

A new Biodegradable Elastomeric Polyester Amide for Soft Tissue Engineering Applications

Abdulrahman Talat Essa, MSc

Thesis submitted to the University of Nottingham for the degree of Doctor of Philosophy

February 2018

Abstract

Elastomeric scaffolds play an important role in the field of soft tissue engineering, and recently, studies investigating different medical applications for these scaffolds have been increasing rapidly. New thermoset bioelastomers have demonstrated promising applications for myocardial, vascular and nerve tissue engineering. Nevertheless, these elastomers have several disadvantages, including the toxicity of the degradation products of the polyester family and the poor solubility of the poly(ester amide) (PEAs) family in the most commonly used polar and nonpolar solvents, which restricts fabrication. Therefore, this PhD project aims to develop a novel biodegradable and biocompatible elastomer to overcome the disadvantages of currently available PEA elastomers, such as the poor solubility of the PEA pre-polymer and the limitations of its mechanical properties, in order to create an elastomer which is similar to protein-based polymers, thus allowing for wider use in soft tissue engineering applications.

The major outcomes of this project include:

(1) In order to build biodegradable and biocompatible elastomers with a satisfactory combination of a soluble pre-polymer, mechanical flexibility and an improved biodegradation profile, an amino alcohol, serinol, was used to synthesise poly(serinol sebacate) (PSS). The synthesised PSS pre-polymer exhibited excellent solubility in a variety of solvents, including methanol, dimethyl sulfoxide and dimethylformamide, while the crosslinked PSS became insoluble in any type of solvent. More importantly, the mechanical properties of PSS could be fine-tuned by changing the curing conditions. In addition, the 3T3 fibroblast cells cultured in the PSS demonstrated good cell attachment and proliferation. No cytotoxicity responses were detected for the PSS samples.

(2) In order to build fibrous elastic materials that resemble the extracellular matrix architecture and mechanical properties of soft tissues, an elastomeric PSS scaffold was fabricated by utilising an electrospinning technique using polyvinyl alcohol (PVA) as a carrier polymer to facilitate fibre formation. After electrospinning, the PSS was cured via thermal treatment and the PVA was partially removed by water. The newly fabricated PSS fibrous scaffold demonstrated diverse characteristics with respect to its mechanical properties, with average rapture elongation (450%) and tensile modulus (~200 kPa) as soft as many types of soft tissues.

(3) The correlation between solution rheology and electro-spinnability, fibre morphology and fibre alignment of polycaprolactone (PCL) with different molecular weights was studied. The produced PCL scaffolds were then treated with an uncured PSS polymer to improve their hydrophilicity and biocompatibility. The PCL/PSS composite scaffolds were fabricated using a safe and cost-effective method. The results showed that cell adhesion and proliferation improved for the PCL/PSS composite scaffolds, which may be attributed to the higher hydrophilicity of these scaffolds in comparison to the pure PCL scaffolds.

In conclusion, novel biodegradable PEA elastomers were successfully designed and synthesised from serinol and sebacic acid by polycondensation reaction. The PSS elastomers exhibited tuneable degradation and mechanical profiles by varying the curing time. Thus, the developed PSS polymer shows excellent potential for various biomedical applications, including tissue engineering applications, drug delivery and coating material.

Publications

The studies presented in this PhD thesis has given rise to the following presentations:

Oral Presentation

Essa, A. ; Aied, A. ; Hamid, O. ; Rose, F. ; Shakesheff, K. (2017), 'Synthesis and Characterization of Biodegradable Elastomeric Polyester Amide for Tissue Engineering Applications', World Academy of Science, Engineering and Technology, International Science Index, Medical and Health Sciences, 11(5), 2120.

Accepted Poster Presentation

Abdulrahman T. Essa, Ahmed Aied, Felicity R. A. J. Rose, Kevin M. Shakesheff, Synthetic and elastic biodegradable polyester amide fibrous scaffold for tissue engineering applications. Accepted at TERMIS-EU Meeting, Davos, Switzerland June, 2017

Acknowledgements

I would like to thank my supervisors Professor Kevin Shakesheff, Dr. Felicity Rose and Dr. Mischa Zelzer for their guidance and support throughout my PhD studies. Many thanks to the all members of the Regenerative Medicine and Cellular Therapies group for making my time at Nottingham University so enjoyable.

Finally, I would like to say thank you to my family especially **Mum and Dad**, brothers and sisters, Faisal, Faris, Maria and Yousif for all their support and love during my PhD.

Table of Contents

Abstract **2**

Acknowledgements **4**

Chapter one **14**

1.1. Tissue engineering **15**

1.1.1. Introduction **15**

1.1.2. *In vitro* tissue engineering **17**

1.1.3. *In situ* tissue engineering **17**

1.1.4. Tissue engineering scaffolds **19**

1.1.5. Elastomers for soft tissue engineering **21**

1.1.5.1. Natural elastomer **24**

1.1.5.2. Synthetic elastomer **24**

1.1.6. Thermoplastic elastomer **25**

1.1.7. Thermoset elastomer **26**

1.1.8. Polyester thermoset elastomer **27**

1.1.8.1. Poly(glycerol sebacate) **27**

1.1.8.2. Poly(diol citrate) **29**

1.1.9. Polyester amide **31**

1.1.10. Fabrication of scaffolds **33**

1.2. Electrospinning **34**

1.2.1. Electrospinning concept **34**

1.2.2.1. Collectors **36**

1.2.2.2. Applied voltage impact **38**

1.2.2.3. The impact of the distance between needle and collector **38**

1.2.2.4. Flow rate **39**

1.2.2.5. Spinneret **39**

1.2.2.6. The impact of polymer concentration and solution viscosity **40**

1.2.2.7. The impact of solution conductivity **41**

1.2.2.8. Surface tension **41**

1.2.2.9. The implications of solvent choice **42**

1.2.2.10. Choice of polymers **42**

1.2.2.11. The impact of environmental factors **43**

1.2.3. Medical applications of Electrospinning **43**

1.2.3.1. Wound dressing **43**

1.2.3.2. Abdominal laparotomy **44**
1.2.3.3. Delivery of chemotherapeutics **44**
1.2.3.4. Controlled release **45**
1.2.3.5. Clinical applications **45**
1.3. Project aims **47**
2.1. Introduction **49**
2.2. Materials and methods **51**
2.2.1. Materials **51**
2.2.2. Synthesis of poly(serinol sebacate) and film fabrication **51**
2.2.3. Gelation point and solubility test **52**
2.2.4. Chemical characterization **53**
2.2.5. Thermal characterization **54**
2.2.6. Mechanical properties **54**
2.2.7. Crosslinking density **55**
2.2.8. Hydration properties **55**
2.2.9. Uncured monomers **56**
2.2.10. In vitro degradation studies **56**
2.2.11. *In vitro* cytocompatibility **57**
2.2.12. Statistics **58**
2.3. Results and Discussion **59**
2.3.1. Synthesis optimization and solubility of PSS **59**
2.3.2. Chemical characterization **63**
2.3.3. Thermal analysis **68**
2.3.4. Hydration properties and Uncured monomers **70**
2.3.5. In vitro degradation **73**
2.3.6. Mechanical properties and crosslinking density **78**
2.3.7. Cytotoxicity and Cell Adhesion **82**
2.4. Conclusion **86**
3. Chapter Three **87**
3.1. Introduction **88**
3.2. Experimental Procedure **90**
3.2.1. Materials **90**
3.2.2. Synthesis of poly(serinol sebacate) (PSS) pre-polymer **90**
3.2.3. Solution preparation for electrospinning **91**
3.2.4. Preparation of PSS fibrous scaffolds **91**

3.2.5. Scaffold morphology 94
3.2.6. Fourier Transform Infrared (FTIR) 94
3.2.7. Mechanical properties 94
3.2.8. Hydration properties 95
3.2.9. In vitro degradation study 95
3.2.10. Cytocompatibility assessment 96
3.2.10.1. Sterilisation of PSS fibrous scaffolds 96
3.2.10.2. Cell culture 96
3.2.10.3. Cell attachment 96
3.2.10.4. Cell proliferation 97
3.2.11. Preparation of PSS fibrous scaffolds with tailored pattern 97
3.2.12. Statistics 97
3.3. Results and Discussion 98
3.3.1. Optimisation of PSS fibre fabrication conditions 98
3.3.2. Effect of PSS:PVA ratio on the fibre properties 99
3.3.3. Curing of PSS:PVA fibrous scaffold 101
3.3.4. Chemical characterisation 103
3.3.5. Mechanical properties 105
3.3.6. *In vitro* degradation 109
3.3.7. Swelling study and pH value 112
3.3.8. Cytotoxicity of PSS scaffolds 115
3.4. Conclusions 118
4. Chapter four 119
4.1. Introduction 120
4.2. Experimental Procedure 122
4.2.1. Materials 122
4.2.2. Synthesis of PSS pre-polymer and PSS/PCL composite scaffold 122
4.2.3. Solution preparation and electrospinning setup 123
4.2.4. Rheology 123
4.2.5. SEM of the electrospun scaffold 124
4.2.6. Fourier Transform Infrared (FTIR) 124
4.2.7. Water contact angle 124
4.2.8. Cytocompatibility 125
4.2.8.1. Sterilization of Nanofiber Mats. 125
4.2.8.2. Cell culture 125

4.2.8.3. Cell viability and attachment 125
4.2.8.4. Cell proliferation 126
4.2.8.5. Fluorescent nuclear staining 126
4.3. Statistics 126
4.4. Results and discussion 127
4.4.1. Rheological properties of PCL solutions 127
4.4.2. Electrospinning 130
4.4.3. Fibre alignment 133
4.4.4. Chemical characterization 139
4.4.5. Characterization of PCL Nanofibers and PSS/PCL composites 141
4.4.6. Water contact angles 141
4.4.7. Cell attachment and proliferation 143
4.5. Conclusions 147
5. Chapter five 148
General discussion, future work and conclusion 148
5.1. General discussion 149
5.2. Future work 152
5.2.1. In vivo studies 152
5.2.2. Surface modification of PSS 152
5.3. Conclusions 152
References 153

List of Figures and Schemes

Chapter one

Figure 1.1 The main elements making tissue engineering. 18
Figure 1.2 *In vitro* and *In situ* tissue engineering approach. 22
Figure 1.3 Biomedical elastomers classess. 27
Figure 1.4 Illustrate the basic electropinning setup: pump, polymer solution, collector, electrical field and mechanism. 30
Figure 1.5: Schematic illustration a plate collector for creating the unwoven nanofibres. and rotating mandrel to create aligned fibres. 35
Scheme 1.1 Reaction scheme for poly(glycerol sebacate). ……...28

Scheme 1.2 Synthesis scheme of poly(diol citrate) from citric acid and aliphatic diols**……..**30

Scheme 1.3 Synthesis scheme of APS (1,3-diamino-2-hydroxypropane and sebacic acid)…32

Chapter two

Scheme 2.1: Synthesis of PSS elastomers……60
Figure 2.1: The cured PSS sheets did not show a tendency to flow under heating up to 50^{o}C or dissolve in DMF and can be subjected to deformation without fracturing the structure. 65
Figure 2.2: ^{1}H NMR spectra, in DMSO-d_6, of sebacic acid, serinol and PSS pre-polymer synthesised at 110^{o}C for 22h. 65
Figure 2.3: ^{13}C NMR Spectra of the PSS pre-polymer.. 66
Figure 2.4: FTIR spectra of PSS pre-polymer synthesised at 110^{o}C for 22 hours and PSS film cured at 110^{o}C for 24h showed strong signals of amide and ester bonds at 1650 cm^{-1} and 1760 cm^{-1}, respectively. 67
Figure 2.5: DSC traces for cured PSS elastomers at 110^{o}C for different periods…….. 69
Figure 2.6: Swelling properties of PSS films in methanol and PBS, the swelling experiment of PSS films was performed to determine the water uptake at 37^{o}C in PBS. 71
Figure 2.7: Percentage of mass loss versus degradation time for PSS-24, PSS-48 and PSS-72 in PBS at 37^{o}C and 60^{o}C. 75
Figure 2.8: SEM micrographs of PSS-24 films before and after 14 days degradation. PSS-24 film was sectioned and imaged using SEM. After 14 days, PSS film exhibited degradation by surface erosion without formation of cracks or pores. 76
Figure 2.9: Variation in the pH of PBS against degradation time for PSS-24, PSS-48 and PSS-72 in PBS at 37^{o}C…… **77**
Figure 2.10 , 2.11: Tensile properties of PSS-24, PSS-48 and PSS-72 films throughout degradation in PBS at 37^{o}C for 14 days. 80,81
Figure 2.12: Light microscopy Images of 3T3 mouse fibroblast cells cultured on PSS polymers on day 1, 3 and 5 post seeding. 83
Figure 2.13: Confocal fluorescence images of 3T3 cells spreading on cured PSS polymers after 5 days of cell culture. 84
Figure 2.14: Proliferation of 3T3 cells cultured on PSS-24, PSS-48 and PSS-72 for 5 days. 85

Chapter three

Figure 3.1: Illustrates the electrospinning setup kit. 92
Figure 3.2: SEM images show the effect of varying PSS:PVA ratio on fibre morphology.. 100
Figure 3.3: Fibre morphology of PSS:PVA (1:1) electrospun scaffolds analysed by SEM. 102
Figure 3.4: FTIR absorbance spectra for PVA, PSS48 sheet, unwashed PSS48/PVA fibre mat and washed PSS48/PVA fibre mat. 104
Figure 3.5: Typical stress-strain curves of PSS48 and PSS72 fibrous scaffolds under wet condition and dry condition. 106
Figure 3.6: The effect of testing conditions (dry and wet) on the mechanical properties of PSS48 and PSS72 fibrous scaffolds. 108
Figure 3.7: Degradation profile of electrospun scaffolds of PSS48 and PSS72. 110
Figure 3.8: SEM micrographs of PSS72 fibrous scaffolds before and after 14 days degradation. 111
Figure 3.9: Swelling ratio of PSS48 and PSS72 fibrous scaffolds during degradation in PBS at 37^{o}C for up to 2 weeks. 113
Figure 3.10: Variation in pH values of degradation media for PSS48 and PSS72 fibrous scaffolds throughout degradation for 14 days in PBS. 114
Figure 3.11: SEM images of 3T3 fibroblast cells cultivated on PSS48 and PSS72 fibrous scaffolds..... 116
Figure 3.12: Proliferation of 3T3 cells cultured on PSS48, PSS72 and PLGA for 5 days. .. 117
Figure 3.13: new setup was made to focus the spinning on the stencil directly..... **Error! Bookmark not defined.**

Chapter four

Figure 4.1: Viscosity curves of PCL 80 as a function of PCL concentration (w/v %). 128
Figure 4.2: Plot of specific viscosity dependence on PCL80 concentration to determine the entanglement concentration..... 129
Figure 4.3: Plot of specific viscosity dependence on PCL45 concentration 129
Figure 4.4: SEM micrographs of electrospun PCL 45 fibres (C_e = 12 wt%) at different concentrations. 131
Figure 4.5: SEM images of electrospun PCL 80 fibres (C_e = 5.5 wt%) at different concentrations..... 132
Figure 4.6: Schematic of the electrospinning stable jet using different PCL80 solution concentrations. 134
Figure 4.7(a)(b)(c): SEM images of a random, partially aligned and aligned electrospun PCL fibres. FFT output images. Plots of Pixel intensity versus the angle acquisition for random, partially aligned and aligned electrospun PCL fibres……..136,137,138
Figure 4.8: Optical images of the produced electrospun PCL80 scaffolds...**Error! Bookmark not defined.**
Figure 4.9: FTIR spectra of aligned PCL80 scaffold, P3, P6 and PSS pre-polymer synthesised at 110^{o}C for 22 hours showed strong signals of amide and ester bonds at 1650 cm^{-1} and 1760 cm^{-1}, respectively. 140
Figure 4.9: SEM images of (a) PCL aligned fibre scaffolds and composite with different amount of PSS coating. 142

Figure 4.10: SEM images showing 3T3 fibroblast cells growing at day one on. 144
Figure 4.11: Fluorescence microscopy images of the PCL aligned scaffolds, P3 and P6 surface cultured with fibroblasts for 5 days. 144
Figure 4.12: Proliferation of 3T3 cells cultured on PCL aligned scaffolds, P3 and P6 for 5 days. 146

List of Tables

Chapter one

Table 1.1: Advantages and disadvantages of natural and synthetic elastomers……. 23.

Chapter two

Table 2.1: Solubility data of PSS pre-polymer and thermally cured samples of PSS in dH_2O and different organic solvents (1 ml) at room temperature 61
Table 2.2: Theoretical and experimental molar ratios of PSS pre-polymer. 64
Table 2.3: Summary of the sol contents, water contact angles and crosslinking densities of PSS samples cured at 110^{o}C for 24, 48 and 72 h. 75

Chapter three

Table 3.1: The variables used to optimise the electrospinning processes of PSS fibrous scaffolds..... 93

Abbreviations

°C	Degree Celsius
µg	microgram
µm	micrometre
2-D	2-dimensional
3-D	3-dimensional
ANOVA	One-way analysis of variance
cm	centimetre
DAPI	4',6-Diamidino-2-phenylindole
DCM	Dichloromethane
dH2O	Distilled water
DMEM	Dulbecco's modified eagle's medium
DMSO	Dimethylsulphoxide
DSC	Differential scanning calorimeter
ECM	Extracellular matrix
FDA	Food and drug administration
g	gram
Mw	weight average molecular weight
n	number of samples
3T3	Swiss mouse embryonic fibroblasts
PBS	Phosphate buffered saline
PCL	Poly(ε-caprolactone)
PGA	Poly(glycolic acid)
PLA	Poly(lactic acid)
PLGA	Poly(lactic-co-glycolic acid)
SD	Standard deviation
SEM	Scanning electron microscopy or Standard error of mean
Tg	Glass transition temperature
w/v	weight/volume
NMR	Nuclear magnetic resonance
PVA	Poly(vinylalcohol)
TCP	Tissue culture plastic

Chapter one

General introduction

1.1. Tissue engineering

1.1.1. Introduction

In the last century, many deadly diseases have been cured by natural and chemical medicines that have revolutionised disease treatment and health care worldwide. Nevertheless, some diseases such as renal failure, muscle dystrophy, and neuron damage as a result of neurological problems are difficult to treat because medications are incapable of restoring the normal functions of affected organs. Surgical transplantation is the main method of treating these ailments. However, following surgery, the risk of infections or complications in patients that use immunosuppressive medications is high, and organs for transplant are in high demand. Also, patients waiting for organ transplants often experience a high degree of mortality because of the large shortage of donors.[1]

In recent decades, regenerative medicine has become a substantial field of study and has begun to address the aforementioned clinical challenges. This field includes different approaches such as tissue engineering, cell therapy and gene therapy to repair damaged or diseased tissues or organs[2,3]. Tissue engineering is one field that relies on advances in bioengineering, molecular biology and materials science to develop biological substitutes for maintaining or restoring the functions of affected tissues or organs (figure 1.1). One example is the development of implantable scaffolds[4]. Such scaffolds can be combined with growth factor to encourage living cells to grow on the scaffold and to develop new tissues that are functionally and structurally similar to native tissues[5].

The domains of tissue engineering and regenerative medicine are enjoying fast development but are frequently lost in the fanfare and marketing possibilities surrounding them. Despite the fact that several experts emphasised that the two terms refer to distinct ideas, they are still regularly used[6]. A wide range of definitions have been proposed in various studies or have been sanctioned by governmental bodies to back regulatory objectives. Thus, tissue engineering was defined by the National Institute for Biomedical Imaging and Bioengineering as the creation of functional structures for damaged tissue or entire organ repair, maintenance or enhancement based on integration of scaffolds, cells and molecules with biological activity in functional tissues[6]. Meanwhile, regenerative medicine was described by the Institute as being concerned with both tissue engineering and self-repair, whereby the body regenerates cells, tissues and organs by employing its own systems and occasionally relying on extrinsic biological material. The interchangeable use of tissue engineering and regenerative medicine has been justified by some on grounds that the aim is not to treat chronic conditions of great complexity but to cure them. For instance, Badylak and Nerem[7] addressed tissue engineering and regenerative medicine advances and considered both of them as references to the same series of research efforts. Likewise, in their review study, Fisher and Mauck[8] suggested that the two terms could be combined into a single one to create the wider field of tissue engineering and regenerative medicine (TERM).

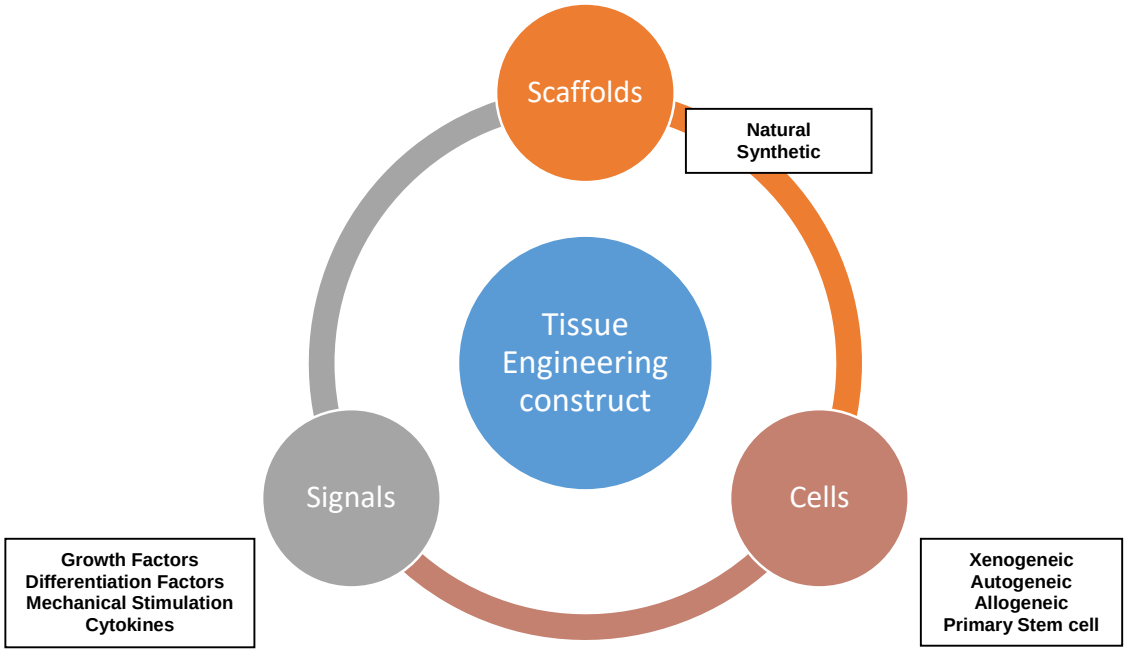


Figure 1.1: The main elements making tissue engineering possible are cells, signals, which derive either chemically or physically from growth factors or a bioreactor, respectively, and the scaffold, which enables cell migration, adherence and tissue production, thus providing a tissue formation template.

1.1.2. *In vitro* tissue engineering

The typical tissue engineering paradigm is *in vitro* tissue engineering, which requires the combination of three elements: cells, scaffolds and growth factor. This process traditionally requires the use of harvested cells that are expanded and then seeded onto a natural or synthetic scaffold that provides a suitable environment. The scaffold will then be completely re-absorbed by the body following the formation of new tissue. In this context, scaffolds are triggered by appropriate mechanical and chemical stimuli to initiate the process of building a new extracellular matrix (ECM). The tissue-engineered construct would be then implanted and integrated with native tissues to replace diseased tissues[9–11] (Figure 1.2).

1.1.3. *In situ* tissue engineering

The concept of *in situ* tissue engineering has recently introduced the possibility of utilising the body's own endogenous cells and biologic resources. In this case, a biodegradable scaffold can be placed to recruit progenitor or stem cells to the site of diseased tissues and organs and to encourage regeneration without cell transplantation[12] (Figure 1.2). Decellularised tissues or organs can be used as *in situ* replacements; however, disease transmission or immunogenic response are possible outcomes[13].

Materials from a foreign host that have been subjected to alterations to serve as a graft are known as allogenic materials. The major strength of these materials is that they retain tissue structure and content and do not differ much from the tissues they are intended to supplant. Thus, in theory, tissue remodelling and repair could be achieved with allogenic materials without triggering an immune response[14,15]. Graft decellularization is a preliminary step in the treatment of an allogenic material and is geared towards eliminating antigens that trigger an unfavourable immune response without disrupting the integrity of the ECM, which serves as the scaffold. Scaffold integrity is usually reflected in the content of collagen, elastin, s-glycosaminoglycan and growth factor, and in structural and ultrastructural integrity.

However, an innate immune response may still be triggered by tissue residue post-decellularization in the case of allogenic and xenogenic materials. To give an example, decellularization may not remove damage-associated molecular pattern proteins (DAMPs), which are present in the native tissue as well as being produced during cell necrosis and by macrophages activated by acute tissue damage. DAMPs are responsible for the upregulation of HMGB1, which in turn promotes the expression of chemokine and TLR4 mRNA[16], thus stimulating a pro-inflammatory response. In theory, there are three strategies for modifying DAMPs, namely, inhibiting their release through the use of platinum or ethyl pyruvate, inhibiting them directly via anti-HMGB1 and pro-apoptotic treatments, or inhibiting DAMP-Rs or the related downstream signalling targets TLR4 antibodies[17].

Moreover, the differentiation and proliferation of recruited cells can be guided by incorporating bioactive groups to scaffolds[12]. The main advantages of this approach are that the process does not require a source of cells and or much time for cell expansion and instead uses the human body as a bioreactor for the formation of new tissues.

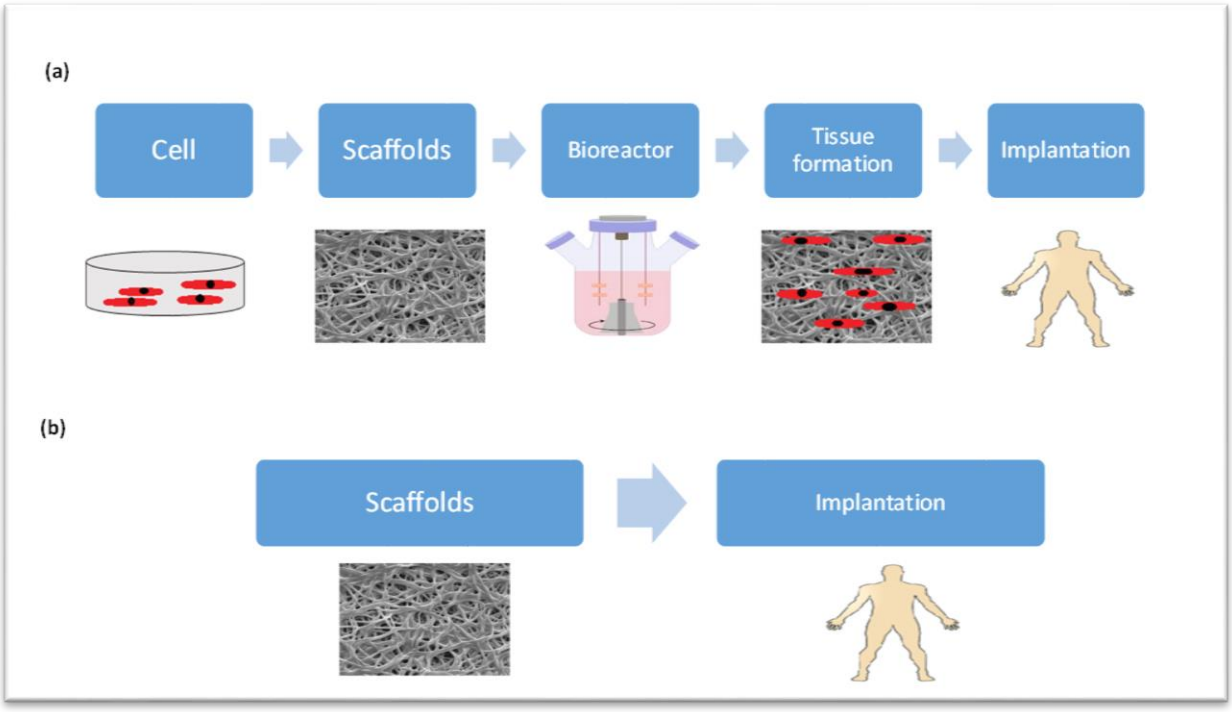


Figure 1.2: (a) *In vitro* tissue engineering approach. The cells seeded onto a scaffold, then placed in a bioreactor. After tissue growth, the scaffold is implanted in the body. (b) *In situ* tissue engineering approach. Scaffold (cells-free) is implanted in the human body, which serves as bioreactor.

1.1.4. Tissue engineering scaffolds

The utilised biomaterials determine the chemical properties of the scaffold and the interaction between the living cells and the scaffold[18]. They also define the mechanical properties of the scaffold. Recent studies have suggested that the mechanical properties of elastomeric scaffolds enhance tissue regeneration[18,19].

Overall, the objective of employing scaffolds in tissue engineering is to guide tissue formation *in vitro* and *in vivo* for the replacement or repair of damaged tissues and organs. Scaffolds also support the transport of growth factors and nutrients to enhance vascularisation and tissue formation. The chemical and physical properties of scaffolds are important to consider during their design and can be dictated by the choice of materials and processing methods. The properties of functional tissue scaffolds will vary depending on the target tissues. Also, the utilised materials and their degradation products must be non-toxic, must not produce any undesirable immunological or thrombogenic responses and must allow for rapid vascularisation[20,21].

Furthermore, scaffolds should have some level of bioactivity to accommodate for cellular attachment, proliferation and differentiation in the case of association with multipotent or pluripotent cells[22]. Scaffolds should also be biodegradable. In some cases, such as transplantation, scaffolds can incorporate into targeted tissues after cells are incorporated; over time, cells produce their own ECMs, which would ideally concur with scaffold degradation and elimination from the body. In addition, the mechanical properties of scaffolds should ideally match those of the ECMs of targeted tissues, should allow for cell ingrowth and should produce an appropriate ECM. In the case of bone tissues, for example, scaffolds must have high strength[23,24]. Some tissue types require specific scaffold designs. For example, in some cases, scaffold porosity should be taken into account to allow for nutrient and gas exchange. Meanwhile, for heart tissues, cardiac inflow/outflow patterning and directionality should be considered[25]. Therefore, to design or assess how appropriate a scaffold is for the purposes of tissue engineering, several important aspects must be taken into account:

(i) Biocompatibility

Tissue engineering scaffold must demonstrate biocompatibility to enable cell adherence, normal function, and migration on its surface and subsequently through it before starting proliferation and forming new matrix. The immune response triggered by the implanted scaffold or tissue engineered structure must be minimal, otherwise a significant inflammatory reaction may occur that may interfere with healing or even lead to the body rejecting the implant.

(ii) Mechanical properties

Consistency should exist between the mechanical attributes of the scaffold and the anatomical area targeted for implantation. Additionally, the scaffold should also demonstrate sufficient strength so that it can be surgically handled when it is implanted, which is crucial for every tissue, but is particularly problematic for cardiovascular and orthopaedic applications. A major difficulty in the context of bone or cartilage engineering endeavours is creation of scaffolds that have suitable mechanical attributes, because bone and cartilage necessitate a scaffold that exhibits enough mechanical integrity to remain in place from the moment it is implanted until the process of remodelling is finished[26].

(iii) Biodegradability

The implanted scaffold or tissue engineered structure are only temporary and should gradually be substituted by the body's own cells, which is the overall intent of tissue engineering. As a result, the scaffold must demonstrate biodegradability otherwise cells will be incapable of forming extracellular matrix[27]. Furthermore, it is not enough for the scaffold to be biodegradable, but the residues of its breakdown must not be toxic and must leave the body without affecting other organs. It is necessary to combine an inflammatory response with controlled introduction of cells (e.g. macrophages) so that breakdown happens alongside tissue development. This is why immunology has become more and more important for research since clinical practice has started to adopt tissue engineering approaches on an increasingly regular basis[28].

(iv) Scaffold architecture

The structure of tissue engineering scaffolds is highly important. To help cells disseminate and make sure that a suitable supply of nutrients reaches the cells in the construct and the extracellular matrix that they form, scaffolds must be highly porous and provide an interlinked pore structure. Such a structure is also essential for elimination of waste products and scaffold breakdown products should not affect other organs and tissues when leaving the body. tissue engineering specialists have particularly expressed worries about core deterioration caused by absence of vascularisation and elimination of waste from the middle of tissue engineered constructs[29].

The mean size of pores in the scaffold has great importance as well. Chemical groups called ligands and present on the surface of the material underpin the interplay between cells and scaffolds and they are naturally present as Arg-Gly-Asp (RGD) binding sequences in scaffolds produced from natural extracellular materials such as collagen. On the other hand, ligands may need to be intentionally introduced in synthetic material scaffolds through processes such as protein adsorption. The specific surface area, representing the pore surface that is available for cell attachment, determines how dense the ligands are, and is in turn determined by the mean size of scaffold pores. More specifically, the pores must be sufficiently large to enable cell penetration into the structure, where the cells attach to the scaffold ligands, and at the same time the pores must be sufficiently small to create a specific surface area that is expansive enough, resulting in the lowest density of ligands to enable a sufficient number of cells to attach to the scaffold[30]. Hence, more than one option of pore size is available for all scaffolds[31], according to the nature of the employed cells and the tissue targeted for engineering.

1.1.5. Elastomers for soft tissue engineering

Elastomer materials are made from polymers that have the ability to stretch several times their length yet return to their original dimensions without permanent deformation. Also, these materials have a glass transition temperature (Tg) below room temperature[32]. The mechanical properties of elastomers, such as their ultimate elongation and Young's modulus, can be tuned by modifying the degree of crosslinking[33]. For these reasons, elastomers are desirable materials for building scaffolds for mechanically dynamic tissues such as myocardial and skeletal muscle tissues.

Generally, the elastomers used in soft tissue engineering can be classified into two main categories: natural and synthetic elastomers. Natural elastomers can be divided into protein-based elastomers and hydrogels, while synthetic elastomers can be divided into chemically crosslinked elastomers (thermosets) or physically crosslinked elastomers (thermoplastics)[34]. Figure 1.3 presents the important biomedical elastomer classes described in the literature[35–38].

Elastomeric biomaterials such as heparinised polymers, poly(vinyl chloride), silicone and polypeptides elastomers have been used in different biomedical applications, including transdermal therapeutic interventions, cardiovascular devices, orthodontics and prosthetic devices[39]. Moreover, increasing uses for elastomeric biomaterials will likely be found in the field of tissue engineering because of the biocompatibility, biodegradability, flexibility and economy of cost of these materials.

Traditional synthetic biomaterials used in soft tissue engineering include poly(lactic acid) (PLA)[40], poly(ethylene glycol) (PEG)[41,42] and polyurethanes[43,44]. However, these types of biomaterials undergo plastic deformation, have a high modulus and demonstrate inappropriate mechanical properties when evaluated in the long term. As a result, other more promising synthetic elastomers have been developed for soft tissue engineering. Table 1.1 shows Advantages and disadvantages of natural and synthetic elastomers.

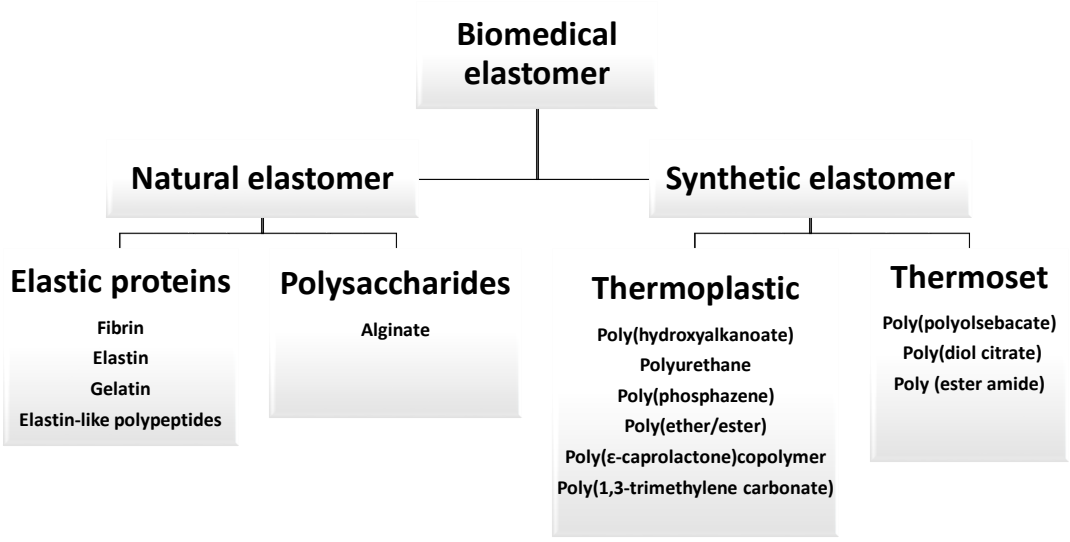


Figure 1.3 Biomedical elastomers classes[35–38]**.**

Table 2.1 Advantages and disadvantages of natural and synthetic elastomers[34].

	Natural elastomer	**Synthetic elastomer**
Advantages	Elastic	Elastic
	Analogous structure to natural Extracelluler matrix	Mechanical properties, purity and degradation kinetics can be contrlloed
	Bioactive and Provide receptor – binding ligands	Structure stability during degradation
	Natural remoulding	
Disadvantages	Possible of immunogenic response	Inflammation due to foreign body response
	Need Purification processes	Poor processibilty
	Unpredictable degradation profile	Release of acidic by-products
	In vivo calcification	
	Complication in processing and preparation	
	Disease transmission	

1.1.5.1. Natural elastomer

Natural elastomers used in soft tissue engineering offer the advantage of containing signalling motifs that enhance cell adhesion, proliferation and differentiation. These natural biomaterials include proteins such collagen[45], elastin[46] and fibrin[47] or hydrogels made of polysaccharides such as chondroitin sulfate[48] and alginate[49]. Many studies have demonstrated the feasibility of collagen and alginate for building natural scaffold constructs for use in myocardial tissue engineering[50,51]. Although several studies have demonstrated the advantages of using natural biomaterials that demonstrate cytobiocompatibility and biodegradability, constraints include long purification processes, batch-to-batch variability and the possibility of disease transmission[36,52].

1.1.5.2. Synthetic elastomer

Synthetic elastomers are one branch of polymeric biomaterials that have three important characteristics in comparison to other polymer biomaterials. They have a stable, three-dimensional structure with mechanical properties similar to the ECMs of soft tissues and organs. Also, they are flexible and therefore able to induce mechanical stimulation for tissue engineering process. Finally, they have a biodegradation profile that is modifiable through controlling different factors such as the crosslinking density of synthesised elastomers[53].

In addition, synthetic elastomers can be synthesised using different types of polymerisation techniques such as ring-opening polymerisation, polycondensation, photo- and thermally-initiated radical polymerisation and have the ability to integrate into co-polymers. These characteristics allow for a large variety of physical and chemical properties[53,54]. The degradation rates of synthetic elastomers can also be controlled by different factors such as segment length and composition, molecular structure (monomers), molar ratios, curing type, polymerisation duration and temperature of the reaction[53].

From a material standpoint, synthetic elastomers can be produced in large batches and can also have adjustable properties that are modifiable depending on the processing conditions and synthetic schemes. From clinical and biological perspectives, these materials should demonstrate biocompatibility and mechanical capacities that resemble the proteins of natural ECMs.

1.1.6. Thermoplastic elastomer

Many research studies have aimed to develop materials that can be utilised as alternatives for natural rubber. This interest has led to the discovery of different types of thermoplastic elastomers[55]. Thermoplastic elastomers possess many of the mechanical properties of natural rubbers such as elasticity and softness. Moreover, in contrast to thermoset elastomers that do not flow once cured, thermoplastic elastomers have the advantage of being easily processed as thermoplastic biomaterials by solvent or melting processes[56]. The general synthetic design is based on the formation of a physical crosslinked network using multi-block co-polymers that consist of soft and hard segments. The polyester segments within the polymer chains, such as poly(glycolic acid) (PGA) or poly(lactic acid) (PLA)[57], are responsible for the biodegradation properties of the materials[58].

The most widely used thermoplastic elastomers are polyurethanes, which were approved by the Food and Drug Administration (FDA) for different applications. Polyurethanes have a wide range of mechanical and degradation properties and include both degradable and stable materials with hydrophilic to hydrophobic characteristics depending on the segmented structure and synthesis process[59,60]; these characteristics can be adjusted for different tissue engineering applications[34,61]. In addition to vascular grafts[62], polyurethanes have been studied for their applications in medicine, including soft tissue engineering, such as cardiovascular tissue[63], intestine[64] and blood vessel[65] engineering, as well as hard tissue engineering involving bones[66], cartilage[67] or ligaments[68]. Polyurethanes as scaffolds for tissue engineering applications must be bioresorbable; therefore, polyester polymers such as PGA, PLA and PCL are mainly included in the synthesis process[69].

PCL is one of the first thermoplastic elastomers that was reported. It is synthesised through the co-polymerisation of PCL and DL-lactide via ring-opening polymerisation[70]. In particular, PCL has been co-polymerised with PLA and PGA to synthesise thermoplastic elastomers for various types of tissue engineering[71,72]. The degradation rate of PCL co-polymers is generally faster than that of PCL polymer alone. For example, PCL-PGA co-polymer scaffolds degrade 50% of their original weight after 6 weeks of incubation, while traditional PLC scaffold took up to 12 months to degrade[73].

Thermoplastic elastomers have certain advantages such being biodegradable, biocompatible and tailorable with respect to their mechanical and physical properties. Nevertheless, thermoplastic elastomers generally contain crystalline regions that could resist degradation. Therefore, these polymers have a heterogeneous degradation profile[58,74] that can cause a non-linear loss of mechanical properties and lead to the mechanical failure of the scaffold before the process of tissue regeneration is completed. In addition, the three-dimensional structure of scaffolds is critical during degradation processes. The presence of crystalline regions that control the architecture of the network of thermoplastic biomaterials can result in unpredictable outcomes[37].

1.1.7. Thermoset elastomer

Unlike thermoplastic elastomers, thermoset elastomers are more predictable in the loss of their mechanical properties and have a consistent degradation profile because of their amorphous structure, which results in the maintenance of their three-dimensional structure throughout the degradation process[37]. For these reasons, the focus of the literature review is on biodegradable thermoset elastomers. The first biodegradable thermoset elastomer was developed for drug delivery, wherein the maintenance of the elastomer network during drug release was important for controlling the drug release process by diffusion[75].

Thermoset elastomers are elastic as a result of polymer chains connected by chemical bonds. This bonding process may occur following the reaction of monomers containing reactive functional groups, which are able to connect to other monomers. The process of crosslinking could be initiated by radiation or thermally. In addition, to form a chemically crosslinked network, at least one of the reacting monomers must build at least three linkages with neighbouring monomers. Once the molecules are fully crosslinked, the molecules will exhibit their final physical properties and will not flow or melt under heat unless the molecules undergo chemical degradation processes. Recently, biodegradable thermoset elastomers have gained increasing attention in the field of tissue engineering[76–78].

When loading drugs into thermoset elastomers, the drug should not be dissolved in mutual solvent or it will be affected by the crosslinking procedure; however, this can be avoided if the drug is in the solid particle form, with the polymer photocrosslinked[79]. The drawback of the latter approach is that a smaller amount of drugs is produced from these elastomers. When compared to thermoplastic elastomers, thermosets are preferable from the point of view that they degenerate more homogeneously because they do not contain either crystalline or high glass transition temperature domains, which would degrade at a slower pace than amorphous areas. Homogeneous degradation leads to more predictable changes in mechanical properties. In addition, an inflammatory response late in the degradation period is connected to crystals being released when thermoplastics degrade[80].

1.1.8. Polyester thermoset elastomer

1.1.8.1. Poly(glycerol sebacate)

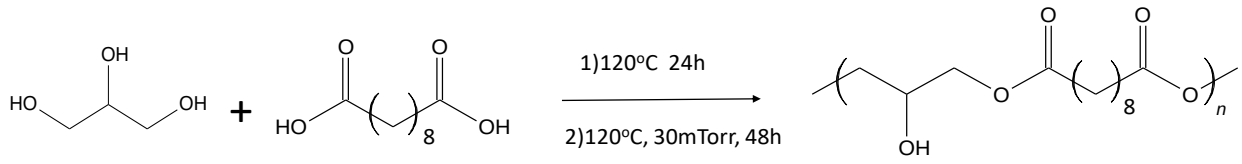
PGS was first developed for biomedical applications by the Langer Group in 2002. This biodegradable thermoset elastomer was intended to mimic the mechanical properties of soft tissues[81]. In particular, PGS is synthesised from sebacic acid (dicarboxylic acid) and glycerol (an alcohol containing three hydroxyl groups), which involves polycondensation between the carboxylic acids in sebacic acid and the alcohol groups in glycerol to yield transparent material (Scheme 1.1). The synthesis process is typically carried out in two steps: First, the pre-polymerisation step is conducted by heating a mixture of sebacic acid and glycerol under a purge of nitrogen gas to prevent reactant oxidation. The esterification reaction in the first step is preferentially between carboxylic acid and primary hydroxyl groups of glycerol to form the polymer chains. Second, the pre-polymerised material is crosslinked for several days under vacuum and high temperature conditions. During the second step, the secondary alcohol groups of glycerol react with the carboxylic acid of sebacic acid, thus leading to crosslinking between polymer chains[34].

The mechanical properties of PGS are related to the crosslink density of the polymer chains. The Young's modulus of PGS elastomers is in the range of 0.056–1.5 MPa, which is indicative of soft materials, and the strain to failure is from 40–400% depending on the crosslinking density[52]. These mechanical properties make PGS suitable for different soft tissue applications in dynamic environments involving ligaments (~1.5 MPa)[82,83] and muscles (~0.5 MPa)[84].

The degradation and mechanical properties of PGS can also be tailored via the co-polymerisation of acrylate groups and polyethylene glycol (PEG) diacrylate in the polymer chains[85]. Photocured PGS-acrylate elastomers exhibit elongation at break and a Young's modulus ranging from 40–190% and 0.05–1.4 MPa, respectively[85]. In addition, the spectrum of PGS-acrylate could be further tailored by incorporating other acrylated groups such as PEG-acrylate[85]; these modified materials demonstrated human primary cell attachment and proliferation and therefore have potential for tissue engineering processes that require the encapsulation of growth factors or that have cells that are sensitive to high temperatures[85].

The degradation rates of PGS have been studied *in vivo* and have demonstrated complete resorption of PGS elastomers after 60 days; *in vitro* degradation studies showed a slower rate of degradation than *in vivo* studies. Although PGS degradation is mainly caused by caused by surface erosion, the difference between *in vivo* and *in vitro* degradation was attributed to macrophage activity and the action of enzymes such as lipase[86] and esterase[87] that may catalyse the hydrolysis of the ester bonds of PGS polymer chains[88].

Various studies have revealed the biocompatibility of PGS with different types of cells such as fibroblasts[85], Schwann cells[89] and endothelial progenitor cells[90]. *In vivo* studies have demonstrated that PGS does not cause chronic inflammation and results in less fibrous capsule formation; however, PGS showed similar inflammatory responses in comparison to poly(lactic-co-glycolic acid) PLGA[81]. Moreover, PGS scaffolds can guide the direction of cardiac muscle cells with a honeycomb structure and can also contract under electric field stimulation[91].



Scheme 1.1 Reaction scheme for poly(glycerol sebacate).

1.1.8.2. Poly(diol citrate)

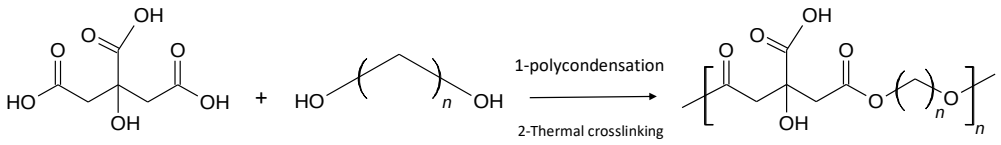
A new biodegradable polyester elastomer based on citric acid and diol groups was developed by Ammer's Group, which has expanded the current availability of thermoset elastomers[92]. (Scheme 1.4). Citric acid is an intermediate metabolite of the Krebs cycle and is a non-toxic, inexpensive monomer that has widely been used in the food industry.

Poly(diol citrate) is synthesised via a polycondensation reaction, similar to PGS. The first step involves producing pre-polymerised material via the thermal polycondensation of citric acid and linear aliphatic diol. This step is followed by a crosslinking process at the desired temperature and duration. Unlike PGS, poly(diol citrate) can be produced without vacuum conditions under low temperatures (37˚C)[93].

One of the main advantages of poly(diol citrate) elastomers are their customisable degradation and mechanical properties according to the diol choice (1,12-dodecanediol, 1,10-decanediol, 1,8- octanediol, 1,6-hexanediol)[92] and the synthesis conditions, such as the mole ratio, crosslinking duration and temperature and vacuum conditions. For instance, increasing the crosslinking time from 24 to 144 h at 120 °C will decrease the strain to failure from 253–117% and increase the Young's modulus from 2.84–6.44 MPa. The mechanical properties of poly(diol citrates) can be further tailored by including fumarate and acrylate groups as crosslinkers; the resulting elastomers have a Young's modulus that ranges from 16.4–38.3 MPa for fumarated elastomers and from 7.4–75.9MPa for acrylated elastomers[94].

Poly(diol citrates) have been reported to have a faster degradation rate when crosslinked under mild conditions (no vacuum, low temperature) versus relatively harsh conditions (vacuum, high temperature). The degradation rate of poly(diol citrates) in phosphate buffered saline (PBS) at 37 °C was six months, while the subcutaneous implantation of poly(diol citrates) was shown to remain for only two months because of enzymatic and cellular effects[92].

Poly(1,8-octanediol) citrate is the most extensively studied elastomer of this group, as 1,8-octanediol is the longest aliphatic diol that is water soluble and has no reported toxicity. Initial biocompatibility studies with human aortic endothelial cells and human aortic smooth muscle cells demonstrated that the cell attachment and proliferation of poly(1,8-octanediol) citrate scaffolds was as good as poly-L-lactic acid scaffolds[92,93]. The hemocompatibility of this elastomer in another *in vitro* study resulted in sufficient reductions in clot formation, platelet adhesion and inflammation response[95]. In addition, tubular scaffolds made from poly(1,8-octanediol) citrate displayed good cell attachment and mechanical matching with blood vessels. Tubular scaffolds are fabricated in two layers: a porous exterior layer made of poly(1,8-octanediol) citrate and a nonporous interior layer made of poly(1,12-dodecanediol) citrate[96].



Scheme 1.2 Synthesis scheme of poly(diol citrate) from citric acid and aliphatic diols.

1.1.9. Polyester amide

The development of poly(1,3-diamino-2-hydropropane-co-polyol sebacate) (APS) elastomers was motivated by the desire to overcome the lack of rapid degradation polyester elastomers such as PGS and PGS-acrylate[97]. The synthesis of APS occurs via the thermal polycondensation of four non-toxic monomers: 1,3-diamino-2-hydroxypropane, sebacic acid, D,L-threitol and glycerol[97] (Scheme 1.5).

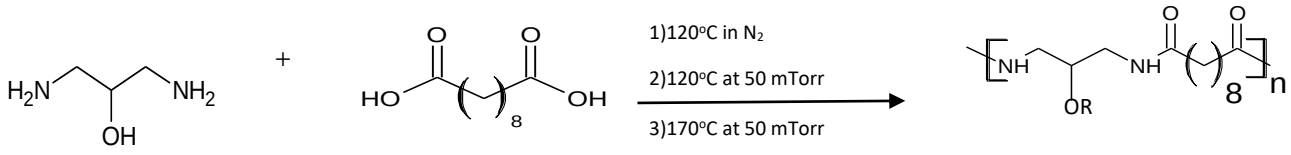
The mechanical properties of APS elastomers corresponded with a low Young's modulus ranging from 1.45–4.34 MPa and a strain to failure ranging from 21–92%; these properties can be increased by reducing crosslinking time. Finally, the ultimate tensile strength (UTS) ranges from 0.24–1.69 MPa[97].

Degradation studies of APS demonstrated an extended degradation profile that can have potential utility in applications where elastomer scaffolds with long half-lives are necessary, such as scaffolds for peripheral nerve regeneration conduits or cardiovascular grafts. In particular, APS showed hydrolytic degradation of 42.8–97.0% when incubated in a sodium acetate buffer with a pH of 5.2[97]. The presence of amide groups in APS can cause a reduction in the hydrolysis effect and in the action of esterase enzymes during degradation processes[36]. In addition, APS elastomers are capable of post-crosslinking modification via the functionalisation reactions of free amines.

Biocompatibility studies with primary human foreskin fibroblasts maintained metabolic activity and demonstrated healthy cell morphology when cultured on APS. Moreover, *in vivo* assessments have revealed that APS produces fewer macrophages and foreign body responses around implants in comparison to PLGA[36].

PGS and APS elastomeric biomaterials are biodegradable and biocompatible. However, many issues associated with these biomaterials and its derivatives remain to be mentioned. For example, PGS can cause cytotoxicity due to acidic degradation by-products. The degradation rate of PGS biomaterials is generally fast, hindering their utilisation as scaffolds for tissue engineering. Moreover, APS has poor solubility in most commonly used polar and nonpolar solvents, restricting its fabrication.

To overcome the disadvantages of currently available biomaterials, and extend the properties of biodegradable elastomers, I hypothesis that the new polyester amide should follow some important design principles, including the following: (1) incorporation of amide groups to promote cell adhesion, (2) insertion of ester bonds to the polymer backbone to enable enzymatic degradation and hydrolysis, (3) tuneable crosslinking to control mechanical properties and (4) use of non-toxic monomers whose degradation products can be eliminated by natural metabolic pathways.



1,3-diamino-2-hydroxypropane **sebacic acid** **APS**

Scheme 1.3 Synthesis scheme of APS from 1,3-diamino-2-hydroxypropane and sebacic acid.

1.1.10. Fabrication of scaffolds

Tissues inside the human body are organised as three-dimensional structures. Therefore, scaffolds should mimic ECMs and the biological and mechanical properties of the targeted tissues to be replaced in order to act as temporary templates. The fabrication and design process of scaffolds for soft tissue engineering present challenges stemming from the complexity of the desired architecture and from the need to create ideal environments for cell viability. In this respect, scaffold design should allow the transport of nutrients, facilitate consecutive multicellular processes and provide suitable mechanical properties[98].

Different techniques can be utilised to fabricate biomaterials into various scaffolds. These techniques can be classified into four categories[99,100]: solvent casting with particulate leaching, solid freeform fabrication (SFF), fibre network formation and phase separation.

Nanofibre technology has been accelerated in recent years to create nanofibre scaffolds from a range of different polymeric materials. Various techniques exist for generating fibres at a nanometre scale such as self-assembly, phase separation template synthesis, drawing and electrospinning. However, of the several techniques for creating fibre scaffolds, the electrospinning technique is most popular because of its simplicity and cost effectiveness. This technique can also be used to create fibres at micro to nanometre scales. Therefore, the next part of the literature review will focus on the electrospinning technique[101].

1.2. Electrospinning

1.2.1. Electrospinning concept

The essence of the electrospinning process is to produce a solution jet which can be divided into smaller jets by a sufficient balance between the electrical force and surface tension force, which hold the solution jet together. Initially, the surface tension held the polymer solution in the form of a droplet at the end of the needle. When the charge was induced on the solution surface by increasing the voltage, pendent droplets of the solution were produced, known as Taylor cones, at equilibrium of the surface tension and electric forces.

When the electrical repulsion between the charges overcome the surface tension on the surface of the drop, a solution jet is ejected from the apex of the Taylor cone[102]. The critical voltage can be identified by Taylor cone, at which the following process would occur[103]:

$V^2 = 4\ H^2/L^2\ (\ln 2L/R - 3/2)(0.117\pi\gamma R)$

V is the critical voltage; H is the distance between the needle and the collector; L is the length of the needle; R is the radius of the needle; and ɣ is the surface tension of the solution.

The Taylor cone is the critical point of the equilibrium between the electrical force and the surface tension force. When the voltage increased above the critical voltage, electrical forces on the droplet distorted the equilibrium, and a solution jet was ejected from the Taylor cone toward the electrical ground or electrode of opposite polarity (collector); at the end of this segment, a conical shape was observed. Electrospinning is a rapid process, and only the conical envelopes of the splaying filaments could be observed because of the fast whipping of the jet[104]. A schematic illustration the basic electrospinning setup and various physical phenomena occurring during electrospinning is shown in Figure 1.4.

The solution jet in the electrospinning process can be divided into four regions[105]: (1) The base, which is the region where the solution jet emerges from the Taylor cone; (2) The jet, which is where the jet is stretched and accelerated by the electrical force; (3) Splaying, which refers to when a single jet is divided into an equal jets diameter and charges; and (4) Splitting, which occurs when the jet is divided into two equal jets.

SEM image of nanofibres

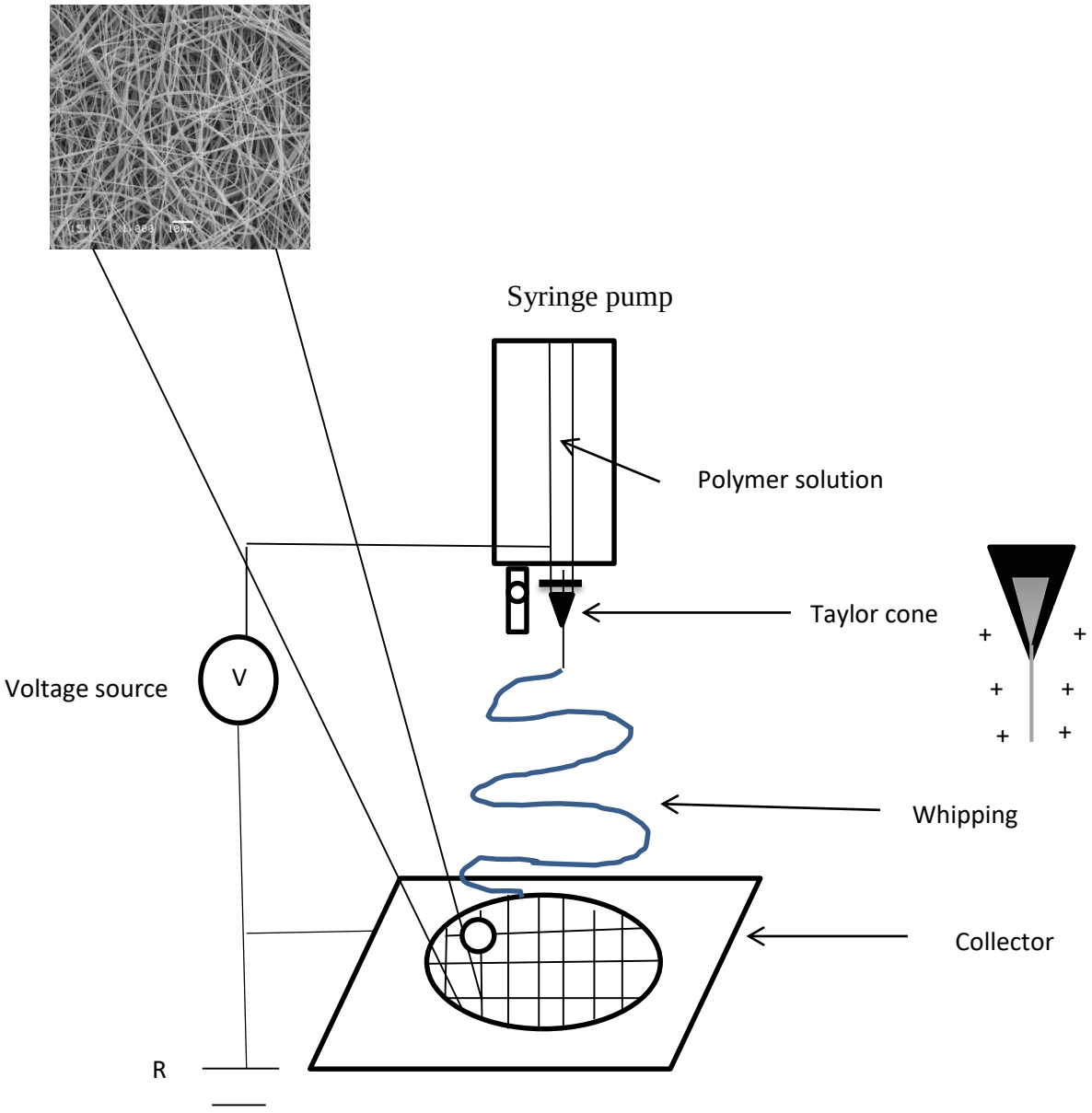


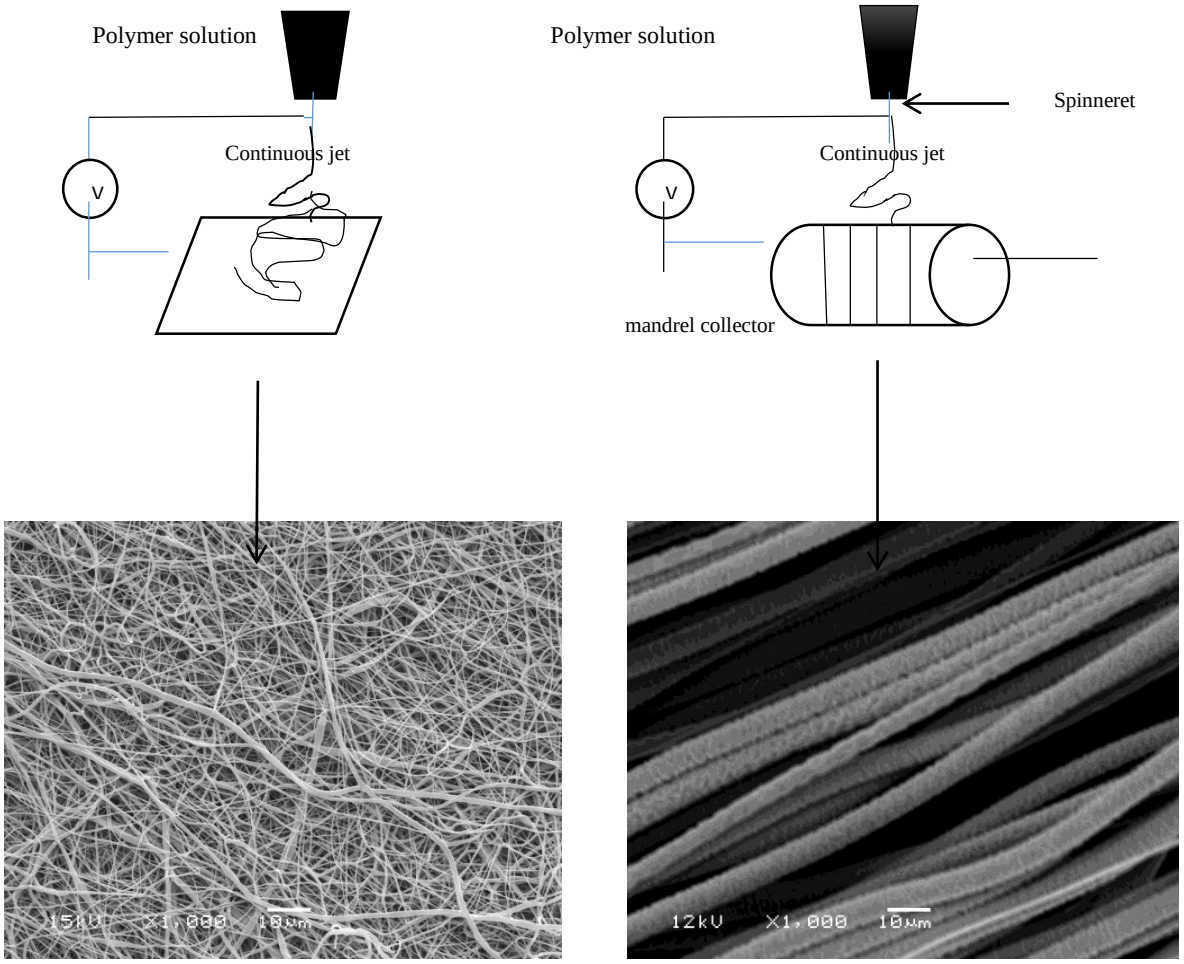
Figure 1.4: The basic electropinning setup: pump, polymer solution, collector, electrical field and mechanism, also the figure shows the main stable jet that undergoes whipping stage before binding to the collector.

1.2.2. Impact of factors on electrospinning

Electrospinning is influenced by three groups of factors, namely, electrospinning factors (e.g. applied electric field, needle-collector distance, flow rate, needle diameter and collector type), solution factors (e.g. solvent, polymer concentration, viscosity and solution conductivity) and environmental factors (e.g. relative humidity, temperature). The production of smooth electrospun fibres without beads depends on all groups of factors. As such, comprehension of the effects of these factors is necessary to improve knowledge about the process of electrospinning and production of polymeric nanofibres.

1.2.2.1. Collectors

The assembly and morphology of the fibres can be influenced by the type of the collector. For instance, random fibres can be produced by using the collector plate, whereas aligned fibres can be produced by using different designs of collectors such as drums, spinning disks and mandrel collectors. In addition, the movement of the collector should be considered to avoid breaking nanofibres into fragments[106,107]. The mat of the fibres can be partially aligned by slowing the rotation of the collector. Figure 1.6 shows an example of the plate and disc collectors. Porous hollow tubes were also produced, which can be used in different applications, such as vascular tissue engineering[108]. In addition, the packing density of the fibres can be determined by the porosity and the conductivity of the collector[109]. For example, cellulose acetate nanofibres were electrospun with copper mesh, and a high yield of the porous structure was produced by using a non-conductive collector. The authors attributed this to the ability of the conductive collector to scatter the residual charge that can be found in the fibres, whereas a non-conductive collector can cause the fibres to repel from each other and thus reduce the density of packing[110].



A B

Figure 1.5: Schematic illustration of the electrospinning setup. (A) SEM image of electrospun PCL(80 kDa) fibres were collected onto a plate collector for creating the random nanofibres and (B) electrospinning setup using rotating mandrel to create PCL (80 kDa) aligned fibres.

1.2.2.2. Applied voltage impact

Deformation of a round droplet into a Taylor cone and formation of ultrafine nanofibers at a critical voltage occur when current from a power supply of high voltage flows into a solution through a needle made of metal[111]. That critical voltage is not the same for all polymers. Polymer solution expansion coupled with charge repulsion in the polymer jet is considered to be the reason why nanofibers of smaller diameter develop as the applied voltage increases[110]. Beads or beaded nanofibers develop when the applied voltage exceeds the critical value. The reduction in Taylor cone size and jet velocity increase at identical rate of flow are the determinants of diameter enlargement and development of beds or beaded nanofibers as the applied voltage increases. Poly(ethylene oxide) (PEO)/water was used by Deitzel and colleagues to demonstrate that beads developed as the applied voltage increased, while Meechaisue and collegueas and Zong and colleagues corroborated that observation[112].

1.2.2.3. The impact of the distance between needle and collector

The morphology of an electrospun nanofiber is largely the product of the distance separating the tip of the metallic needle from the collector. This distance differs depending on the polymer system, in much the same way as the applied electric field, viscosity and flow rate. The reason why the distance influences the morphology of the nanofiber is that it is determined by the time of deposition, rate of evaporation, and whipping or instability interval[113]. Therefore, preparation of smooth and homogeneous electrospun nanofibers necessitates the maintenance of a critical distance, as nanofiber morphology will be directly impacted by modifications on both sides of the critical distance[114]. The effect of the needle tip-collector distance has been the focus of ample study, with findings revealing that too small a distance led to the development of faulty nanofibers with a large diameter, while increase in the distance shrunk the nanofiber diameter[113]. Furthermore, some instances have also been reported where alterations in distance did not affect the nanofiber morphology[115].

1.2.2.4. Flow rate

The polymer solution properties, including concentration, viscosity and spinneret diameter greatly determine the flow rate of the electrospinning process; a lower flow rate is recommended to ensure there is enough time for the solvent to evaporate. However, the flow rate also effects the fibre diameter[116]. The bead formation and the thickness of the nanofibres can be increased by using a high flow rate and large volume of the solution owing to the short drying time[117]. In addition, the vertical configuration is the ideal position to prevent the gravity effect on the electrospinning process[117]. In addition, Megelski et al. studied the correlation between the flow rate and the structure of the polystyrene/tetrahydrofuran solution[118]. In this study, increasing the flow rate led to an increase in the pore size and diameter, and beads were formed at a high flow rate due to incomplete solvent drying before reaching the collector, which can also increase the possibility of the formation of ribbon-like fibres.

1.2.2.5. Spinneret

In 2007, Macossay conducted a comprehensive investigation of the spinneret tip diameter, reporting that the inner spinneret diameter and the average fibre diameter were not correlated in any way[119]. Nevertheless, the flow rate of the polymer solution and the shape and size of the interface between the solution and air are affected by the inner diameter, thus implicitly affecting the critical voltage necessary for initiation of electrospinning[120]. Different studies have proposed different spinneret designs. The majority of applications employ a simple hypodermic needle with blunted tip to create a flat aperture. Custom-built spinnerets are provided with electrospinning units available on the market and some of them possess an in-built heating component to permit the spinning of high temperature solutions or melts. For instance, various different spinneret tips are manufactured for the electrospinners offered on the market, including a heating spinneret and the alternative of remote (tube-fed) and local (syringe in place) spinneret. Meanwhile, the development of core-shell copolymer fibres and hollow fibres is widely undertaken with the spinneret designs of co-axial spinneret systems[121]. The creation of these two types of fibres involves insertion of a polymer solution within the centre of a stream of a different solution based on a dual funnel design. Dissolution of the middle polymer reveals the shell, thus achieving hollow fibres.

1.2.2.6. The impact of polymer concentration and solution viscosity

The charged jet uniaxial stretching underpins the process of electrospinning and is massively impacted by modifications in the polymeric solution concentration. To give an example, the intertwined polymer chains fragment prior to arriving at the collector owing to the applied electric field and surface tension under conditions of low concentration of polymeric solution[122]. In turn, the fragments induce beads or beaded nanofibers to develop. Viscosity is increased when the polymeric solution concentration is augmented, and in turn, makes the polymer chains even more intertwined, thus being able to surpass the surface tension and eventually giving rise to homogeneous electrospun nanofibers without beads. Moreover, when the concentration exceeds the concentration of development of homogeneous nanofibers without beads, known as the critical value, the solution flow through the tip of the needle is obstructed due to the drying of the polymer solution at the metallic needle tip, thus causing blockage. Consequently, faulty nanofibers with beads develop[123]. Additionally, changes in the solution viscosity cause the bead morphologies to alter in shape from a spherical shape resembling a droplet, in the case of solutions with low viscosity, to an elongated droplet or ellipse and smooth fibres, in the case of solutions with adequate viscosity[124].

1.2.2.7. The impact of solution conductivity

Besides impacting the development of the Taylor cone, solution conductivity contributes to modulation of nanofiber diameter as well. When a solution is poorly conductive, no electrospinning will occur because the droplet surface lacks the charge needed for the development of a Taylor cone. By contrast, when solution conductivity is elevated to a critical value, the droplet surface charge will increase, leading to Taylor cone formation, whilst the diameter of nanofiber will diminish[125]. However, the Taylor cone will not develop and electrospinning will not occur when conductivity exceeds a critical value. The whole process of electrospinning must be considered to elucidate this phenomenon. The Coulomb force between the fluid surface charge and the force generated by the external electric field determines the electrospinning process. On the other hand, the electrostatic force associated with the surface charges generated by the applied external electric field (this electrostatic force is triggered by the field element tangential to the fluid surface) is the main determinant of Taylor cone development. An ideal dielectric polymer solution cannot migrate on the fluid surface because it lacks sufficient charges in the solution, and as a result, Taylor cone will not develop and electrospinning will not occur as the applied electric field will not be able to produce an appropriate electrostatic force. Nevertheless, migration on the fluid surface is possible in the case of a polymer solution with conductivity, which has enough free charges, thus leading to development of a Taylor cone and electrospinning activation[126].

1.2.2.8. Surface tension

Surface tension can be altered by adding a surfactant[127]. Bead formation can also be increased due to high surface tension[128]. The beads have a high volume. Thus, bead formation becomes an undesirable phenomenon leading to a decrease in the surface area and surface energy of the nanofibres, which opposes the aim of the electrospinning process[129]. Yang et al. studied the effect of the surface tension on the morphology of the nanofibres with poly(vinylpyrrolidone) (PVP) and using DMF, ethanol and DCM as solvents. They found that using different solvents can affect the formation of beads. The results were attributed to the reduction of the surface tension when using different solvents[130].

1.2.2.9. The implications of solvent choice

Polymer solubilisation and conversion into nanofibres via electrospinning are directly dependent on solvent selection, which needs to take into account how soluble the polymer is in a particular solvent and how volatile the solvent is, as reflected in its boiling point. Solvents demonstrating volatility are usually deemed most suitable because they have a reduced boiling point and evaporate rapidly, thus being able to help nanofibres dehydrate quicker over the distance between capillary tip and collector surface. On the other hand, solvents with extreme volatility and minimal boiling points are not a good option because of the possibility of evaporation at the capillary tip and consequently the polymer solution flow rate may become blocked. Meanwhile, flat nanofibre morphologies resembling ribbons or nanofibre conglutination at boundaries may occur in the case of solvents with high boiling points as their dehydration may not finish before the collector is reached[131]. The movement of the jet through the atmosphere in the direction of the collector, which depends on solvent volatility and impacts the porosity of developed nanofibres, leads to phase separation at the interface between liquid and air[110]. Using a combination of two solvents with distinct boiling points can help to attain the intended porosity and topography of the nanofibres.

1.2.2.10. Choice of polymers

The choice of polymer depends on the application and properties of the polymer. For example, increasing the molecular weight of the polymer can cause an elevation in the viscosity of the solution[132]. Koski and his group studied the influence of changing the molecular weight on the nanofibres' formation[132]. They found that reducing the molecular weight and keeping the concentration constant can lead to an increase in the possibility of bead formation, whereas elevating the molecular weight can create smooth nanofibres. However, further increasing of the molecular weight can lead to the formation of a micro-ribbon shape and sometimes patterned fibres with a very high molecular weight[133].

1.2.2.11. The impact of environmental factors

Recent evidence suggests that nanofiber diameter and morphology depend not only on electrospinning and solution factors, but also on environmental factors, especially relative humidity and temperature[134]. The charged jet solidifies according to humidity, which therefore can alter the diameter of nanofibers. The chemical character of the polymer has an influence over this entire phenomenon. In a study by Pelipenko and colleagues, PVA, PEO and their blend solution PVA/hyaluronic acid (HA), PEO/(chitosan (CS)) were employed to investigate how humidity fluctuations impact nanofiber diameter. It was observed that, as humidity rose from 4% to 60%, the nanofiber diameter experienced a reduction from 667 nm to 161 nm and from 252 nm to 75 nm, in the case of PVA and PEO, respectively. The reduction in nanofiber diameter was even more pronounced in the case of the blend, decreasing from 231 nm to 46 nm for both PVA/HA and PEO/CS, as the humidity was increased from 4% to 50%. When the humidity was increased even more, separate polymers acquired bead fibre and the blends lacked electrospinning almost entirely[135].

1.2.3. Medical applications of Electrospinning

1.2.3.1. Wound dressing

Generally the properties of an ideal wound dressing are the ability to enhance the healing of the wound by working as a barrier against bacteria, the ability to absorb the exudates from the wounds and the ability to allow gas exchange[136]. Loading drugs in the system can also enhance the effectiveness of the wound healing and can be used as electrospin scaffolds for wound dressing, which have some important advantages, such as the porosity of the surface, a nanofibrous scale and a large surface area, that can improve the efficiency of the system[137]. Moreover, different antibiotics and antifungals, such as cefazolin and itraconazole, were evaluated and produced for the electrospinning wound dressing to treat or prevent the local infections [138]. Thakur et al. used the electrospinning to create a dual drug release for the wound dressing. The author used the single and dual spinneret to electrospin two different PLLA solutions with lodocain and another solution with mupirocin. They were collected together to form a dual drug release system for wound dressing. In the dual spinneret, the lidocain was released immediately from the system to reduce the pain with a sustained release profile of the mupirocin, which was used to inhibit the growth of staphylococcus aureus for several days[139].

1.2.3.2. Abdominal laparotomy

Electrospinning of the sheet structure can be used as a physical barrier for post-surgical adhesion, which can help to prevent abdominal complications that occur after surgery. The main criteria of the electrospinning sheet that can be used in such cases should be biodegradable, stable at the site of surgery, anti-adhesive and be able to be loaded with suitable drugs[140]. In 2007, ornidazole was successfully electrospun with PCL, and the results showed a decrease in the post-surgical adhesion, while the matrices without the drug did not show an effect[140]. In addition, the electrospinning matrices were also introduced to increase and prevent the infections after abdominal laparotomy, which was applied to minimise the complications of trauma[141]. Hong et al. loaded antibiotic tetracycline with PLGA and then blended poly(ester urethane) urea (PEUU) with tet-PLGA to form an elastic composite sheet. The composite was implanted on the rat abdominal wall; the composite demonstrates a significant decreasing in the abscess of the rat abdomen. The shrinkage limitation of the PLGA matrices was overcome by using PEUU and electrospinning with PLGA [141].

1.2.3.3. Delivery of chemotherapeutics

Electrospinning matrices have another application in the field of post-surgical chemotherapy. For instance, the sustained release of the chemotherapies from electrospun matrices can enhance the median survival duration after the resection of the tumour cells, such as malignant glioma, compared to traditional methods[142]. An animal study showed a significant reduction in the growth of the brain tumour when using paclitaxel electrospun matrices. For example, Sudhir et al. electrospun paclitaxel with PLGA to produce a sustain release system for post-surgical glioma. An apoptosis study showed the advantage of using paclitaxel electrospun matrices compared to taxol.

1.2.3.4. Controlled release

In the context of medical therapy, medication delivery can be successfully achieved via controlled release, which ensures balanced delivery kinetics, diminishes toxic effects and side-effects, and makes the process more convenient to the patients[143]. The procedure of controlled release involves loading of the active substance into a carrier or device and releasing it at an expected rate *in vivo* during oral or subcutaneous administration. Electrospun nanofibers present numerous benefits as possible drug delivery carriers. For instance, electrospinning facilitates drug loading without affecting drug activity due to the high applied voltage. Furthermore, compared to bulk material, such as film, the release rate of nanofiber drug systems is higher, owing to the high specific surface area and short length of diffusion passage. Moreover, regulation of nanofibers in terms of morphology, porosity and content permits effective control of the release profile. Polymers demonstrating biodegradability, including PLA[144], PCL[145], poly(D-lactide)[116], PLLA[146], PLGA[147], and hydrophilic polymers, including PVA[148], PEG[149] and PEO[150], are the major sources of nanofibers used in drug release systems. In addition, research has focused on model drugs such as drugs with good water solubility[151], poor water solubility[152], and without water solubility[153], while examinations of the release of macro-molecules, including DNA[147]and proteins with bioactivity[154], from nanofibers have been conducted as well.

1.2.3.5. Clinical applications

The original application of collagen nanofibers was for the purposes of determining whether the culturing of smooth muscle cells was feasible[155]. The procedure involved stimulation of cell development on the collagen nanofibers, followed by integration of the cells in the nanofiber network after a week of seeding. Good attachment and proliferation were exhibited by smooth muscle cells on nanofiber membranes derived from other polymers via electrospinning, including poly (ethylene-co-vinyl alcohol)[156], poly(ester urethane) urea (PEUU)/collagen blend[157], poly(L-lactide-co-ε-caprolactone) (PLLA-CL)[158], PCL/ collagen[159]. In addition to making fibres more elastic and enhancing their tensile strength, the collagen integrated in nanofibers also helped cells to adhere better[159]. Furthermore, cell adhesion was noted to be affected by the hydrophobicity of the surface of fibres and considerable increase in fibre wettability occurred as a result of surface treatment of PS nanofibers with argon plasma, doubling the rate of cell adhesion[160].

Ample research has been focused on PCL nanofibers for the purposes of bone tissue engineering[161]. Studies reported that, after seven days of seeding, the PCL matrix was permeated by mesenchymal stem cells (MSCs) alongside plentiful extracellular matrix, while after one month, mineralisation and production of type I collagen happened. In the context of an *in vivo* experiment, a four-week PCL construct cultured from MSCs was introduced in rat omenta[162], preserving the shape and size of the initial scaffold and resembling bone after one month. In addition, bone scaffolding has also been attempted based on other polymer nanofibers, such as polyester urethanes (PEU)[163], polyphosphazenes[164], poly(lactic acid) (PLA), PLLA containing montmorillonite (MMT) nanoplatelets[165], silicate fibres[166] and poly(propylene carbonate)[167].

The location and function of blood vessels determine their size, mechanical and biochemical attributes, cellular composition and ultra-structure. Therefore, engineered vascular grafts must demonstrate the intended features. In this regard, particular difficulties are posed by substitution of blood vessels, especially vessels with a diameter of less than 6 mm[168].

Research has been conducted to determine whether vascular endothelial cells (ECs) could be cultured on electrospun nanofiber mats. One study compared cell development on electrospun PLLA nanofibers and cast smooth PLLA film and reported that vascular ECs exhibited improved function on the smooth PLLA film but not on the electrospun nanofiber mat[169]. Therefore, an effective three-dimensional scaffold for blood vessel tissue engineering could be attained through integration of smooth film and electrospun nanofiber mat, as the latter can promote the development of vascular smooth muscle cells[158].

According to the findings of an *in vitro* study of neural stem cells cultured on a scaffold made of PLLA nanofibers, the scaffold helped NSCs to differentiate and encouraged neurite outgrowth and NSC attachment[170]. Furthermore, another study that employed aligned PLLA nanofiber or microfiber scaffolds reported that, although orientation was not markedly altered in terms of fibre diameter, NSC lengthening and neurite outgrowth directions were parallel to the fibre alignment direction[171]. Moreover, *in vitro* research was also conducted to investigate how Schwann cells responded to a range of categories of polymer nanofibers, including poly(3-hydroxybutyrate) (PHB), PHBV, PCL, PLLA and chitosan, alongside their solution-cast films[172].

1.3. Project aims

Elastomeric scaffolds play an important role in the field of soft tissue engineering, and recently studies of these scaffolds for different medical applications have been increasing rapidly. This literature review focuses on synthetic biodegradable elastomers and electrospinning techniques.

The degradation rate of PGS biomaterials is generally fast and can cause cytotoxicity due to acidic degradation by-products. Therefore, hindering their utilisation as scaffolds for tissue engineering. Moreover, APS pre-polymer has poor solubility in most organic solvents, restricting its fabrication.

In this project, we hypothesise that nontoxic monomers, sebacic acid and serinol, can be used to produce a new biodegradable polyester amide elastomers with controllable mechanical and biodegradation properties, to be used in different soft tissue engineering applications, which can be synthesised under mild conditions without using cross-linking reagents or toxic catalysts. In the first step towards testing the hypothesis, it is necessary to characterise the chemical structure, mechanical properties, and biodegradation profile of these materials to support fibroblast attachment and proliferation.

The objectives of this research project are:

- to develop a new polyester amide biodegradable material to overcome the disadvantages of currently available materials, and extend the properties of biodegradable elastomers to allow for broader use in soft tissue engineering applications;
- to fabricate an elastic, porous scaffold from the newly developed polyester amide biomaterial using electrospinning techniques for utilisation as an elastomeric scaffold to support the growth of cells; and
- to study the correlation between PCL rheology and fibre structure alignment, and investigate the applicability of the newly developed polyester amide biomaterial as a coating to enhance the hydrophilicity of PCL-aligned scaffolds.

2. Chapter two

Synthesis and Characterization of Biodegradable Elastomeric Polyester Amide for Soft Tissue Engineering Applications

2.1.Introduction

The primary objective of tissue engineering is the development of biological substitutes for the restoration or replacement of damaged tissues and organs[173]. To meet the demands of different types of tissues and organs[174], there is a need for developing more materials that are functionally suitable and for devising different fabrication techniques. These medical demands have inspired many researchers to attempt to modify existing natural and synthetic materials or to produce novel synthetic biomaterials, with diverse properties, for multiple tissue engineering applications[35,97,175–178].

Natural biodegradable materials, such as collagens, have been widely investigated, in various forms of scaffolds and hydrogels, for cellular attachment, proliferation and differentiation for soft tissue engineering[179,180]. Similarly, materials such as elastin, fibrin, gelatine and alginate have also been extensively employed for an array of tissue engineering applications including heart muscles[181], ligaments[182], cartilage[183] and blood vessels[184]. Although natural elastomers confer advantageous properties, such as biocompatibility and biodegradability, they also might cause disease transmissions upon implantation and are subject to difficulties in relation to extraction processes and regulatory issues[36,185]. Conversely, synthetic biodegradable thermoplastic polymers, such as PCL, PLA, PGA, polyurethanes and their copolymers, are the most widely investigated family of biodegradable materials, presenting tuneable chemical and mechanical properties suitable for soft tissue regeneration[37,171,186–189]. Nevertheless, this polymer class has demonstrated undesirable heterogeneous degradation behaviour and non-linear loss of mechanical properties due to the presence of structure-encompassed crystalline segments that could cause mechanical failure of the scaffold prior to completion of the tissue regeneration process[190]. Moreover, most of these thermoplastic polymers have a high modulus and undergo plastic deformation. Therefore, these polymers poorly withstand different dynamic environments subsequent to implantation inside the body[191,192].

Such shortcomings shape the motivation of researchers in regard to developing synthetic biodegradable elastomers for employment in a range of tissue engineering applications. For instance, biodegradable elastomers, based on polyester linkage, such as PGS[81], have been developed and used as elastomeric scaffolds for various biomedical applications[193–195]. However, these still present specific drawbacks such as cytotoxicity due to the acidic by-products of these elastomeric polyesters and rapid degradation by hydrolysis upon implantation[88,196]. The APS elastomer belongs to the class of poly(ester amide), and was

developed to enhance the PGS degradation profile[97,197]. The APS elastomer has previously been investigated for tissue engineering applications[198] due to its biocompatibility[97,197]; however, APS is only soluble in hexafluoroisopropyl alcohol (HFIP) and has poor solubility in most commonly used polar and nonpolar solvents, restricting its fabrication processes[36,199] and limiting the chemical characterisation and structural modification of the APS pre-polymer. Consequently, it would prove worthwhile to develop an alternative biodegradable poly(ester amide) elastomer with expanded chemical and physical properties.

Amino-1,3-propanediol (serinol) is a non-toxic amino alcohol that is a structural analogue of the amino acid serine. Serinol is biocompatible[200,201], inexpensive and has been widely applied in medicine[202,203], tissue engineering applications and surface functionalization[204–206]. Sebacic acid is a natural metabolite of fatty acids[207,208] and has been studied in diverse applications of tissue engineering[34,209].

For the purposes of this chapter, a synthetic, biodegradable and elastic poly(ester amide) polymer based on serinol and sebacic acid was synthesised and termed poly(serinol sebacate) (PSS). I hypothesise that the trifunctional monomer with amine and hydroxyl groups is important for the formation of amide and ester bonds, as well as enabling the polymerisation of crosslinked chains with tuneable chemical, mechanical and biodegradation properties; hence, broadening the properties of available biodegradable polymers for tissue engineering applications. Herein, I report the synthesis and characterisations of equal molar ratios of serinol and sebacic acid with varying curing durations.

2.2. Materials and methods

2.2.1. Materials

Sebacic acid (99.5%), serinol (98%), deuterated dimethylsulfoxide-d_6 (DMSO-d_6), hexafluoroisopropanol (HFIP, 99.5%) and trypsin EDTA solution were purchased from Sigma Aldrich, UK. Reagent grade dimethylformamide (DMF, 99.8%), tetrahydrofuran (THF, 99.6%), dimethyl sulfoxide (DMSO, 99%), acetone (99.7%), methanol (99.8%), chloroform (99.6%), dichloromethane (DCM, 99.6%), ethyl acetate (99.8%) and resazurin sodium salt (Prestoblue®) were purchased from Fisher scientific and used without further purification. Dulbecco's Modified Eagle's Medium (DMEM) media (Gibco Life Technologies, UK), (1% v/v) L-glutamine, 1% antibiotic (penicillin/streptomycin) and (10% v/v) fetal calf serum (FCS) were purchased from Thermo Fisher Scientific, UK.

2.2.2. Synthesis of poly(serinol sebacate) and film fabrication

PSS was synthesised in two steps. (1) A polycondensation reaction between serinol and sebacic acid for which equal molar ratios of sebacic acid and serinol were placed in a 100 ml three-neck round bottom flask. The mixture was heated to 130ºC under a flow of nitrogen gas (~120 cm^3\min) with continuous stirring until the sebacic acid was melted. The temperature was then maintained at 110˚C and the contents were allowed to react for 22 hours. (2) PSS films were prepared by dissolving the viscous PSS pre-polymer in methanol (50% w/v) and pipetting in a fume hood and then thermally cured in a vacuum oven at 110 ºC for 24 hours 48 hours and 72 hours. The produced samples were coded as PSS-24, PSS-48 and PSS-72 respectively. Afterwards, the samples were incubated in methanol for 12 h and washed with dH_2O to remove sol part from the cured polymers.

2.2.3. Gelation point and solubility test

The gelation point was defined by the stage at which mechanical stirring became difficult and the polymer no longer dissolved in methanol. Pre-polymer samples were collected for chemical characterisation. The solubility of the pre-polymer PSS (25 mg) in H_2O and different organic solvents (1 ml) at room temperature was visually evaluated.

2.2.4. Chemical characterization

The chemical structures of PSS polymers were characterised by different chemical methods. Molecular weight analysis was performed using a PL50 Polymer Laboratories system in combination with a refractive index detector, using two mixed bed columns at 50^{o} C, DMF and 0.1% LiCl as the mobile phase, with a flow rate of 1 mL min^{-1}. Poly(methyl methacrylate) standards were used for the calibration.

The chemical composition of the crosslinked PSS was also analysed using Fourier Transform Infrared (FTIR) spectroscopy. The FTIR spectra were recorded using a Thermo Scientific Nicolet IR 200 FT-IR spectrometer over the range of 700–4000 cm^{-1} and the results were analysed using Omnic 8.0 software (Thermo). An analysis of spectral images was conducted via correlation with a comparison spectral image that was selected as a reference due to its recurring appearances on the chemical map.

The ^{1}H (100 MHz) and ^{13}C NMR (400 MHz) spectra of the PSS pre-polymer were recorded on a Bruker Avance 400 spectrometer at 25^{o} C using a relaxation delay of 1 s. The pre-polymer samples were dissolved in deuterated DMSO and then placed in the NMR tubes of 5 mm diameter. The chemical shifts were analysed relative to the peak of the solvent as a secondary standard. NMR spectral data were analysed using MestReNova version 7.0.3-8830 from Mestrelab Research S.L. (MestReNova Manual). ^{1}H NMR (400 MHz, DMSO-d_6 q): 7.45, 7.68, 7.90 (N*H*CO), 3.70-4.22 (group, C(C*H*$_2$O)$_n$ –(CH2OH)3-n), 3.40 (C(CH$_2$O)$_n$(C*H*$_2$OH)$_{3-n}$), 227 (OCOC*H*$_2$(CH$_2$)$_7$-CONH),2.19,2.07 (OCO(CH$_2$)$_7$C*H*$_2$CONH), 1.51, 1.48(OCOCH$_2$C*H*$_2$(CH$_2$)$_4$C*H*$_2$CH$_2$CONH and CC*H*$_2$CH$_3$), 1.24 (OCO(CH$_2$)$_2$(C*H*$_2$)$_4$(CH$_2$)$_2$CONH). ^{13}C NMR (400 MHz, DMSO-d_6): 175.05 (*CO*OH), 173.24, 173.09 (NH*CO*), 172.77, 172.64, 172.60 (CH$_2$O*CO*), 53.22, 50.02, 47.07 (*C*(CH$_2$OCO)$_n$(CH$_2$OH)$_{3-n}$), 63.37, 62.94, 60.81, 60.72 (C(*C*H$_2$OCO)$_n$(*C*H$_2$OH)$_{3-n}$), 35.91, 35.88, 34.31, 33.95, 33.85, 25.79, 25.03, 24.87 (OCO*C*H$_2$(CH$_2$)$_6$CH$_2$CONH), 29.23, 29.16, 29.09, 28.92 (OCOCH$_2$(*C*H$_2$)$_6$CH$_2$CONH). The samples were dissolved in DMSO-d_6.

2.2.5. Thermal characterization

Glass transition temperature (T_g) was determined by differential scanning calorimetry (DSC) (TA Instruments, USA). All samples were scanned twice at temperatures between −40° C and 150° C. The first scan started at −40° C, followed by heating to 150° C at a rate of 10° C/min. The samples were then cooled from 150° C to −40° C at rate of 100° C/min. The samples were then subjected to a second heating cycle that was identical to the first cycle. The T_g was determined from the heating second cycle (step change). All measurements were performed using aluminium pans with lids (TA Instruments, Belgium) under a nitrogen atmosphere and the data of the second heated scans were analysed using TA universal analysis software.

2.2.6. Mechanical properties

Tensile properties of the PSS were measured using Instron 5969, following the ASTM standard D412-06a, equipped with a 50 N load cell and the cross-head speed of 10 mm/min was used. The crosslinked PSS (n = 3) were cut into a dog-bone shape with dimensions of 1.5 mm(T) × 7 mm(W) × 30 mm(L). The samples were stretched at a constant speed of 10 mm/min till failure. The strain was calculated from the displacement ($(L-L_0)/L_0 \diagup 100$)), where L_o and L were the initial and final length of the specimen. The stress was calculated by dividing the applied force by the cross-section area. The obtained stress–strain curves were used to determine the ultimate tensile strength, Young's modulus and elongation at break. Tensile strength was considered as the highest stress at sample failure and Young's modulus was determined as the gradient of the initial linear section in stress-strain curve (between 0.05% and 0.25% of strain). Elongation to break was determined as the percentage of strain at failure of the specimen.

2.2.7. Crosslinking density

The crosslinking densities of the cured samples were calculated by using the theory of rubber elasticity equation (1)[210],where R is the universal gas constant, T is the absolute temperature and E is the Young's modulus (Pa):

$$Crosslinking\ density\ \left(\frac{mol}{m^3}\right) = \frac{E}{3\ R\ T} \qquad (Eq.1)$$

2.2.8. Hydration properties

Hydration properties of PSS samples were determined by swelling study and contact angle analysis. The sessile drop technique was adopted to undertake the measurement of the WCA of homogeneous samples via a Cam200 instrument (KSV Instruments). The software of the instrument is based on the fitting of the Young-Lapace equation. For the purposes of this measurement, deionised water was employed. The procedure involved placing the droplet on the surface and taking 20 images of it (0.5 second interval) and the first two measurements were eliminated for all samples. The baseline was established by hand and determination of the contact angle was undertaken for every image. The plotting of the values was performed in relation to time (t) and the actual WCA was computed via linear regression. The swelling percentage was analysed by measuring the differential weight before (W_{dry}) and after hydration (W_{hyd}). The crosslinked PSS samples, with size of around (10 mm × 10 mm) (n = 3), were incubated with phosphate buffered saline (PBS) at 37º C in a bath shaker (25 RPM) and methanol. Samples were removed from the solution at regular time intervals and vacuum dried for 5 min to remove the water from the surface. The thickness of the samples was measured using digital callipers, and the weight of the samples was measured using the digital lab scale and recorded at different time points until equilibrium was reached. The swelling degree was calculated using the following equation:

$$Swelling\ (\%) = \frac{(w_{hyd} - w_{dry})}{w_{hyd}}\ x\ 100 \qquad (Eq.2)$$

2.2.9. Uncured monomers

For measuring the amount of uncured monomers, the samples measuring ($8 \times 7 \times 1$ mm^3) (n = 3) weighed as W_1, were placed in methanol for 24 h to remove the sols in the cured polymers, then dried in a vacuum oven and weighed as W_2. The uncured monomers was calculated using equation 3:

$$uncured\ monomers\ (\%) = \frac{(w_1 - w_2)}{w_1}\ x\ 100 \qquad (Eq.3)$$

2.2.10. In vitro degradation studies

The degradation rate of PSS was conducted by incubating samples ($15 \times 15 \times 1$ mm^3) (n = 3) in phosphate-buffered saline (PBS) at 37°C and under accelerated condition (in an oven at 60^{o}C) for 14 days. Initial weight (W_i) was recorded and the samples were then soaked in 10 ml of PBS and placed in a shaking incubator at 70 rpm. At every time point, the samples were removed from PBS, washed with dH_2O to remove salts deposited by the PBS, dried and weighed again (W_d). The pH of retrieved PBS solution was measured at each degradation time point and then fresh PBS was added to the samples. The percentage of weight loss W_{loss} was determined using equation (4).

$$weight\ loss\ (W_{loss}\ \%) = \frac{(w_i - w_d)}{w_i}\ x\ 100 \qquad (Eq.4)$$

The morphology of the PSS-24 sample surface before and after degradation was evaluated by using a scanning electron microscope (SEM) (JSM-6060LV). A gold coater (Leica EM SCD005) was used to apply a thin gold layer to the samples. The coater was operated at 10 mA for 300 seconds and the SEM micrographs of the PSS specimens were captured at accelerated voltage of 10 kV.

2.2.11. *In vitro* cytocompatibility

The cytocompatibility of PSS was evaluated by studying the proliferation of mouse fibroblast cells on the sample surface. First, circular samples of PSS were washed with a large amount of dH_2O and sterilised by UV radiation for 30 min before the study. Next, the 3T3 mouse fibroblast cells were cultured in DMEM, supplemented with 1% (penicillin/streptomycin) and 10% FCS and incubated with 5% CO_2 at 37° C. Cells were detached using trypsin, counted and centrifuged 180×g for 5 min. The PSS samples were placed into a 24-well plate (non-tissue culture plate, Falcon, USA) and washed with DMEM for 24 h. The PSS samples were sterilised through exposure to UV light (280 nm) for 30 minutes and seeded with a cell density of 10×10^4 cells/sample, and incubated with 5% CO_2 at 37° C in a humidified tissue-culture incubator.

Cell viability was assessed using a live/dead assay (Life technologies, USA). The live/dead solution was prepared by adding calcein (0.5 µl/ml) and ethidium homodimer (2 µl/ml) to sterile PBS. After 5 days, the culture medium was removed and the PSS samples were washed with PBS. Afterwards, 1 ml of live/dead staining solution was added to the PSS samples and incubated at room temperature for 30 min. The samples were then washed with PBS three times then imaged using a fluorescence microscope (Nikon SMZ1500, Japan). The cell growth and attachment were observed and photographed using a digital camera attached to the inverted Nikon Eclipsa microscope (TS100, Japan).

Proliferation rates of the cells at day 1, 3 and 5 were assessed using PrestoBlue® cell proliferation assay. The culture medium was removed from the PSS samples (n = 3) and washed with sterile PBS. The samples were then treated with 10% PrestoBlue® reagent in culture medium and incubated for 120 min at 5% CO_2, 37°C in the dark. 100-µL Aliquots of the PrestoBlue®/media reagent were collected into a 96 well plate (Flat Bottom Black, Coaster, US). Thearafter, fluorescence intensities were measured using a Tecan microplate reader (Tecan, Reading, UK) at excitation/emission wavelengths of 560/590 nm. Acellular PSS samples were incubated with PrestoBlue® solution (10%) for blank correction. A standard curve was used to correlate cell number with the fluorescence intensity.

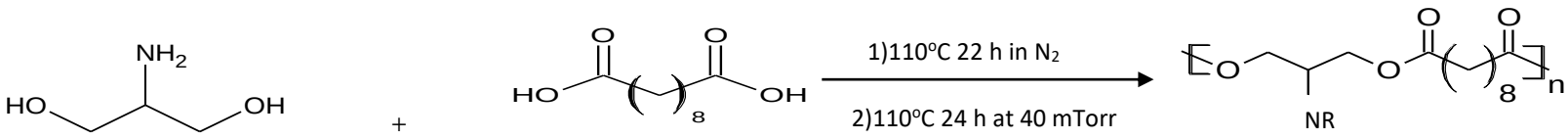
2.2.12. Statistics

All obtained results were reported as mean ± standard deviation (SD), and statistical analysis was carried out by one-way analysis of variance (ANOVA) with Tukey's post-hoc analysis using GraphPad Prism software (v. 6). The data were considered to be significantly different if p-value becomes less than 0.05.

2.3. Results and Discussion

2.3.1. Synthesis optimization and solubility of PSS

PSS pre-polymers were synthesised using a thermal polycondensation reaction (Scheme 2.1). Results revealed the optimal reaction duration for obtaining the soluble pre-polymer to be 22 hours, yielding a yellowish and adhesive product at room temperature. The adhesive was a product of the remaining amine and hydroxyl groups in the PSS pre-polymer. The reaction temperature was adjusted to a temperature between 100^{o}C and 140^{o}C to evaporate the water formed from the polycondensation reaction and prevent a potential etherifying reaction between hydroxyl groups. The solubility of the PSS pre-polymer was evaluated at room temperature and results showed that the pre-polymer was completely dissolved in a wide range of organic solvents, such as DMF, DMSO, methanol, propanol and HFIP, indicating an absence of significant crosslinking between polymer chains during the thermal polycondensation reaction (Table 2.1). The synthesised PSS pre-polymer was subsequently thermally cured in a vacuum oven for 24, 48 and 72 hours at 100^{o}C and fabricated into elastomer sheets (~ 1.5 mm thickness). The cured PSS24 sheet can be subjected to deformation without fracturing the structure (figure 2.1), confirming the success of the thermal curing process (Table 2.1).



Serinol Sebacic acid Poly (serinol sebacate)

Scheme 2.1: Synthesis of PSS elastomers. (1) PSS pre-polymer was synthesised by polycondensation of serinol and sebacic acid under a stream of nitrogen gas with continued stirring. (2) Pre-polymers were cured at 110 °C (40 mTorr) for 24 h 48 h and 72 h. (R = H_2, amide bond)

Table 2.1 Solubility data of PSS pre-polymer and thermally cured samples of PSS in dH_2O and different organic solvents (1 ml) at room temperature

Sample	dH_2O	Methanol	THF	DMF	DMSO	HFIP	Ethyl acetate	propanol	$CHCL_3$
PSS (pre-polymer)	-	+	±	+	+	+	-	+	±
PSS-24	-	-	-	-	-	-	-	-	-
PSS-48	-	-	-	-	-	-	-	-	-
PSS-72	-	-	-	-	-	-	-	-	-

+, Soluble; ±, partially soluble; -, insoluble

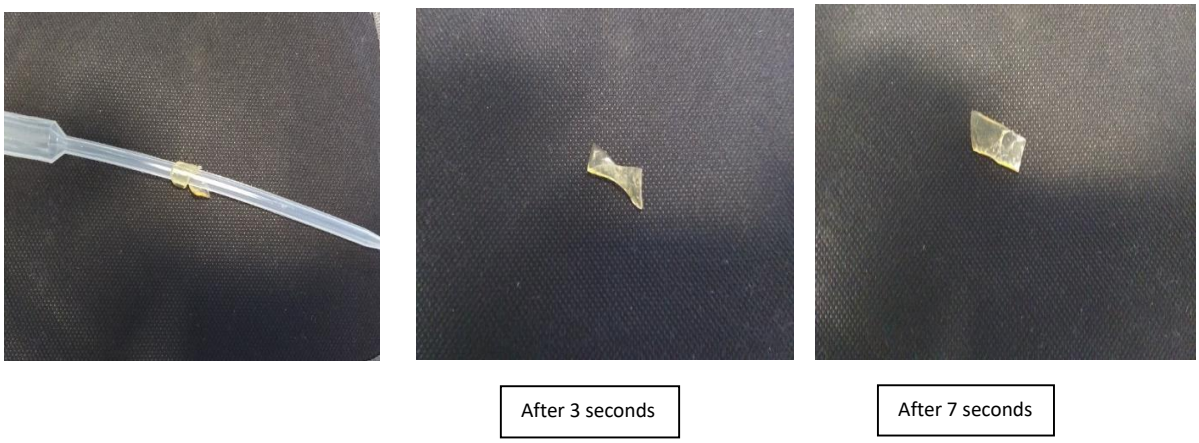


Figure 2.1: The cured PSS24 sheet can be subjected to deformation without fracturing the structure and return to its original shape after 7 seconds.

2.3.2. Chemical characterization

Pre-polymer of PSS (sebacic acid: serinol, molar ratio of 1:1) was synthesised under optimal conditions and subjected to chemical characterisation by ^{1}H, ^{14}C NMR and FTIR spectroscopy. Serinol possesses two hydroxyls and one amide group which each have different reactivity toward amidation and esterification reactions. The main three structures expected from amidation and esterification with sebacic acid are illustrated in Figure 2.2(a). They include monoamide with the terminal unit labelled T, monoamide ester with the linear unit labelled L, and monoamide diester with the dendritic unit labelled D.

Figure 2.2(b) showed the ^{1}H NMR spectrum of PSS pre-polymer using DMSO-d_6 as the deuterated solvent. DMSO-d6 was chosen because the PSS pre-polymer has good solubility in DMSO compared to $CHCL_3$ and NMR signals are solvent dependent[211]. The three signal peaks a, b, c, at 1.25, 1.5 and 2.04-2.3 ppm, respectively, were ascribed to the proton of sebacic acid methylene groups in the polymer backbone, while the three groups of peaks (7.45, 7.66, 7.89 ppm) were attributed to several structure units of the branch groups (linear, terminal, dendritic) in the pre-polymer chain, indicating a successful reaction of amide formation between the amine group and sebacic acid. The peaks at 3.8-4.2 ppm, corresponding to protons adjacent to ester bonds, confirmed the reaction between hydroxyls groups and sebacic acid and the formation of ester bonds. The assignment presented in Figure 2.2(b) is based on integral ratios and chemical shifts and are in agreement with data presented by Xiuru et al.[212] regarding a reaction of multihydroxyl primary amines with dicarboxylic acids.

The molar ratios of pre-polymers of serinol and sebacic acid were calculated from ^{1}H NMR data by comparing the amount of methylene hydrogen within serinol and sebacic acid. The actual mole percent and the comparisons matched with the theoretical ratio, indicating good control over the synthesis process (Table 2.2). The amine group was more prone to reacting with carboxyl groups in sebacic acid. The amine groups were mostly consumed during the pre-polymerisation step and the reaction between hydroxyl groups and carboxyl groups took place to crosslink the PSS chain.

To obtain further confirmation of the result from the ^{1}H NMR spectra, a ^{13}C analysis was performed. The ^{13}C NMR spectrum of PSS pre-polymer, after 22 hours of reaction time, is given in Figure 2.3(b). The chemical shift values for the amide, ester and acid carbonyl are 172.6, 173.25 and 175 ppm, respectively. The split of the amide and ester carbonyl, into

different patterns, likely originated from the substitution of serinol and different sebacic acid structures possible during the reaction. The methylene resonances of sebacic acid are located between 24.8 and 36 ppm and shifted with the substitution. Figure 2.3(b) shows the resonances of serinol methylene and methine carbons. The abundance of the T species is large, which is expected due to amine groups high reactivity to amidation. The chemical shift assignments of the serinol carbons, for the three different species in Figure 2.3(b), are consistent with studies by Rickerby[200] about the dicarboxylic ester amide of serinol.

The FT-IR spectrum of the PSS pre-polymer and cured PSS are illustrated in Figure 2.4. The data revealed further indications of successful completion of the PSS synthesis. The spectrum provided evidence for the functional groups and chemical structure, displaying characteristic carbonyl stretching vibration at 1722-1745 cm^{-1} and the formation of ester bonds between serinol and sebacic acid, while amide carbonyl absorption at 1640-1655 cm^{-1} indicated a reaction of the serinol amine group with sebacic acid in the pre-polymer chain. The vibration of N-H at 1551-1562 cm^{-1} and the band in the range of 3200–3500 cm^{-1} represents the stretching of hydroxyl groups. The band at 3295 cm^{-1} is specific to amide linkage N–H stretching vibrations. During the curing process of PSS, the disappearance of amine absorption at 1610 cm^{-1} indicated that the reaction of amine groups with sebacic acid was complete. In addition, there was an increase in the ester carbonyl peak intensity, while amide carbonyl intensity showed little change during the curing process (Figure 2.4), due to the lower reactivity of hydroxyl groups. Therefore, these results showed the formation of new ester bonds during the curing process, as previously reported[97,213]. Altogether, NMR and FTIR results revealed successful synthesis of the PSS polymer. The PSS pre-polymer had a molecular weight (M_w) of 6670 Da, a number-average molecular weight (M_n) of 5525 Da and polydispersity index (PDI) of 1.21. DMF was chosen in measuring the molecular weight study due to a solubility issue when using THF as the eluent.

Table 2.2: **Theoretical and experimental molar ratios of PSS pre-polymer. In ^{1}H NMR spectrum, the peak from hydroxyl groups overlap with that of H_2O at 3.2-3.5 ppm, which had been eliminated.**

sample	Theoretical molar ratio	Obtained ratio from NMR
PSS pre-polymer	1:1	1:0.928

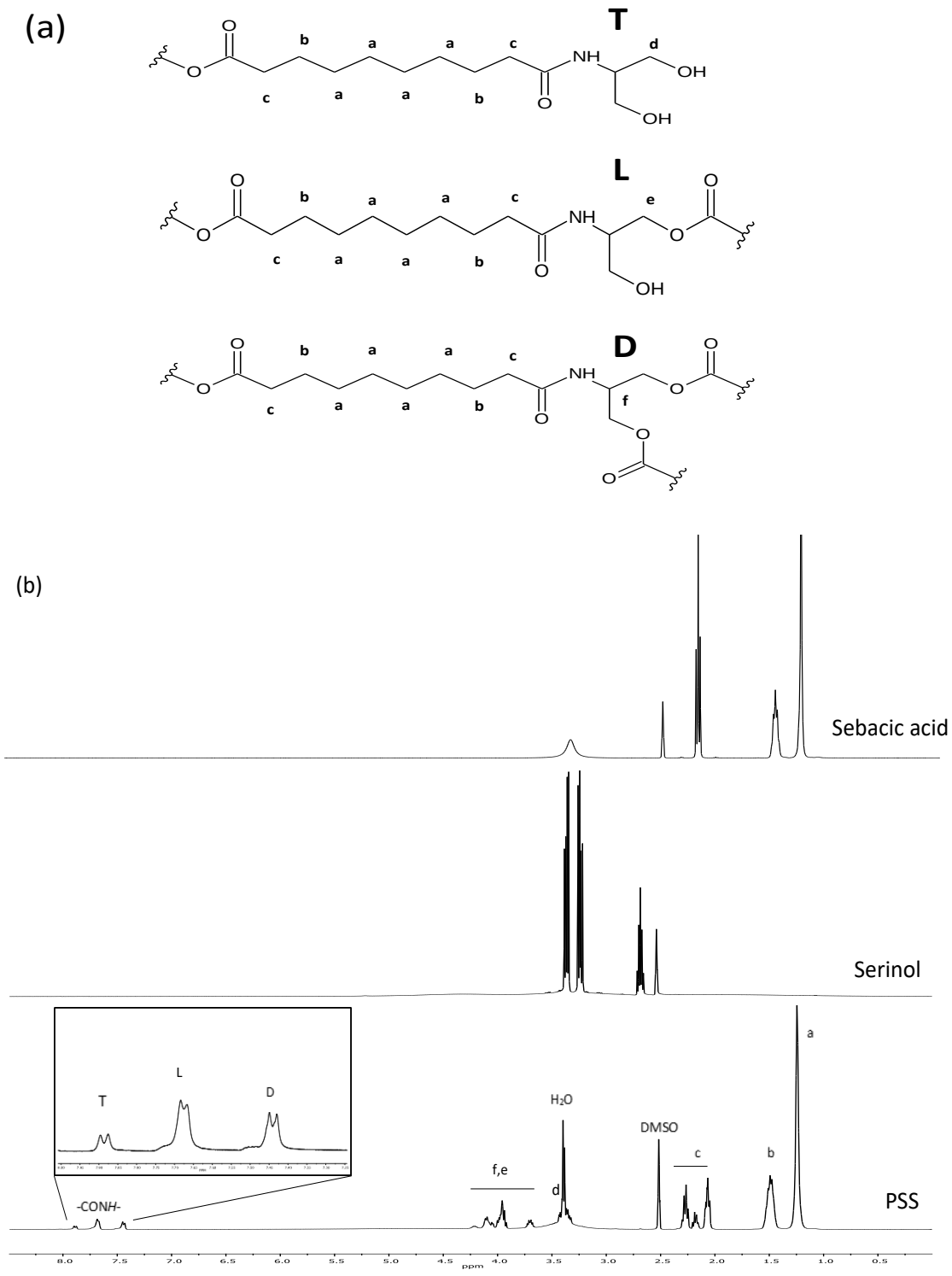
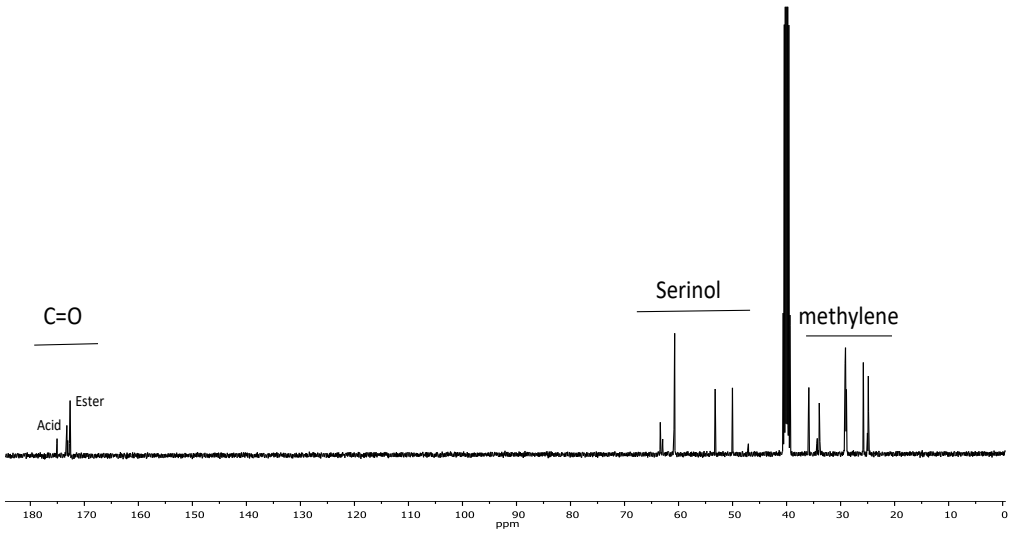


Figure 2.2: ^{1}H NMR spectra, in DMSO-d_6, of sebacic acid, serinol and PSS pre-polymer synthesised at 110^{o}C for 22h; (a) the resonance assignments for PSS pre-polymer of the main three structures T (terminal), L (linear) and D (dendrites), (b) full ^{1}H-NMR spectrum, the peak at 2.5 ppm is due to ^{1}H DMSO solvent.

(a)



(b)

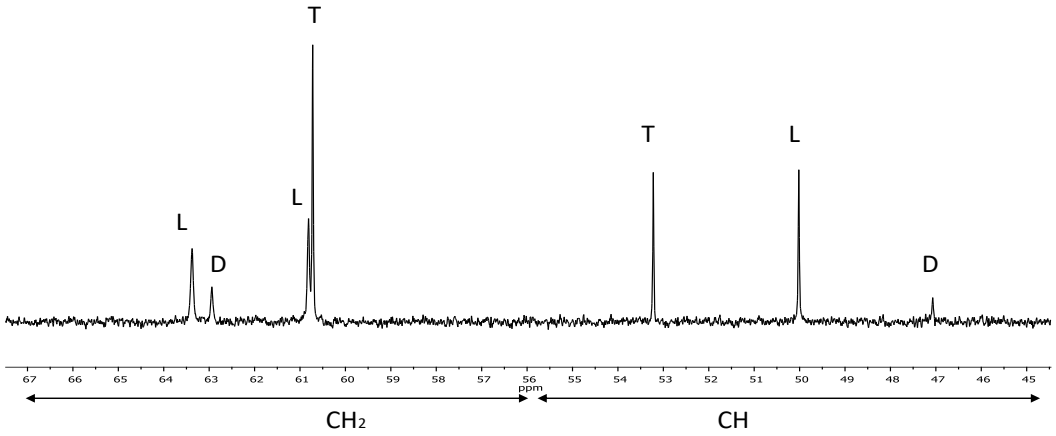


Figure 2.3: ^{13}C NMR Spectra of the PSS pre-polymer; (a) the ^{13}C NMR spectrum of the PSS pre-polymer after 22 hours of reaction time, (b) an expansion of the ^{13}C NMR Spectra of the PSS pre-polymer from serinol and sebacic acid with molar ration of 1:1 as a function of reaction time.

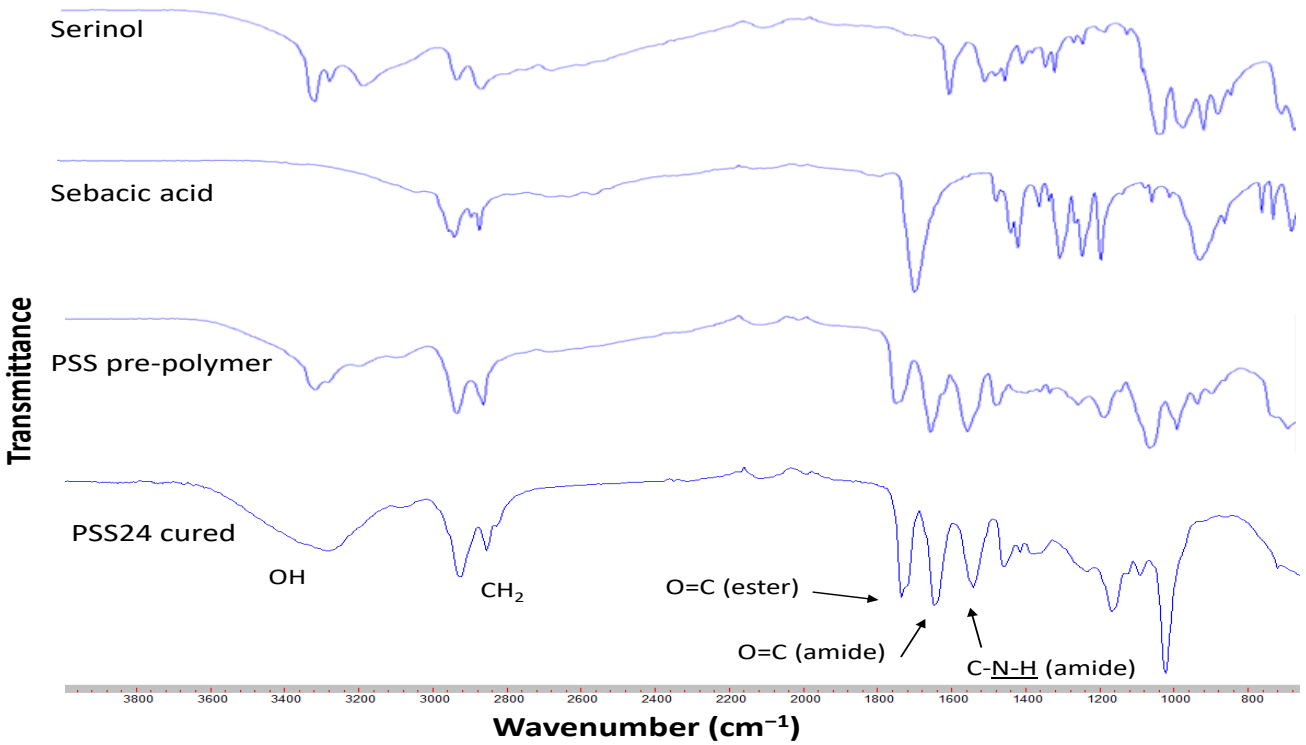


Figure 2.4: FTIR spectra of PSS pre-polymer synthesised at 110°C for 22 hours and PSS film cured at 110°C for 24h showed strong signals of amide and ester bonds at 1650 cm^{-1} and 1760 cm^{-1}, respectively.

2.3.3. Thermal analysis

The thermal properties of PSS polymers were evaluated using a Q10 DSC (TA Instruments, USA; Figure 2.5). The ideal elastomeric scaffold for tissue engineering applications should have a *Tg* lower than the body temperature to ensure that the properties of the scaffold can be maintained in an *in vivo* environment[34]. PSS samples were first heated to 150^{o}C to remove thermal history. The second heating cycle was used to determine the *Tg* of the samples. The *Tg* values for PSS-24, PSS-48 and PSS-72 were approximately -5.3^{o}C, -0.5^{o}C and 6.3^{o}C, respectively. The results indicate that PSS samples would have rubber-like elastomeric behaviour at a physiological temperature. There was no observable melting or crystallisation peaks across the measured range between -40^{o}C and 150^{o}C because of the expected heterogeneous population of molecules, which potentially lead to an amorphous state. The *Tg* of polymer PSS-72 is higher than other polymers, which can be attributed to an increase in the crosslinking density at longer curing periods and can also be inferred by the increase of amide contents, which exhibit less bond rotation and result in relatively rigid polymer segments, ultimately increasing the *Tg*[214–216].

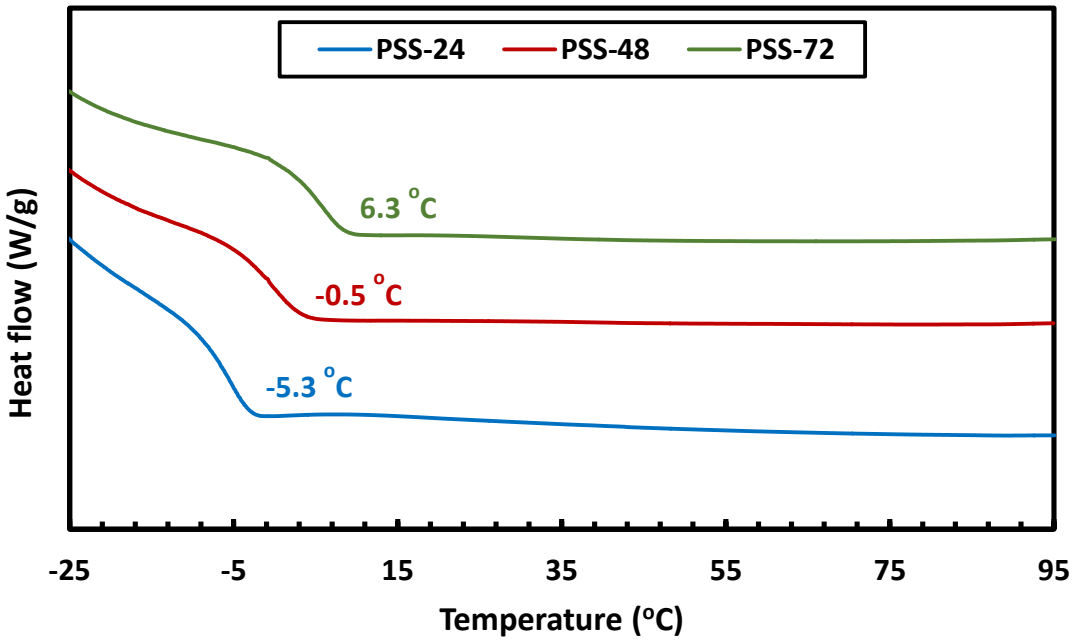


Figure 2.5: DSC traces for cured PSS elastomers at 110°C for different periods; 24, 48 and 72 h.

2.3.4. Hydration properties and uncured monomers

The swelling of PSS experiments were conducted in methanol and PBS at 37^{o}C. The results showed that the maximum amounts of methanol and PBS absorbed by PSS-24, PSS-48 and PSS-72 ranged from 62.77 to 55.95% and from 16.32 to 13.93%, respectively (Figure2.6). PSS reached equilibrium water content (EWC) within 24 hours. Percentages swelling in methanol for all PSS samples were significantly higher ($P<0.0001$) than those in water. Swelling percentage for PSS-72 in methanol was significantly lower ($P< 0.01$) than that for PSS-24 and PSS-48, whilst no significant difference ($P>0.05$) was seen between all samples in water.

The high capability of PSS samples with methanol absorption could facilitated removal of unreacted monomers. The water uptake capacity of PSS decreased slightly, with an increase in curing duration, which can be attributed to the decrease in accessible spaces for PBS diffusion[217] between the PSS molecular chains. However, the eight-carbon chain of the sebacic acid could increase the hydrophobicity of the PSS samples and diminish the degree of the crosslinking effect.

To evaluate the hydrophilicity of cured PSS films, the water-in-air contact angle of the PSS films, from different curing times, was measured (Table 2.3). As for PSS-24, water droplets formed an angle of 92.5˚ on the surface, which decreased to 86.3˚ and 81˚ for PSS-48 and PSS-72 as the curing periods increased for PSS-48 and PSS-72, respectively.

The amount of uncured monomers within the cured PSS samples were evaluated as the weight loss after immersion in methanol for 24 hours. The uncured monomers in the polymer decreased from 27.2 ± 1.1% to 8.3 ± 0.8% by increasing the curing time (Table 2.3). This is suggested to be due to the increase of new crosslinks between cured polymer chains (i.e., crosslinking density) that occur during longer curing periods. The crosslinking density for PSS increased from 24 to 280 mol/m^3 by increasing the curing time from 24 to 72 hour (Table 2.3).

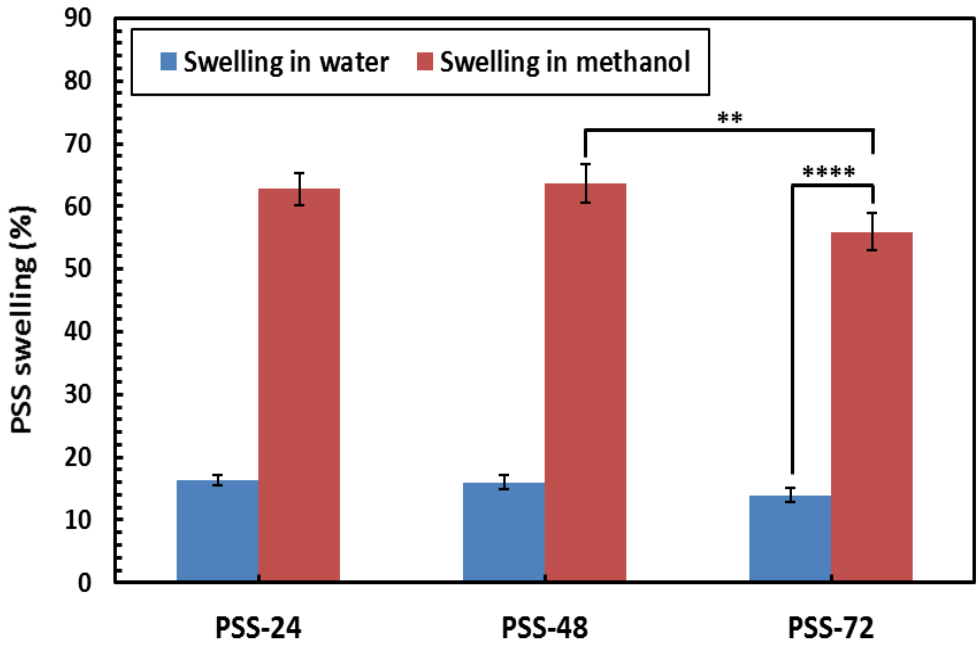


Figure 2.6: Swelling properties of PSS films in methanol and PBS, the swelling experiment of PSS films was performed to determine the water uptake at 37°C in PBS. The error bars represent one standard error. (n=3) (**p < 0.01,****p < 0.0001, ANOVA with Tukey's multiple comparison test)

Table 2.3: **Summary of the uncured monomers, water contact angles and crosslinking densities of PSS samples cured at 110°C for 24, 48 and 72 h. (n=3)**

Formulation	Uncured monomers (%)	Water contact angle (°)	Crosslink density (mol/m^3)
PSS-24	27 ± 1.1	92 ± 3.5	24 ± 4
PSS-48	14 ± 1.3	86 ± 1.7	56 ± 10
PSS-72	8 ± 0.8	81 ± 1.1	280 ± 20

2.3.5. In vitro degradation

The degradation behaviour of PSS was studied by determining the weight loss of the samples in PBS at 37°C and 60°C. After 14 days of in vitro degradation at 37°C, PSS-24 exhibited ~ 10% mass loss. As the curing time increased, the mass loss of PSS-48 and PSS-72 decreased to ~ 6% and ~ 3%, respectively (Figure 2.7 (a)). The rates of mass loss for the PSS films accelerated at 60°C and followed linear trends (Figure 2.7 (b)) to reach approximately 25, 18 and 11% after 14 days for PSS-24, PSS-48 and PSS-72, respectively. At a higher temperature, the rate of degradation accelerated due to the higher amount of energy available for elevated chain mobility and chain scission reactions[218]. With the increase of degree of amidation and esterification, the degradation rate decreased because a higher number of amide and ester bonds were required to be broken during degradation[86,197,219].

The gradual degradation curves suggest that PSS degrades via surface eroding, similar to APS and PGS[86,197]. The degradation mechanism could be evaluated by measuring the change in molecular weight of the polymer during degradation. Nevertheless, it was difficult to examine the molecular weight of PSS samples once they were cured and had become insoluble in solvents. Alternatively, changes in the morphology of the surfaces and cross sections of the degraded PSS films were evaluated using SEM (Figure 2.8). PSS-24, PSS-48 and PSS-72 samples showed a smooth texture for both the surfaces and cross sections before degradation, while irregular surfaces were obtained after degradation (Figure 2.8). More importantly, the cross sections of all PSS samples showed a smooth surface with an absence of cracks or pores, indicating that the core portion of the film had minimal or no degradation. This confirmed that the degradation of PSS films was primarily governed by a surface erosion mechanism.

An inflammatory response was sometimes observed in the surrounding tissue as a result of acidic degradation by-products of the polymers[220]. Most of the degradation studies were performed by incubating the polymer in simulated body fluid (SBF) and PBS to simulate the in vivo degradation profile and replicate the buffer of the body fluid[221]. It was expected that the by-product of the PSS degradation could decrease the pH of the solution. Therefore, the pH changes in PBS were monitored for different PSS samples, throughout degradation experiments, at 37^{o}C (Figure 2.9). The rapid initial decrease in pH observed at day 1 was likely due to the initial cleavage of loosely bounds acids that left behind within the polymer after synthesis. Therefore, washing with PBS for 24 hours is recommended for PSS materials prior to use. Afterwards, the pH of all PSS samples were found to be neutral (at around 7 pH) until the end of the degradation study. These results suggest that PSS material could potentially lead to lower inflammatory effects after implementation. The buffer capacity of PBS solution and presence of amine groups after degradation might buffer the acidic degradation by-products.

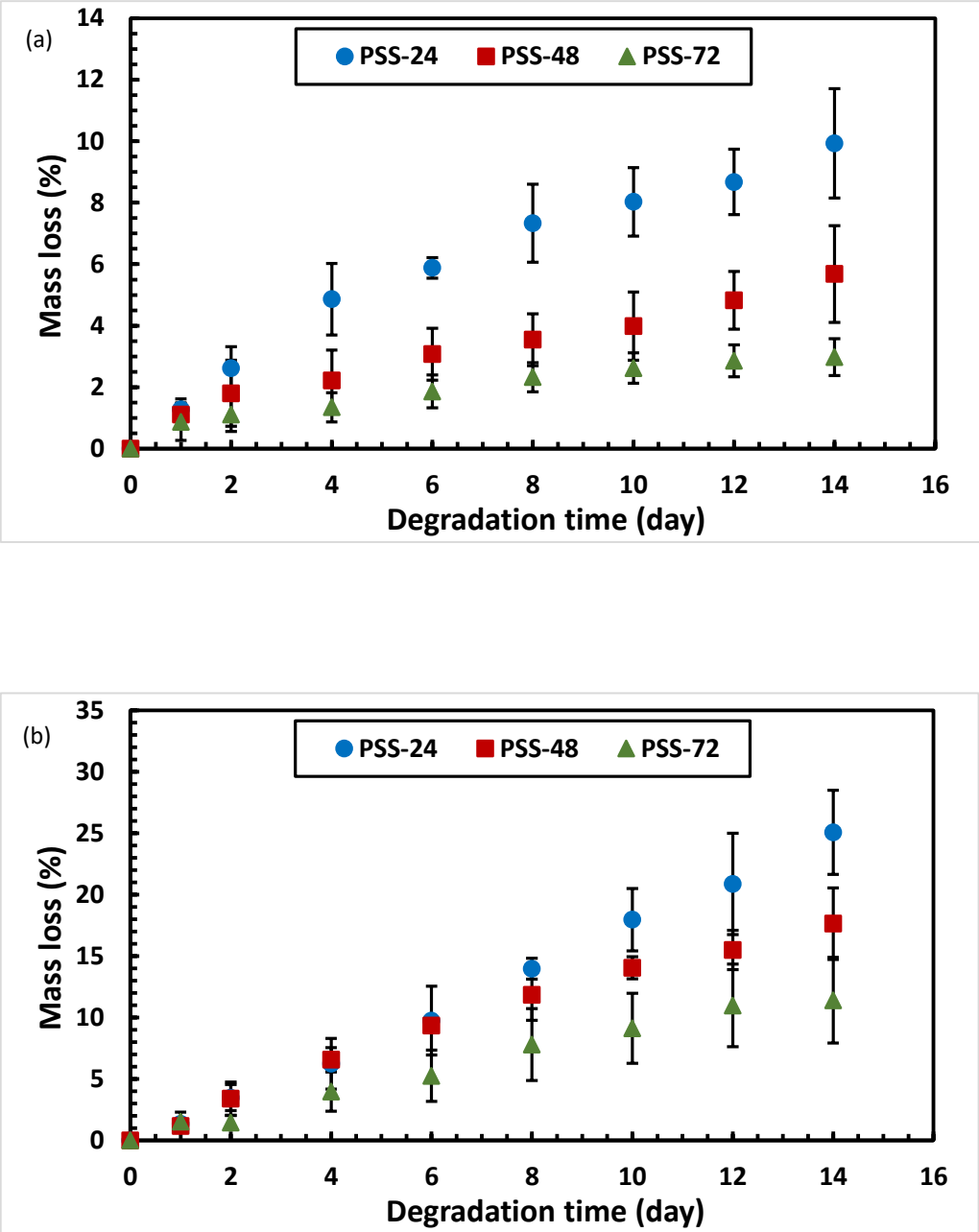


Figure 2.7: Percentage of mass loss versus degradation time for PSS-24, PSS-48 and PSS-72 in PBS at (a) 37°C and (b) 60°C. (n=3)

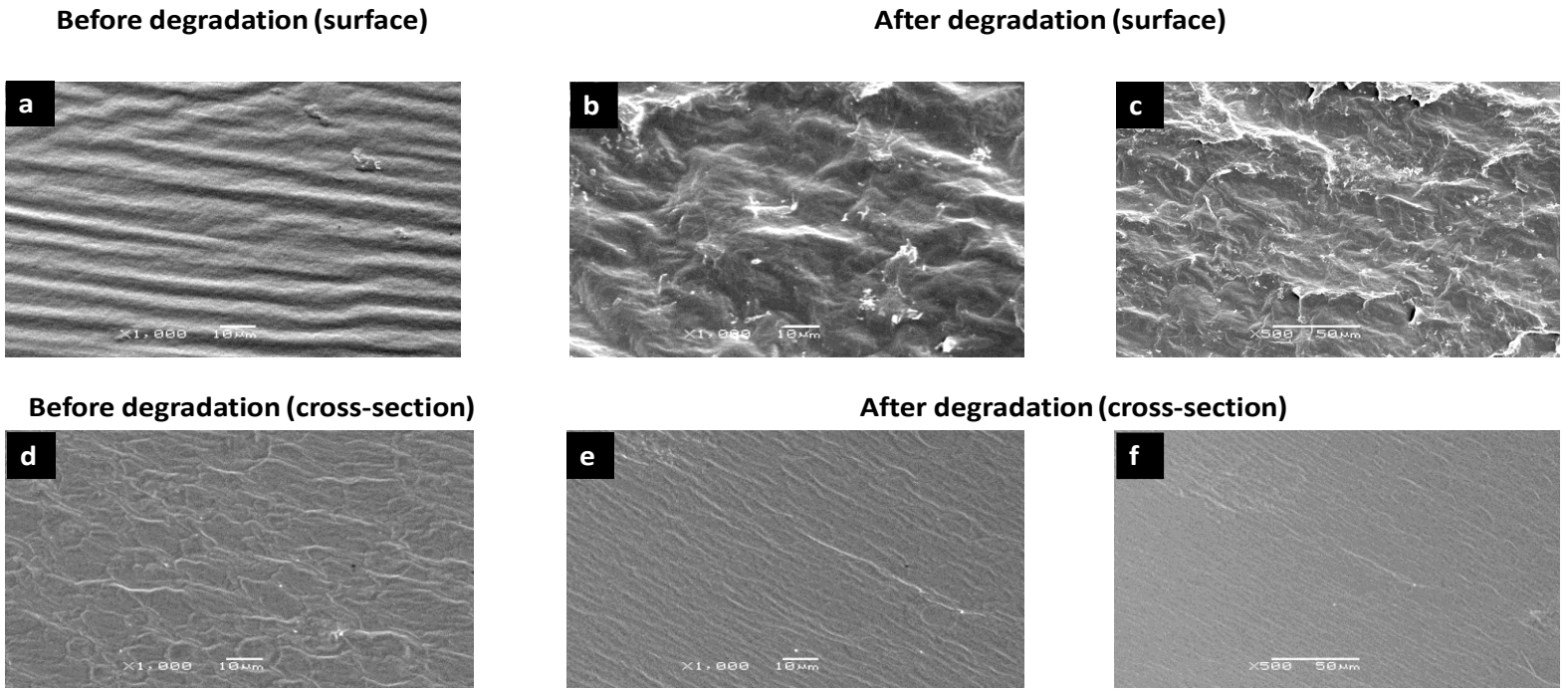


Figure 2.8 SEM micrographs of PSS-24 films before and after 14 days degradation. PSS-24 film was sectioned and imaged using SEM. After 14 days, PSS film exhibited degradation by surface erosion without formation of cracks or pores.

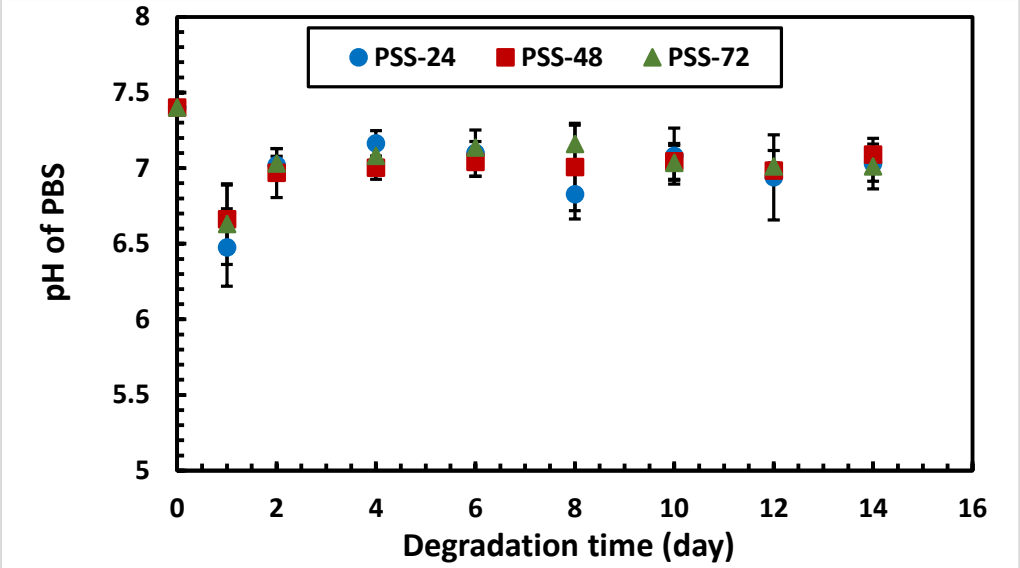


Figure 2.9: Variation in the pH of PBS against degradation time for PSS-24, PSS-48 and PSS-72 in PBS at 37ºC. (n=3)

2.3.6. Mechanical properties and crosslinking density

PSS pre-polymer did not be cured at temperature lower than 110^{o}C, therefore we fixed the curing temperature at 110^{o}C and used range of curing times to tune the mechanical properties of PSS polymer.

The tensile properties of PSS samples were measured at room temperature. Figure 2.10 (a) represents the typical stress-strain curves for as prepared PSS films after curing for different durations. It was observed increasing the crosslinking density by increasing the curing periods which in turn led to increase the tensile strength and the elastic modulus (Figure 2.10 and Figure 2.11). Conversely, elongation to break values decreased with the increase of curing time, see Figure 2.11.

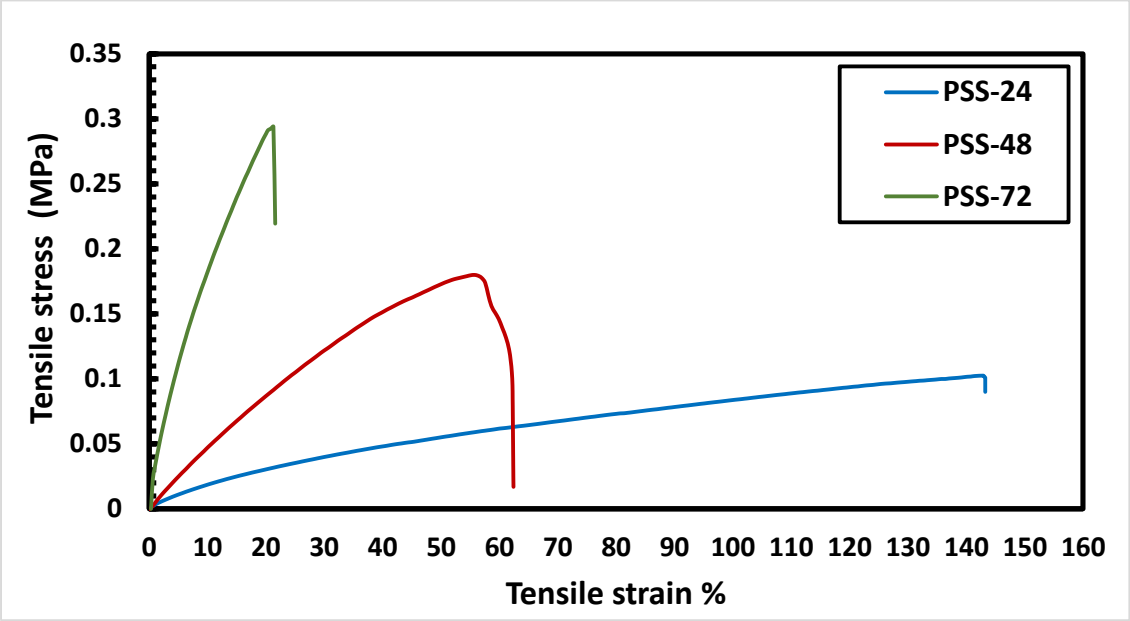
PSS-72 revealed a statistically significant ($P<0.0001$) increase in tensile modulus and strength compared to PSS-24 and PSS-48, while percentages of elongation to failure for PSS-24 were significantly ($P<0.0001$) greater than PSS-48 and PSS-72. For example, PSS-72 showed a three-fold increase in tensile strength (294 ± 24 kPa) and eleven-folds increase in Young's modulus (2086 ± 153 kPa) compared to PSS-24. The total elongations to failure for PSS-24, PSS-48 and PSS-72 were 142 %, 58 % and 22 % which are similar to other thermally cured elastomers[81,92,97,222]. The range of the elastic modulis of PSS samples are those of skeletal muscles which is made of large amount of collagen fibrils[223–225].

The mechanical retention of the degraded PSS-24, PSS-48 and PSS-72 were evaluated to declare the effect of degradation process, see Figure 2.10 and Figure 2.11. No statistical significant changes ($P>0.05$) in elastic modulus, tensile strength and elongation percentage were observed for all PSS samples throughout the degradation experiment for 14 days in PBS at 37^{o}C.

The crosslinking density of the PSS elastomers increased with increasing the degree of crosslinking (Table 2.3). This results are similar to the thermally cured

elastomers that previously reported in which the crosslinking density is directly proportional to the curing time[93]. By increasing the curing time in PSS24 from 24 hours to 48 hours, the crosslinking density increased from 24.2 to 48 mol/m^3.

(a)



(b)

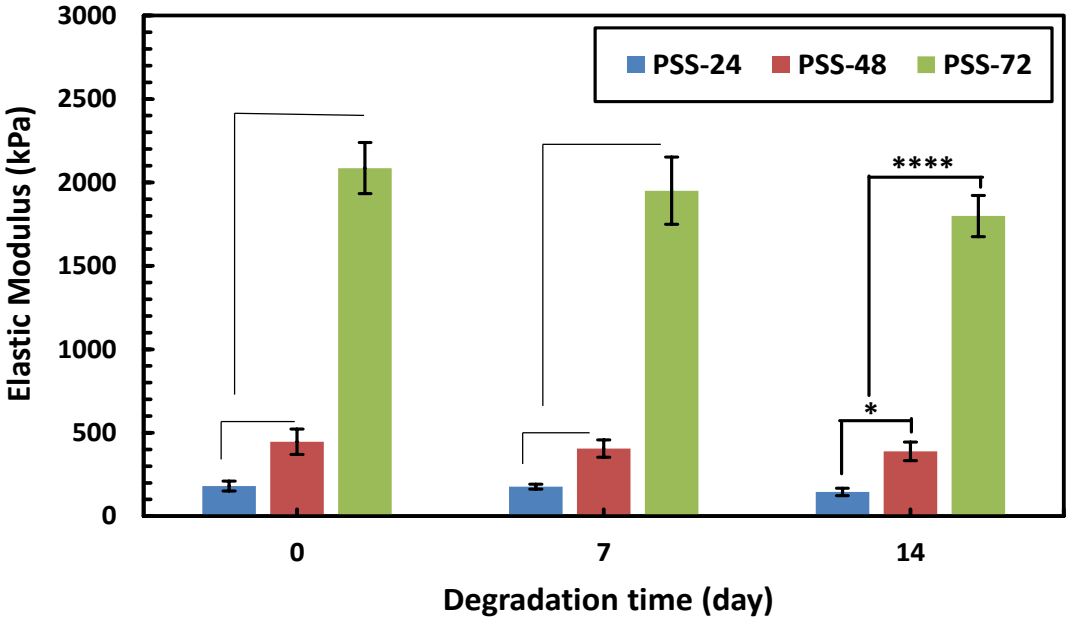
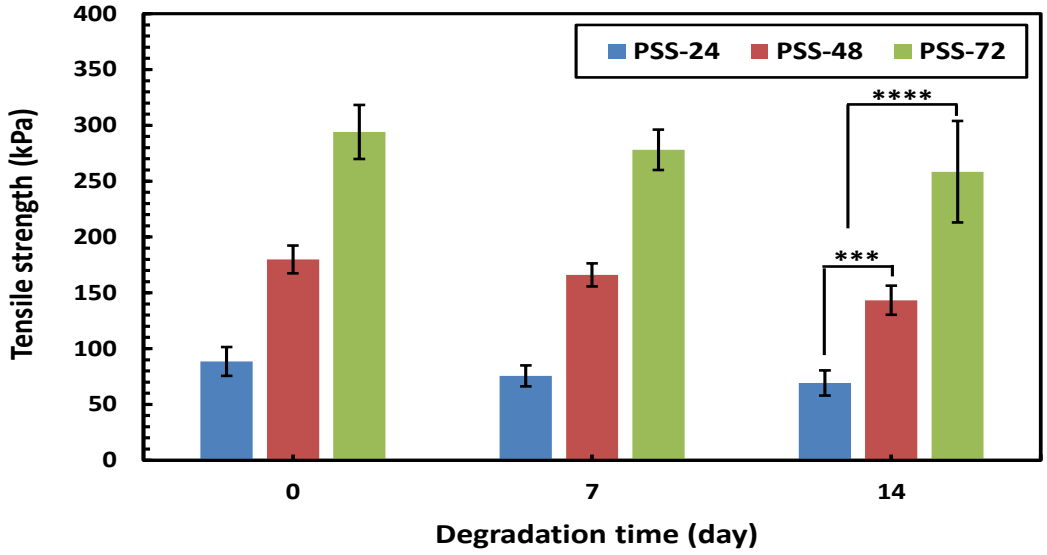


Figure 2.10: Tensile properties of PSS-24, PSS-48 and PSS-72 films throughout degradation in PBS at 37°C for 14 days; (a) stress-strain curves for as prepared materials, (b) tensile strength for PPS samples before and after degradation in PBS at 37°C for 7 and 14 days. The error bars represent one standard error. (n=3) (*$p < 0.05$, ****$p < 0.0001$, ANOVA with Tukey's multiple comparison test)

(c)



(d)

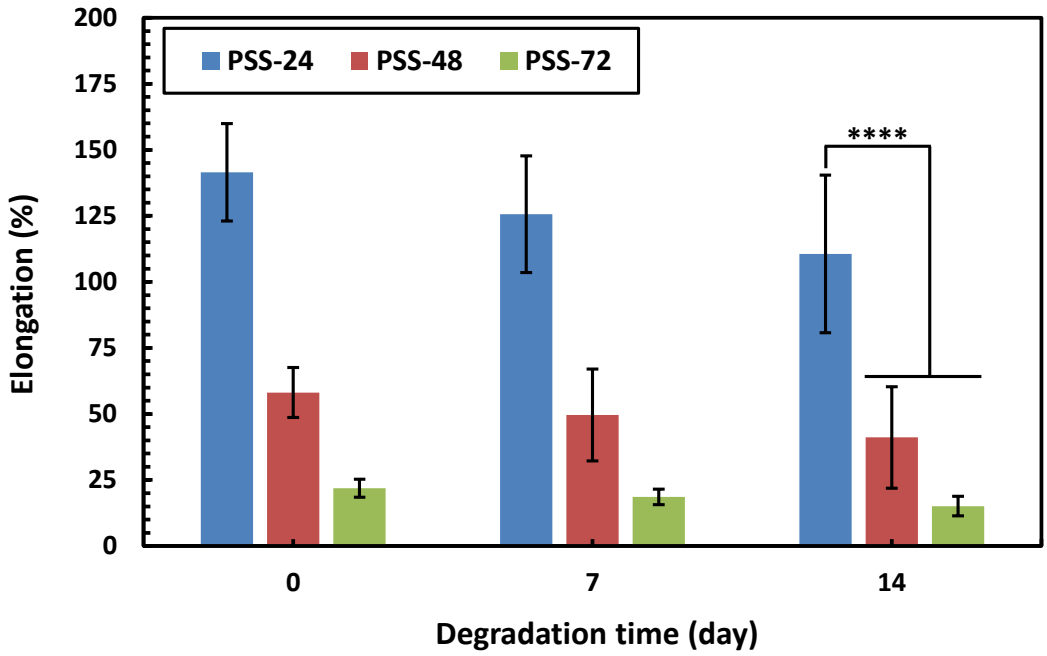


Figure 2.11: Tensile properties of PSS-24, PSS-48 and PSS-72 films throughout degradation in PBS at 37ºC for 14 days; (a) tensile modulus for PSS films and (b) elongation to break for PSS specimens. (n=3) (***p < 0.001, ****p < 0.0001, ANOVA with Tukey's multiple comparison test)

2.3.7. Cytotoxicity and Cell Adhesion

The two monomers, sebacic acid and serinol, used in this study to synthesize PSS are reported to be nontoxic and biocompatible[205,222]. Thus, it was expected that PSS would possess good biocompatibility and could potentially be utilised for different tissue engineering applications. The response of the PSS films, over a 5-day culture period, was examined using LIVE/DEAD staining. Figure 2.13 shows that the cells were found to be viable (green) and distributed on the surface of all the films and there was an increase in cell number over the 5-day culture period, with few dead cells present. The dead 3T3 cells were not clearly visible due to the autofluorescence of PSS films that occurs while imaging. However, from microscopic examination, there appeared to be few dead cells on the PSS films (< 1% of the sample).

On day one, a light microscope examination showed rounded 3T3 cells on all the PSS films with little cell to cell contact. On day three and five, cells became elongated with high cell density and cell to cell contact increased on all PSS films. The films exhibited normal shape and similar morphology to 3T3 cells grown on tissue culture polystyrene (TCP) as a standard control (Figure 2.12). The proliferation of 3T3 mouse fibroblast cells on the polymer surface was analysed using PrestoBlue® assays after 1, 3, and 5 days of seeding. The results revealed that the proliferation rate of cells on the surface of PSS-24, PSS-48, PSS-72 and TCP increased significantly ($P<0.0001$) with culture time (Figure 2.14). At day one, cell proliferation on all PSS samples were similar ($P>0.05$) to the positive control, TCP, and after cell culturing for further time periods, some of PSS specimens were slightly ($P<0.01$) lower than TCP. These results indicated that PSS polymer has good biocompatibility by supporting cell attachment, along with spreading and proliferation, suggesting that PSS may be a promising candidate for different biomedical applications.

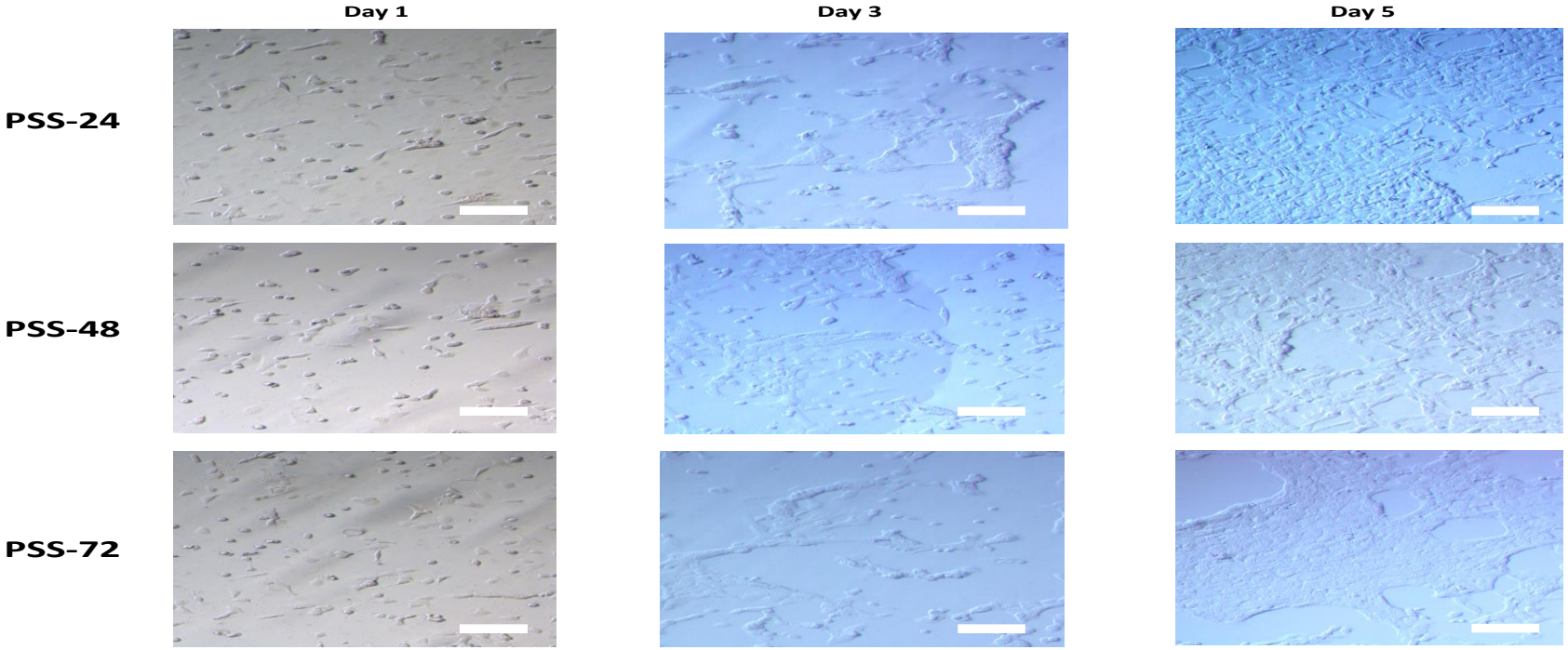


Figure 2.12: Light microscopy Images of 3T3 mouse fibroblast cells cultured on PSS polymers on day 1, 3 and 5 post seeding. 3T3 cells cultured on PSS appeared to have a similar morphology as in tissue culture polystyrene. Scale bars are 50 mm.

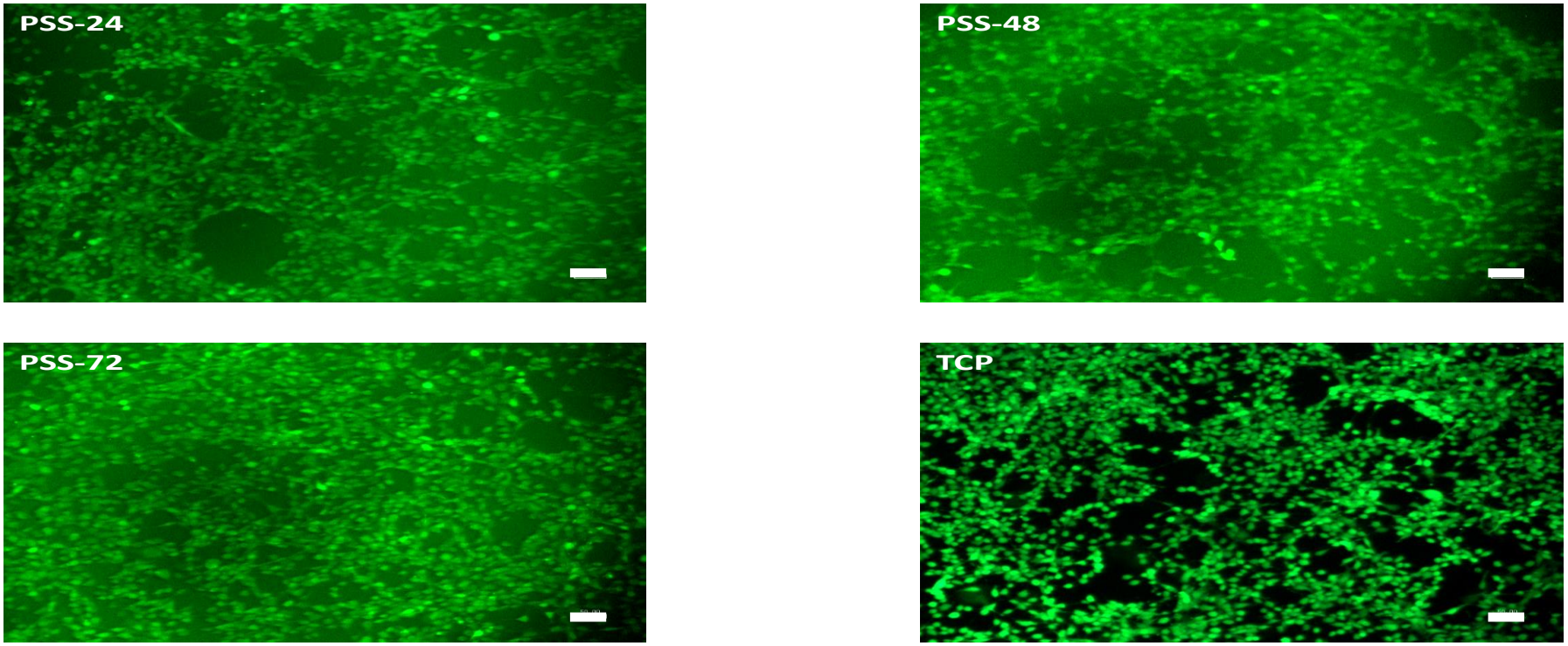


Figure 2.13: Confocal fluorescence images of 3T3 cells spreading on cured PSS polymers after 5 days of cell culture.

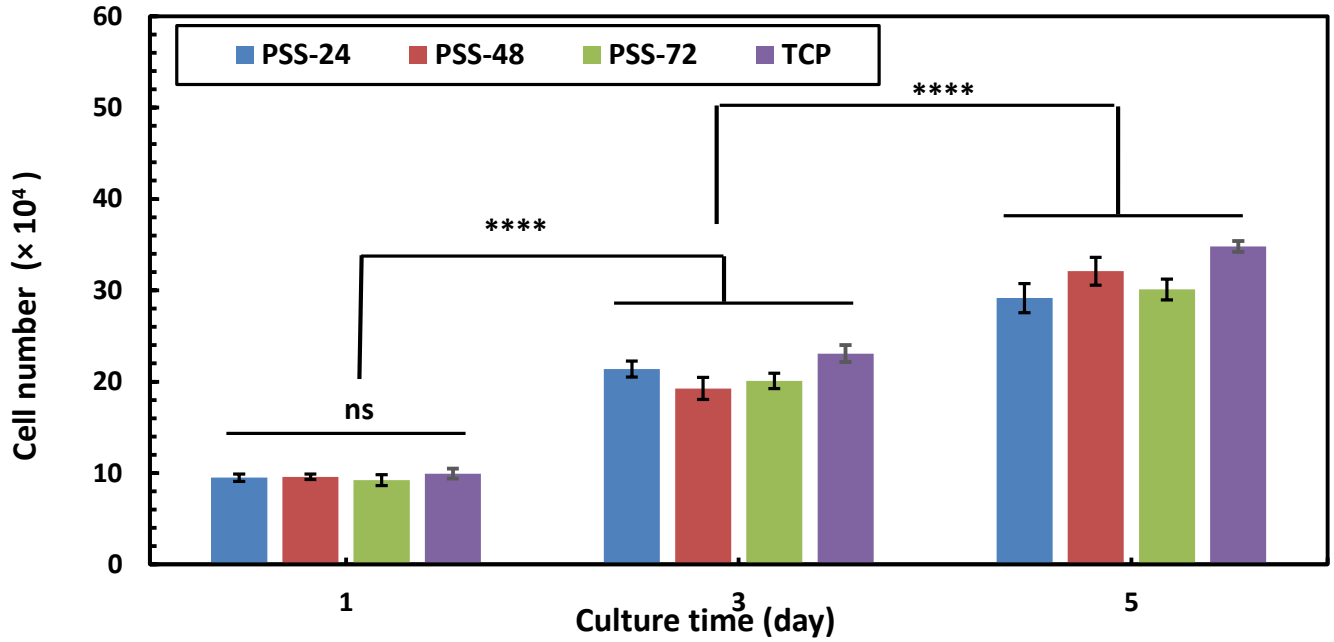


Figure 2.14: Proliferation of 3T3 cells cultured on PSS-24, PSS-48 and PSS-72 for 5 days. Four replicates of each sample were tested using PrestoBlue® assay and the averages are presented ±SD. **** represent significant difference $P<0.0001$ in comparison with TCP and ns refers to non-significant difference ($P>0.05$).

2.4. Conclusion

Novel biodegradable PEAs elastomer were successfully designed and synthesised from serinol and sebacic acid by polycondensation reaction. PSS elastomers exhibited tuneable degradation and mechanical profiles by varying the curing time. Furthermore, The PSS films exhibited low T_g below body temperature and the PSS samples degraded slowly with high UTS and low elastic modulus similar to protein-based polymers. PSS showed good cytocompatibility by supporting attachment, spreading and proliferation of 3T3 fibroblast cells. Thus, the developed PSS polymer shows excellent potential to be applied for various biomedical application such as tissue engineering applications, drug delivery and diagnostic system.

3. Chapter Three

Elastic Fibrous Biodegradable Polyester Amide Scaffold for Soft Tissue Engineering Applications

3.1. Introduction

Scaffolds represent the initial component in the tissue regeneration process and are exposed to dynamic environments *in vivo*. Typical scaffold designs that drive research and development for the regeneration of soft tissues, such as heart valves and skeletal muscles, principally focus on imitation of the extracellular matrix [226], providing initial structural support for different types of seeded cells and allow for diffusion of nutrients through the porous structure; this scaffold also provides tuneable biodegradation and mechanical properties to match the regeneration process of the target tissue. Synthetic biodegradable elastomers are promising polymers because of their chemical and physical optimised properties[34,227]. Moreover, synthetic biodegradable elastomers offer advantages over natural materials as they exhibit less immunogenicity and less batch-to-batch synthesis variation[34,227].

Previous studies have demonstrated the importance of the microenvironment structure on cellular attachment and proliferation. The cellular response to three-dimensional scaffolds, such as fibrous structures, is different to that of two dimensional scaffolds[228,229]. The electrospinning technique has been used widely for different tissue engineering applications to produce fibrous scaffolds with fibre diameters ranging from nanometre to micrometres. The electrospun scaffolds could be customised to mimic a wide range of shapes and mechanical properties of the native extracellular matrices[230,231]. Electrospinning of biodegradable thermoplastic polymers, such as PCL, PLA, PGA and their co-polymers, are the most widely investigated polymers with will-established processes[73,171,186]. However, because of their poor mechanical recovery after deformation, thermoplastic polymers have been generally inappropriate for repair of soft tissues that need to function under dynamic conditions, such as skeletal muscles and heart valve [232,233] . Therefore, there is a demand to use the electrospinning technique to produce elastomeric fibrous scaffolds derived from thermoset elastomeric polymers. Usually these polymers demonstrate a homogenous degradation behaviour with a predictable loss of mechanical properties[37]. As an example, PSS a new biodegradable and biocompatible thermoset elastomer has recently developed. PSS is a degradable polyester amide elastomer, which has flexible mechanical properties and supports cell adhesion; PSS could potentially fill the existing gap in biomaterials needed for the soft tissue engineering. Moreover, the solubility of PSS pre-polymer in different organic solvents was improved compared to APS polymer.

In the electrospinning process, there are number of important parameters, such as molecular weight and solution concentration, which should be considered when attempting to electrospin a new material[105]. Electrospinning chemically cured thermoset polymers, such as PSS, are challenging due to the insolubility of PSS in any organic solvent once cured, yet the fibres from uncured pre-polymer melt during the curing process at high temperature. To overcome these challenges, a carrier polymer can be used. PVA is non-toxic, water soluble, biocompatible and blends successfully with various natural or synthetic polymers to overcome the limitation of the electrospinning process or to add value to the electrospun fibres[234–237]. PVA is approved by the FDA for pharmaceutical and food chemistry applications[238]; and has been investigated in wound dressing, the regeneration of tendons and other tissue-engineered scaffolds[239,240].

Therefore, PVA is an attractive carrier polymer that can be used to facilitate the electrospinning of PSS.

The objective of this chapter was to firstly synthesise PSS pre-polymer that can be cured into networks with a various mechanical and degradation profiles, and then convert it into an elastic biocompatible electrospun scaffold using PVA as a carrier polymer to facilitate the electrospinning process. The degradation, mechanical, biocompatibility properties and optimisation of the electrospinning parameters of the fibrous scaffolds will be explored.

3.2. Experimental Procedure

3.2.1. Materials

Sebacic acid (99.5%), serinol (98%), hexafluoroisopropanol (HFIP, 99.5%) and trypsin EDTA solution were purchased from Sigma Aldrich and used as received. methanol (99.8%), and resazurin sodium salt (Prestoblue®) were purchased from Fisher scientific and used without further purification. Poly (vinyl alcohol) (PVA) with molecular weight of 110,000 (98% hydrolysis) generously provided by Nippon Gohsei (Dusseldorf, Germany). Cell culture supplies including Dulbecco's Modified Eagle's Medium (DMEM) media (Gibco Life Technologies, UK), (1% v/v) L-glutamine, 1% antibiotic (penicillin/streptomycin) and (10% v/v) fetal calf serum (FCS) were purchased from Thermo Fisher Scientific, UK.

3.2.2. Synthesis of poly(serinol sebacate) (PSS) pre-polymer

PSS elastomer with serinol:sebacic acid ratio of 1:1 was synthesized according to the procedure explained earlier in the second chapter. Serinol and sebacic acid were charged in a 100 ml three-neck round bottom flask in 1:1 molar ratio. The flask was maintained at 110^{o}C for 16 hours under inert atmosphere (nitrogen gas) and constant stirring. The resultant PSS prepolymer was cooled to room temperature. The gel point was determined as that when the polymer no longer dissolve in methanol. At the end of the reaction, a viscous, yellow coloured PSS pre-polymer was obtained and stored at 2^{o}C prior to use.

3.2.3. Solution preparation for electrospinning

The PSS solution with concentration of 9 wt% was prepared by dissolving 9 g of PSS viscous liquid in 100 ml of HFIP for 24 hours at room temperature. PVA solution of 9 wt% was obtained by dissolving 10 g of PVA powder in 100 ml of HFIP with stirring for 24 hours until a clear solution was obtained with a high increase in viscosity. PSS was then blended with PVA solution with different weight ratio (1:1, 2:1, 3:1). All blended solutions were stirred for further 24 hours to get homogenous binary solution.

3.2.4. Preparation of PSS fibrous scaffolds

The process of electrospinning was performed by using an electrospinning kit (IME Technology, Netherland), which has a special syringe pump (Harvard, USA), a special sensor and a condenser to control the humidity and temperature. The solutions were placed in a 5 ml syringe (Becton Dickinson®) and then mounted in the syringe pump. The power supply was connected to the 21-gauge blunt needle (Sterican®) (Figure 3.1). PVA is soluble in water and HFIP but is not soluble in most organic solvents[241]; in contrast, PSS is soluble in several solvents including HFIP, thus HFIP was selected as the common solvent for both to dissolve PSS and PVA. To determine the optimum collector distance and voltage, the effect of varying the collector distance measured from the tip of the needle to the collector (20, 25, 30 cm) and voltage (10, 15, 20 kV) on fibres morphology were studied. The PSS:PVA ratio (1:1), solution concentration (9% w/v) and applied voltage or collector distance were kept constant. Based on optimisation trials, the distance parameter of 25 cm and applied voltage of 20 kV were selected and kept constant for further studies. The effect of varying the PSS:PVA ratio (1:1, 2:1, 3:1) on fibre morphology was also evaluated by keeping solution concentration (9% w/v), collector distance (25 cm) and applied voltage (20 kV) constant. The effect of varying the concentration on morphology of the fibrous scaffold was studied. A constant ratio of PSS to PVA (1:1) solution was electrospun at a constant voltage (20 kV), distance (25 cm), flow rate of 1.5 ml/hours and temperature of 20 ±1 ^{o} C. The produced fibres were collected on aluminium foil, which was placed around the mandrel collector and dried in a fume hood for 48 hours to evaporate any residual solvent. Fibrous scaffolds were then placed in a vacuum oven and cured at 120^{o} C for 24 hours (PSS24), 48 hours (PSS48), 72 hours (PSS72). The crosslinked PSS fibrous scaffolds were purified by soaking in hot water at 90^{o}C for 4 hours to eliminate the PVA carrier and the sol fraction was removed by methanol washes with agitation for 24 hours. Table 3.1 summarises the optimisation process of PSS-PVA fibrous scaffolds.

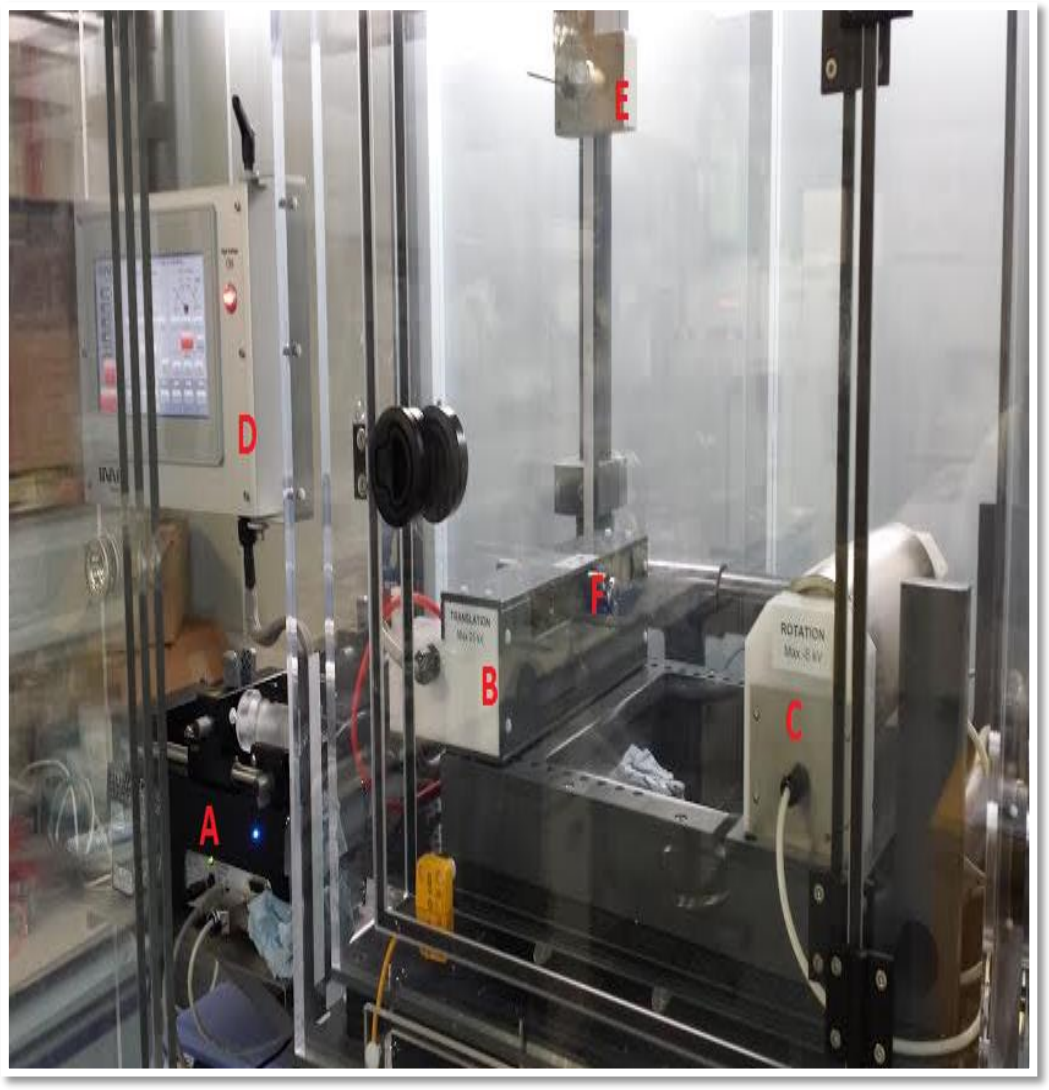


Figure 3.1 The electrospinning setup kit, which requires a (A) pump, (B) Voltage contactor, (c) Mandrel collector, (D) touch screen controller, (E) Temperature and Humidity sensors, (F) Needle holder.

Table 3.1: The variables used to optimise the electrospinning processes of PSS fibrous scaffolds.

Property	Polymer concentration (% w/v)	PSS/PVA ratio	Voltage (kV)	Distance (cm)
Collector distance	9	(1:1)	20	20
	9	(1:1)	20	25
	9	(1:1)	20	30
Voltage	9	(1:1)	10	25
	9	(1:1)	15	25
	9	(1:1)	20	25
Polymer ratio	9	(1:1)	20	25
	13.5	(2:1)	20	25
	18	(3:1)	20	25

3.2.5. Scaffold morphology

The morphology of the produced PSS electrospun fibrous scaffolds were examined using a scanning electron microscope (JSM-6060LV). **T**he electrospun scaffolds were coated with a gold layer before examination. All samples were placed on the carbon tape on the metallic holder and coated with a thin layer of gold using a gold coater (Leica EM SCD005) at 10 mA for 300 seconds. SEM micrographs were captured at 10 mm working distance and accelerated voltage of 15 kV. To calculate the fibre diameters, 200 fibres were selected randomly from the SEM and analysed with ImageJ software (National Institutes of Health, USA) according to the method published previously[242].

3.2.6. Fourier Transform Infrared (FTIR)

The chemical bonds of the PSS24 and PSS48 scaffolds was investigated by Fourier Transform Infrared (FTIR) spectroscopy, The FTIR spectra was in range of 700–4000 cm^{-1} and recorded on Thermo Scientific Nicolet IR 200 FT-IR. The data were analysed using Omnic 8.0 software (Thermo Scientific).

3.2.7. Mechanical properties

Tensile test of the fibrous PSS scaffolds were performed using Instron 5969, with a 100 N load cell and the cross-head speed was 10 mm min^{-1} until failure. The crosslinked fibrous scaffolds (n=3) were cut into rectangular shape with dimensions of 30 mm(L) × 10 mm(W) × 1mm(T). The thickness of the samples were measured using digital callipers. Electrospun scaffolds were hydrated in phosphate buffered saline (PBS) prior to analysis and the stress–strain curves were used to calculate ultimate tensile strength as the highest stress at sample failure, Young's modulus as the linear curve between 0.5% and 2.5% strain and elongation at break.

3.2.8. Hydration properties

Effect of various curing time on water absorption of the scaffolds was investigated via hydration studies. The fibrous scaffolds (5 mm× 5 mm) (n = 4) were incubated in PBS at 37 ^{o}C in a water bath shaker (25 RPM). The weights and the thickness of scaffolds at different time points were recorded until reached equilibrium. The percentage swelling ratio was calculated using equation (1):

$$Swelling\ (\%) = \frac{(w_{hyd} - w_{dry})}{w_{hyd}}\ x\ 100 \qquad (Eq.1)$$

where W_{dry} is initial sample weight and W_{hyd} is the weight of the hydrated samples.

3.2.9. In vitro degradation study

The degradation rate of PSS scaffolds was determined by incubating samples (5×5×1 mm^3) (n=4) in phosphate buffer saline (PBS) solution at 37 ^{O}C for 14 days, and the PBS was replaced every 24 h. The scaffolds were placed in a shaking incubator at 70 rpm. Initial weights (W_i) were recorded. After each time point, the scaffolds were removed, washed in dH_2O to eliminate salts deposited by the PBS and their weights were recorded after drying**.** The weight loss W_{loss} was calculated using equation (2). Morphology of degraded fibrous scaffold before and after degradation was evaluated by SEM.

$$weight\ loss\ (W_{loss}\ \%) = \frac{(w_i - w_d)}{w_i}\ x\ 100 \qquad (Eq.2)$$

3.2.10. Cytocompatibility assessment

3.2.10.1. Sterilisation of PSS fibrous scaffolds

All fibrous scaffold mats were cut into discs (15 mm diameter) and placed in a 24 well-plate and supported with plastic crown (Cell Crown, Sigma-Aldrich) to prevent the fibrous scaffold from floating in the culture medium. Thereafter, all fibrous samples were pre-treated with 70% v/v ethanol/H_2O for 24 h, followed by washing three times with sterilised PBS prior to cell seeding. In addition to sterilisation, the ethanol was also used to remove any unreacted monomers during the polymer fabrication.

3.2.10.2. Cell culture

The fibroblast cells (3T3) cells were cultured in Dulbecco's Modified Eagle Medium (DMEM), supplemented with 1% Penicillin/Streptomycin and 10% Fetal Bovine Serum (FBS). The PLGA (ratio) fibrous scaffold were used as a positive control. The fibrous scaffolds (PSS24, PSS48) and control PLGA fibrous scaffolds were sterilised under UV light for 30 minutes. All scaffolds were placed in 48-well plates (Falcon, BD Bioscience, UK), which contained 1 ml of DMEM, and then seeded with fibroblast cells at the density of 10×10^4 cells/sample. The fibrous scaffolds were then cultured under standard incubation conditions of 5% CO_2 humid air and at 37 ^oC. The media was replaced every 48 hours with a fresh media.

3.2.10.3. Cell attachment

Fibroblast cells were seeded on the scaffolds and harvested at day 1, day 3 and day 5 time points. The fibrous scaffolds were washed with PBS to remove unattached cells and fixed with 3% glutaraldehyde for 2 hours, and washed with PBS. Subsequently, Scaffolds were dehydrated with a series concentration of alcohols (50%, 70%, 90%, 100% v/v). Cell spreading and cell attachment were observed using SEM.

3.2.10.4. Cell proliferation

The cell proliferation was examined over a period of 5 days using PrestoBlue (PB) Assay (thermos fisher scientific, UK) according to the manufacturer's protocol. The Prestoblue assay was used to analyse the time-dependant cell proliferation based on the ability of viable cells to reduce resazurin dye (blue) to resorufin (pink). Briefly, seeded scaffolds (n=4) were transferred to a new 48-well plate containing fresh culture medium. PB (10% v/v) was added into each well and incubated at 37°C for 2 h. Reduced PB (100 μL) was then placed in 96-well plate to measure the fluorescence intensity using a Tecan microplate reader (Tecan, Reading, UK) at excitation/emission wavelengths of 530/590 nm. TCPs and PLGA were used as control.

3.2.11. Preparation of PSS fibrous scaffolds with tailored pattern

To produce patterned features on the PSS/PVA fibre scaffolds, a patterned metal stencil was used as the negative collector. The process of electrospinning was performed by using an electrospinning kit (IME Technology). Figure 1.3 describe a schematic view of the electrospinning process and of the patterned stencil structure. The PSS/PVA electrospun fibres were removed from the stencil used as collector during electrospinning and dried in a fume hood for 48 h to evaporate any residual solvent. Fibrous scaffolds were placed in a vacuum oven and crosslinked at 120^{o} C for 24 h. PSS fibrous scaffolds were purified with dH2O for 48 h to remove PVA and the sol fraction was removed by methanol washes with agitation for 24 h.

3.2.12. Statistics

Statistical analysis was expressed as mean ± standard deviation (SE), and carried out by one-way analysis of variance (ANOVA) with Tukey's post-hoc analysis or student's t-test. The data were considered to be significantly different if p-value becomes less than 0.05.

3.3. Results and Discussion

3.3.1. Optimisation of PSS fibre fabrication conditions

The electrospinning process can be achieved when the polymer retains sufficient chain entanglement that can provide stable jet[243]. Polymer chain entanglement is controlled by molecular weight of the polymer, chain length distribution and polymer concentration[244]. A common method for electrospinning process is to dissolve the polymer in an appropriate solvent, when the solvent is evaporated the jet becomes unstable and enters the bending instability region, which accounts for fibre drawing on the collector[245,246]. This approach was not feasible with PSS because of its low molecular weight that resulted in a low viscosity polymer solution and could not be spun, suggesting that insufficient chain entanglements were available. Despite high polymer concentration, it was not possible to directly electrospin the PSS solution due to a quick coalesce of fibres on the collector. The carrier polymer was believed to facilitate electrospinning process of the PSS.

In this study, the electrospun fibre mats could not be produced at a concentration of PVA less than 4.5% w/v (PSS:PVA 1:1) as a result of low concentration solution, only droplets could be obtained irrespective of the electrospinning conditions and PSS concentration. Thus PVA concentration of 4.5 % w/v were used in the present study.

The PSS fibrous scaffolds were electrospun at the optimised processing conditions such as collector distance, applied voltage and polymers ratio. The collector distance varied between 20 and 30 cm distances and, the optimum distance was found to be 25cm resulting in bead-free fibres with narrow diameter distribution. Whereas distance below 25cm exhibited fibres fusion and Lack of uniformity. Similarly, different voltage (between 1 and 24 kV) was used and stable and continuous jet was produced at 20 kV.

3.3.2. Effect of PSS:PVA ratio on the fibre properties

The effect of PSS:PVA ratio on the scaffold morphology was analysed at different ratios of PSS to PVA (1:1, 2:1 and 3:1) and fixed voltage of 20 kV, distance between needle and collector of 25cm, 18% w/v overall solution concentration and flow rate of 1.5 mL/h. The SEM images for fibrous scaffolds of various PSS:PVA ratios are shown in Figure 3.2. Fibrous scaffolds prepared with 2:1 and 3:1 PSS:PVA ratios resulted in increase the fusion of the fibre, while PSS:PVA with 1:1 ratio yielded regular fibres of 1.3±0.25 μm diameter. These results are in accordance with previous reports where the fibre fusion and diameters of blend electrospun APS and PGS fibre scaffolds increased with increasing proportion of both APS and PGS[199,247]. These findings might be attributed to adhesive nature of PSS pre-polymer due to the presence of hydroxyl groups. Results also indicated that among the three ratios of PSS:PVA, 1:1 ratio was the best composition for fibre yielded uniform and bead-free fibres. Therefore, subsequent investigations of curing, degradation, mechanical properties and cytocompatibility were focused on fibrous scaffolds synthesised from PSS:PVA with 1:1 ratio.

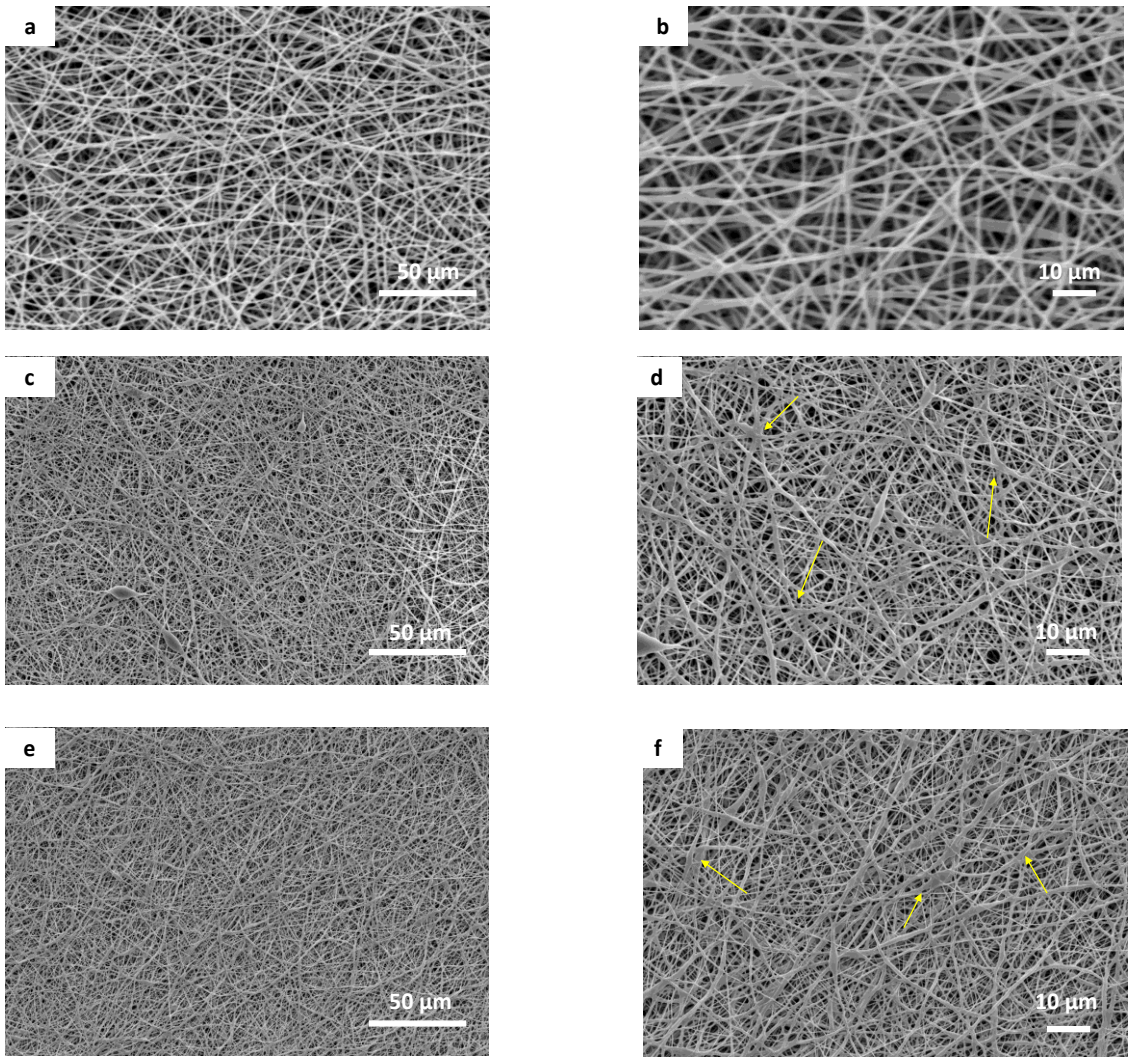


Figure 3.2: SEM images show the effect of varying PSS:PVA ratio on fibre morphology, yellow arrows indicate fused fibres with increased PSS concentration: (a) and (b) 1:1 PSS:PVA scaffold, (c) and (d) 2:1 PSS:PVA scaffold and (e) and (f) 3:1 PSS:PVA scaffold.

3.3.3. Curing of PSS:PVA fibrous scaffold

We have examined the change in the morphology of the PSS:PVA fibrous scaffold after curing the at 110^{o}C for 24, 48 and 72 hours. It was observed that fibre morphology of PSS:PVA fibre did maintained fibre morphology after curing for 48 and 72 hours with fusion restricted to the contact fibre between fibres (Figure 3.3).Thereafter, the scaffolds were soaked in hot water at 90^{o}C for 4 hours to eliminate the PVA carrier.
The remaining mass for PSS48 and PSS72 after water treatment were 65 and 69 %, respectively, both samples had more than 50% mass remaining. This treatment partially dissolved the PVA carrier from the fibrous scaffold. The remaining of PVA residual could be due to physical entrapment within PSS fibres. Chemical curing of PVA with PSS polymer via polycondensation reaction with free carboxylic acid groups in PSS and possible change in the solubility of PVA after thermal curing[240] were suggested as other reasons for the residual PVA within PSS scaffolds after washing with hot water.

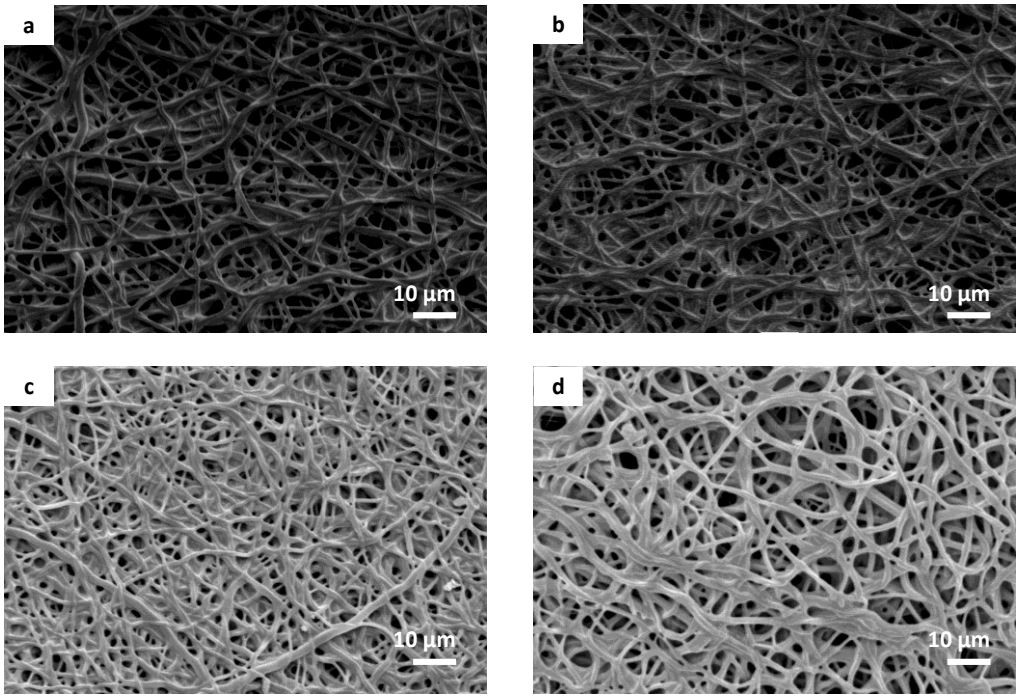


Figure 3.3: Fibre morphology of PSS:PVA (1:1) electrospun scaffolds analysed by SEM: (a) PSS:PVA after curing at 110˚C for 48 hours and washing in water for 4 hours at 90˚C, (b) PSS:PVA scaffold was cured for 72 hours and washed in water for 4 hours at 90˚C, (c) and (d) SEM micrographs of PSS:PVA scaffolds after purification with methanol for 48 and 72 hours respectively.

3.3.4. Chemical characterisation

FTIR spectroscopy was used to study the chemical compositions of the prepared PSS scaffolds. FTIR spectra for PSS48 scaffolds prior to and after soaking scaffold in hot water for 4 hours at 90˚C to remove PVA carrier are illustrated in Figure 3.4, PVA powder and PSS48 sheet were used for comparison. Peaks at 1731 and 1640 cm^{-1} were attributed to carbonyl groups[248] which confirmed the presence of ester and amide functional groups in PSS48 sheet. The intensities of the ester and amide peaks of the washed PSS48/PVA were about 60% of that for the PSS48 sheet, suggesting that some of the PVA had been eliminated after hot water treatment. In addition, these amide and ester peaks were absent in the spectra of PVA polymer. The stretching at 1160 cm^{-1} was assigned to C-O-C bond in the ester group of PSS[248]. The intensity of this peak was weak for the unwashed PSS48/PVA and absent in PVA spectra, while the peak was stronger for the PSS48 sheet and washed PSS48/PVA, confirming that some of the PVA polymer had been removed with water. The peaks at 2840 and 2920 cm^{-1} are corresponding to alkane group present in PSS and PVA, while the broad peak between 3300 and 3500 cm^{-1} was attributed to hydroxyl group in the structure of both PSS and PVA. The intense peak at 1225 cm^{-1} was assigned to the remaining acetate groups in PVA which was not detected for the PSS48 sheet and PSS48 scaffolds. The intensity of the ester peak in the spectra of the washed PSS48/PVA was about 25% of that of the PVA, confirming that some of the PVA had been washed out by hot water. These results confirmed successful electrospun of PSS fibrous scaffold and partial elimination of the carrier polymer from the scaffold.

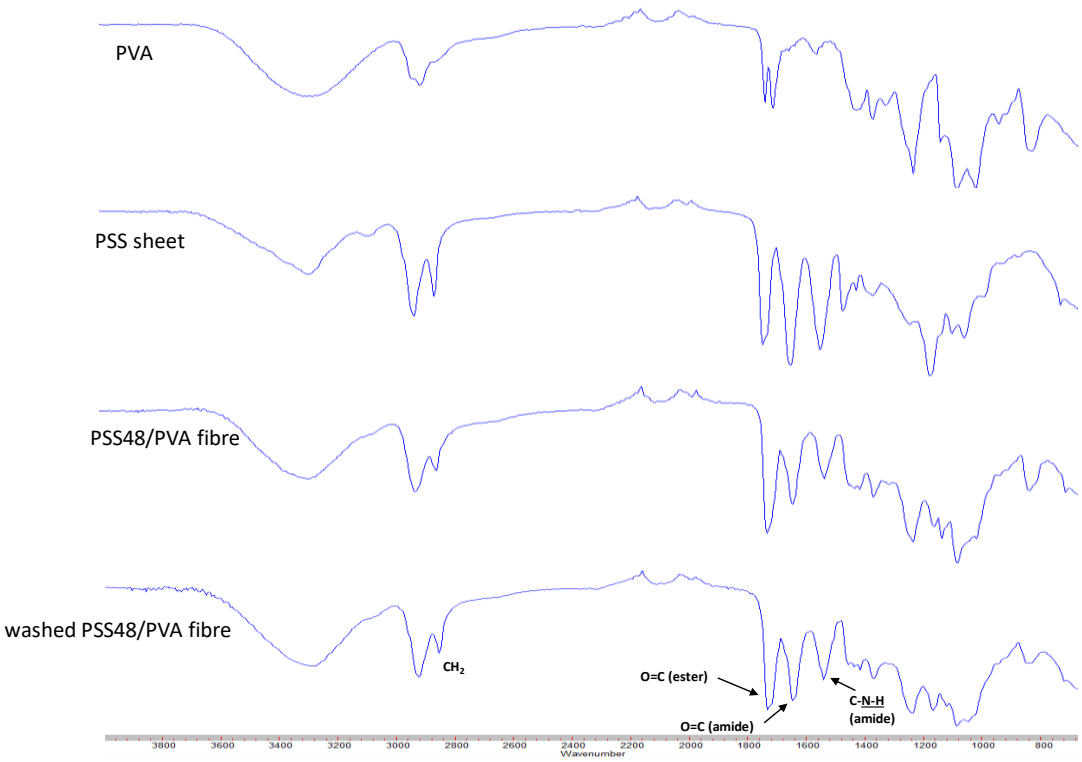


Figure 3.4: FTIR absorbance spectra for PVA, PSS48 sheet, unwashed PSS48/PVA fibre mat and washed PSS48/PVA fibre mat (PSS48/PVA fibre mat by soaking in hot water for 4 hours).

3.3.5. Mechanical properties

The mechanical properties, ultimate tensile strength (UTS), elastic modulus and elongation at break of PSS48 and PSS72 fibrous scaffolds under wet or dry conditions can be seen in figure 3.5, figure 3.6 and figure 3.7. The wet PSS48 and PSS72 fibrous scaffolds demonstrated slightly linear profile, while dry PSS48 and PSS72 fibrous scaffolds exhibited noticeably non-linear curve. The non-linearity of stress-strain curves for PSS scaffolds was attributed to the existence of PVA residual. The dry PSS48 solid film showed almost linear curve consistent with elastomeric polymers. Surprisingly, dry PSS48 and PSS72 scaffolds showed higher UTS and modulus compared to PSS film which was ascribed due to the remaining PVA quantity in the scaffold. PVA is a thermoplastic polymer that has different mechanical properties compared to the PSS materials[249]. Moreover, the elongation percentage of the dry PSS48 and PSS72 fibrous scaffolds were higher than the PSS48 film because the capability of the fibres to realign themselves in the direction of the tensile stress[250]. On the other hand, the UTS and elastic modulus of the wet fibrous scaffolds were significantly lower than dry scaffolds, whilst the elongation percentage were higher. These results can be attributed to the plasticisation effect of water in particular within PVA residuals in the scaffolds[251].

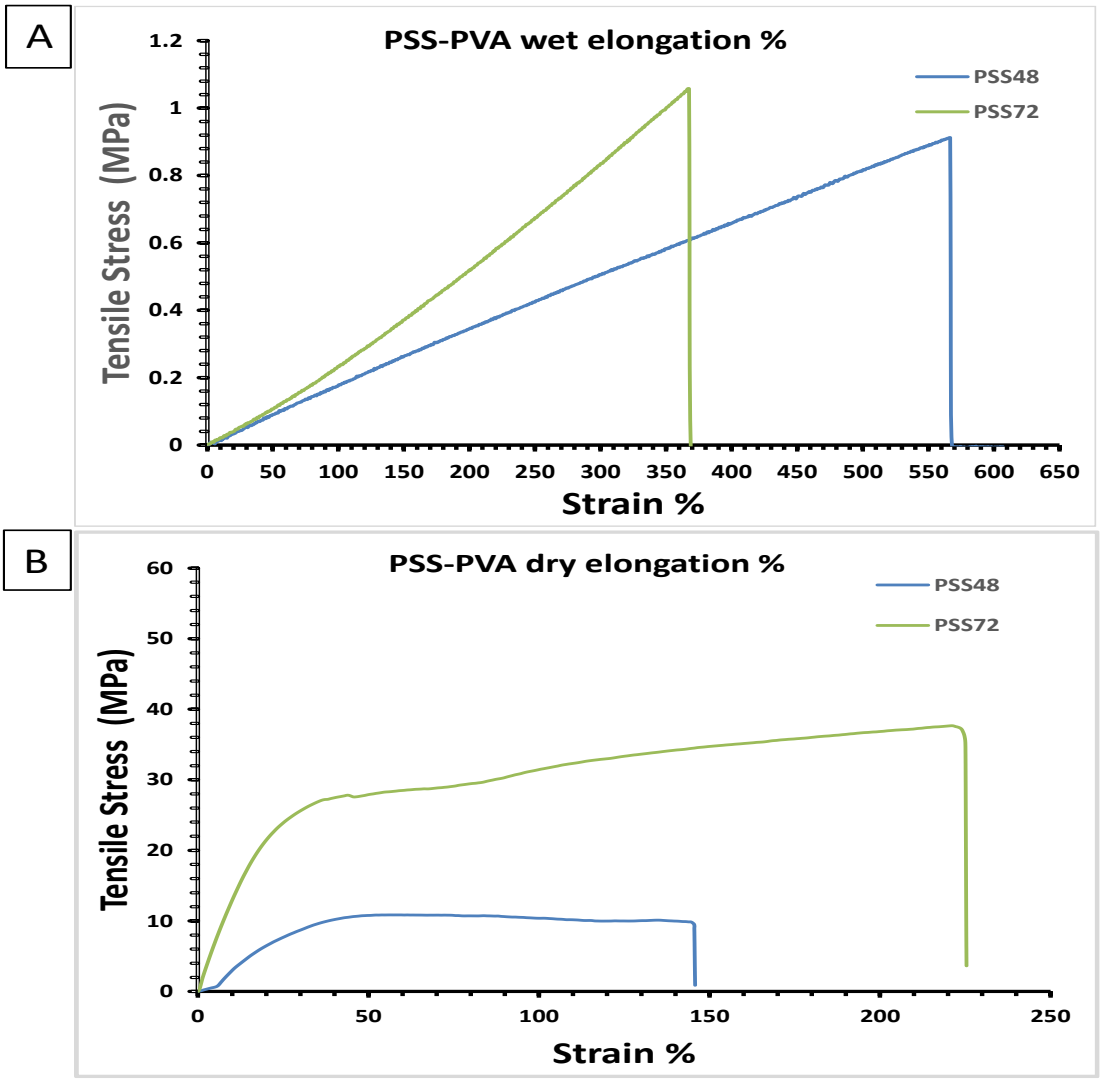


Figure 3.5: Typical stress-strain curves of PSS48 and PSS72 fibrous scaffolds under (A) wet condition and (B) dry condition. The samples were saturated in PBS prior to tensile testing as wet. Triplicates of each specimen were tested to failure.

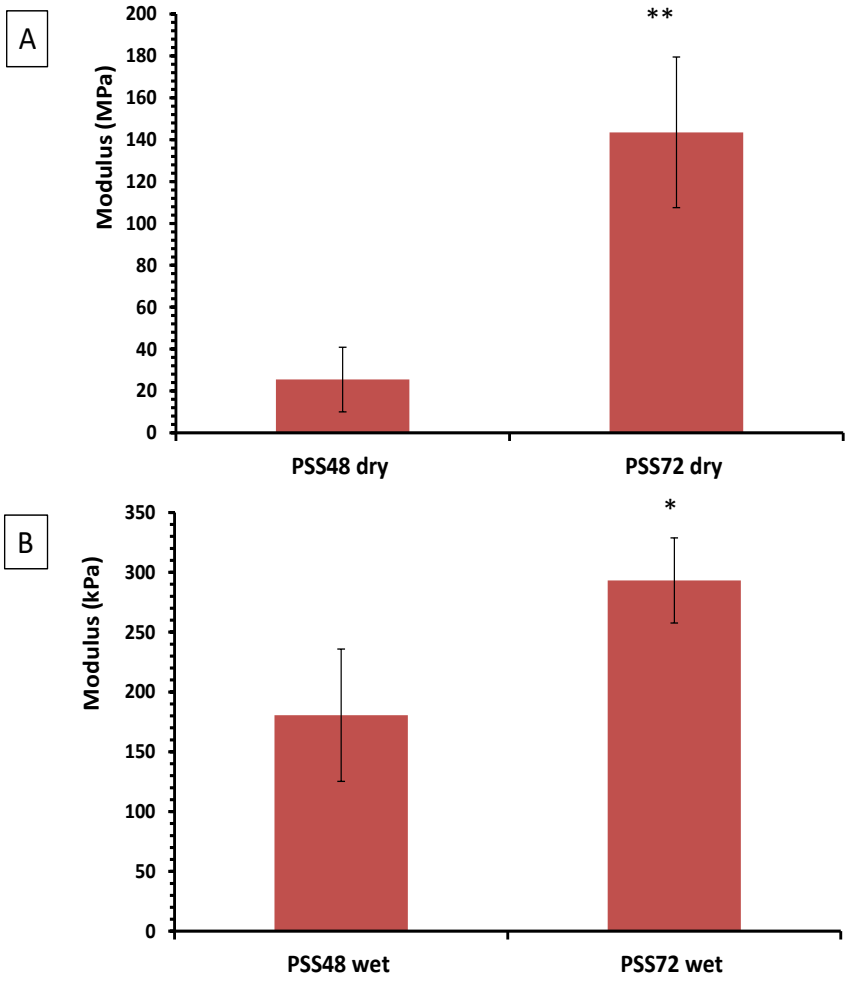


Figure 3.6: The effect of testing conditions (dry and wet) on the tensile modules of PSS48 and PSS72 fibrous scaffolds. The error bars represent one standard error. (n=3)(*$p < 0.05$,**$p < 0.01$).

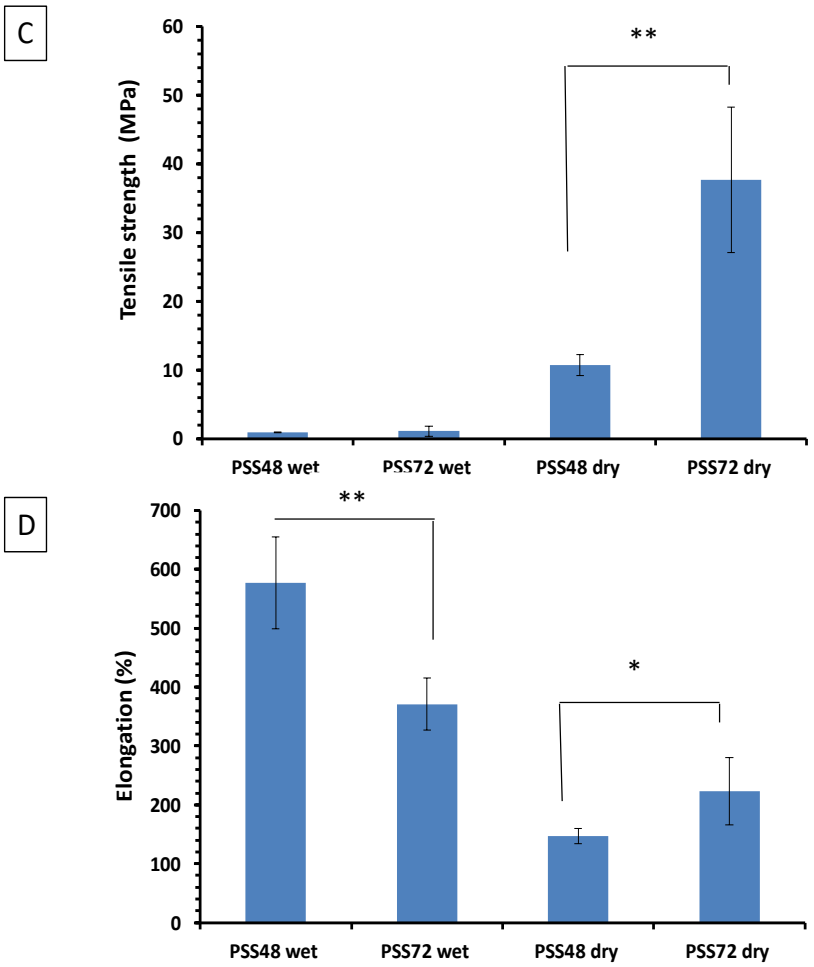


Figure 3.7: The effect of testing conditions (dry and wet) on the mechanical properties of PSS48 and PSS72 fibrous scaffolds. The wet scaffolds were tested after immersed in PBS until saturation; (C) tensile strength and (D) elongation percentage to failure. (n=3)(*$p < 0.05$,**$p < 0.01$).

3.3.6. *In vitro* degradation

In vitro degradation study of PSS48 and PSS72 scaffolds was performed by measuring the percentage of weight change of the scaffolds throughout incubation in PBS for up to 14 days, see figure 3.8. The PSS72 exhibited slower degradation rate compared to PSS48, PSS72 and PSS48 lost 5.5 and 7.5% respectively, after 14 days, which caused by increasing the crosslinking degree that led to a reduction in penetration of water molecules into polymer chain segments. In addition, with the increase of degree of amidation and esterification, the degradation rate would decrease because a higher number of amide and ester bonds would be required to be broken during degradation process[36,62,63]. Moreover, even after 14 days, the SEM images showed that the scaffolds maintained their fibrous structure (Figure 3.9). The gradual degradation of fibrous scaffolds suggested that the scaffold followed surface degradation mechanism[252].

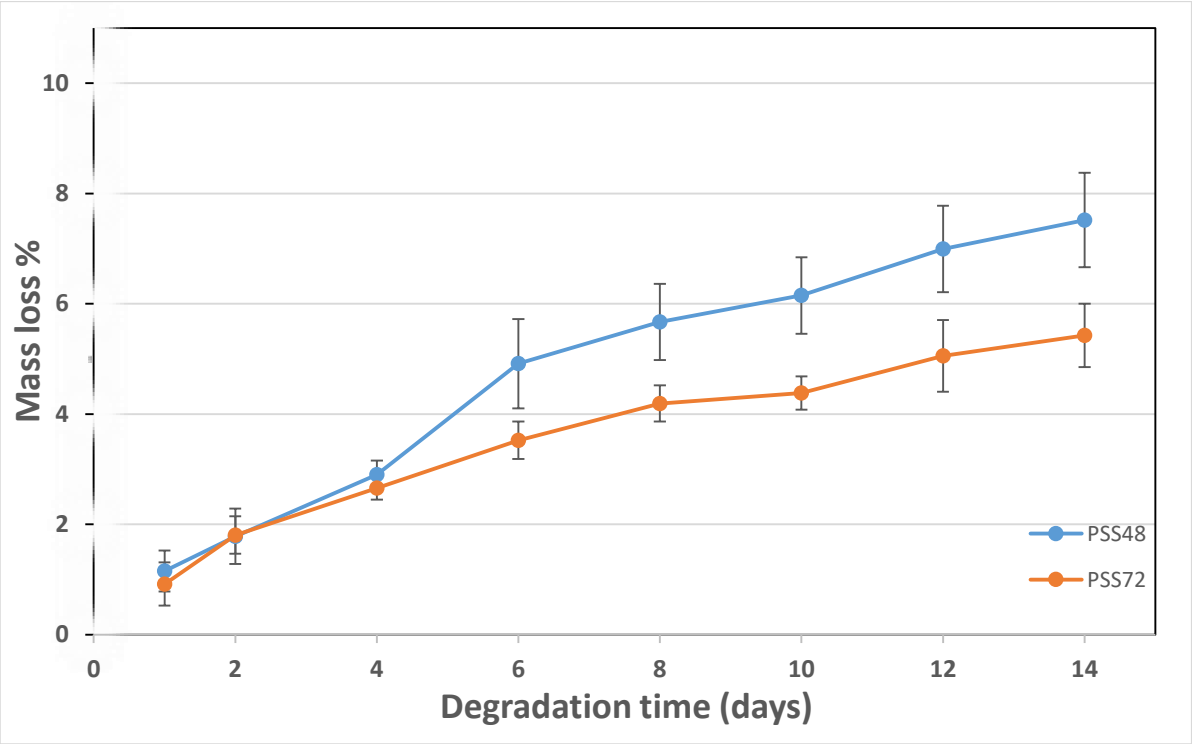


Figure 3.8: Degradation profile of electrospun scaffolds of PSS48 and PSS72. Degradation was determined by weighing the PSS fibrous scaffolds throughout incubation in PBS for 2 weeks at 37^{o}C. (n=4)

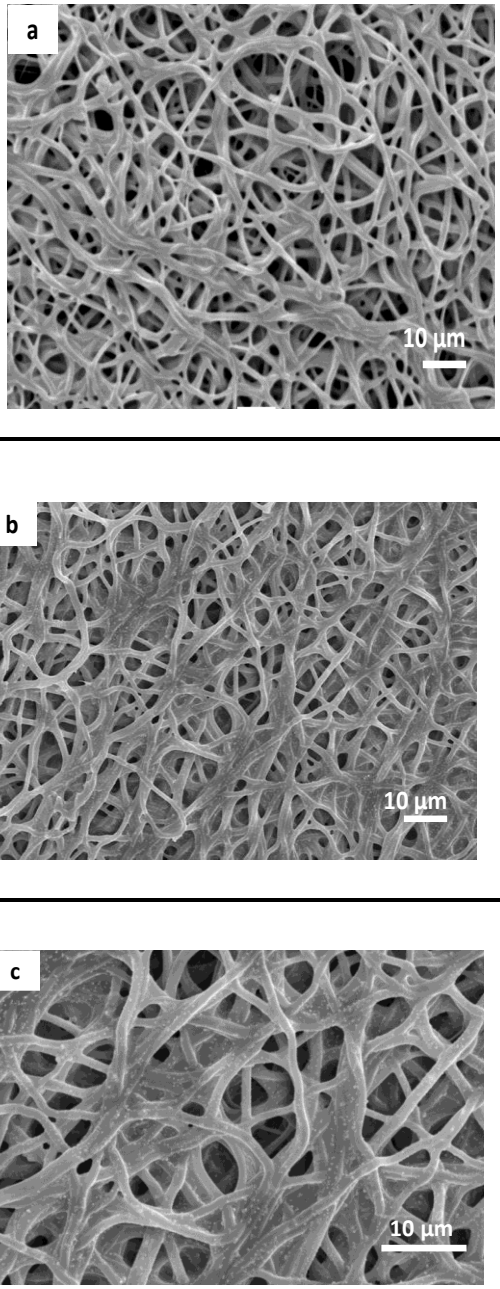


Figure 3.9: SEM micrographs of PSS72 fibrous scaffolds (a) before and (b,c) after 14 days degradation.

3.3.7. Swelling study and pH value

Figure 3.10 illustrates the swelling ratio of PSS48 and PSS72 fibrous scaffold immersed in PBS up to two weeks. The water uptake of the for PSS48 and PSS72 fibrous scaffolds increased initially to 75% and 70% after one week and reached 92% and 112% at week two. The initial increase in swelling ratio could be due to the absorption of water in the first stage of degradation[253].

Acidic degradation products of polymers are commonly followed by *in vivo* inflammatory responses in the surrounding host tissue[220]. Therefore, pH changes of the media (PBS) of the PSS fibrous scaffolds were monitored during degradation (Figure 3.11). It was depicted that both fibrous scaffolds PSS48 and PSS72 showed slightly lower pH throughout the study compared with the initial pH of ~7.4. It was reported that pH of 5% PVA/water solution ranged between 5.0 and 6.5[254], thus the decrease in the pH for PSS scaffolds might be attributed to the gradual release of PVA residuals over the degradation time. Therefore, this mild acidity of degradation media of PSS fibrous scaffolds can be avoided through careful removal of PVA carrier after curing of PSS scaffolds.

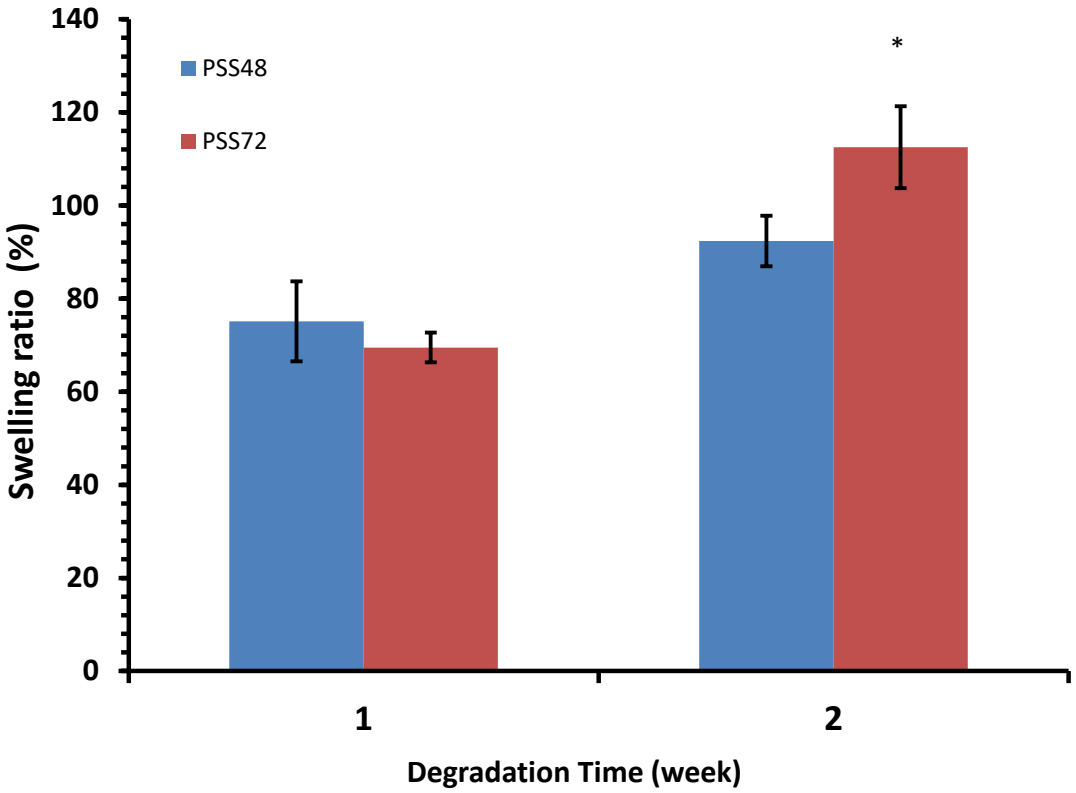


Figure 3.10: Swelling ratio of PSS48 and PSS72 fibrous scaffolds during degradation in PBS at 37^{o}C for up to 2 weeks (n=4) ($p < 0.05$).

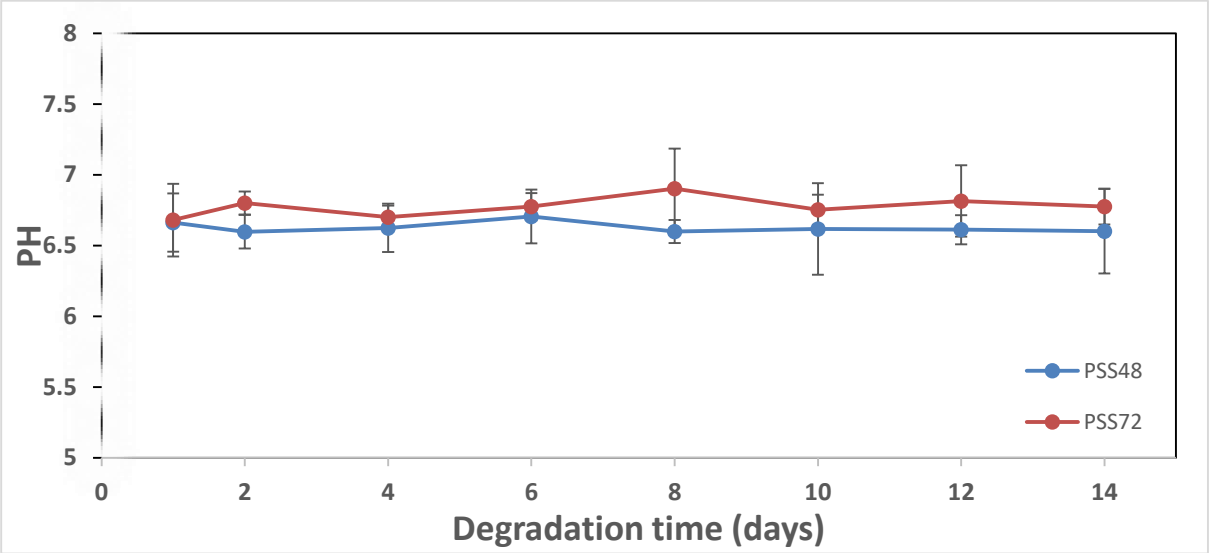


Figure 3.11: Variation in pH values of degradation media for PSS48 and PSS72 fibrous scaffolds throughout degradation for 14 days in PBS.

3.3.8. Cytotoxicity of PSS scaffolds

Cytocompatibility is a very important factor in order to evaluate any biomaterial for medical applications. Since the PSS fibrous scaffolds were crosslinked thermally without using chemical crosslinker, it was expected that the scaffolds would cytocompatibility similar to PSS elastomer. Moreover, the unreacted monomers were eliminated from all fibrous scaffolds which were believed to be harmful for the cells[255]. *In vitro* cytocompatibility assessment was performed through culturing 3T3 cells on different PSS scaffolds. SEM examination revealed good cell attachment with healthy cell morphology that varies from round to elongate in all samples. Figure 3.12 shows the cell morphology of different test samples. After 5 days culture, the number of cells increased and almost covered the whole surfaces of both kinds of the scaffolds. Proliferation of the cells seeded on the scaffolds was examined by Alamar blue assay (figure 3.13), the results showed an increase in the florescence reading from day one to day five which indicates that all the fibrous scaffolds supported cell proliferation. In addition, there was no significant difference in cell proliferation between cells seeded on PSS scaffolds compared with PLGA, suggesting minimal effect of residual PVA. These results indicate that PSS fibrous scaffolds are cytocompatible and can be explored further for different soft Tissue Engineering applications.

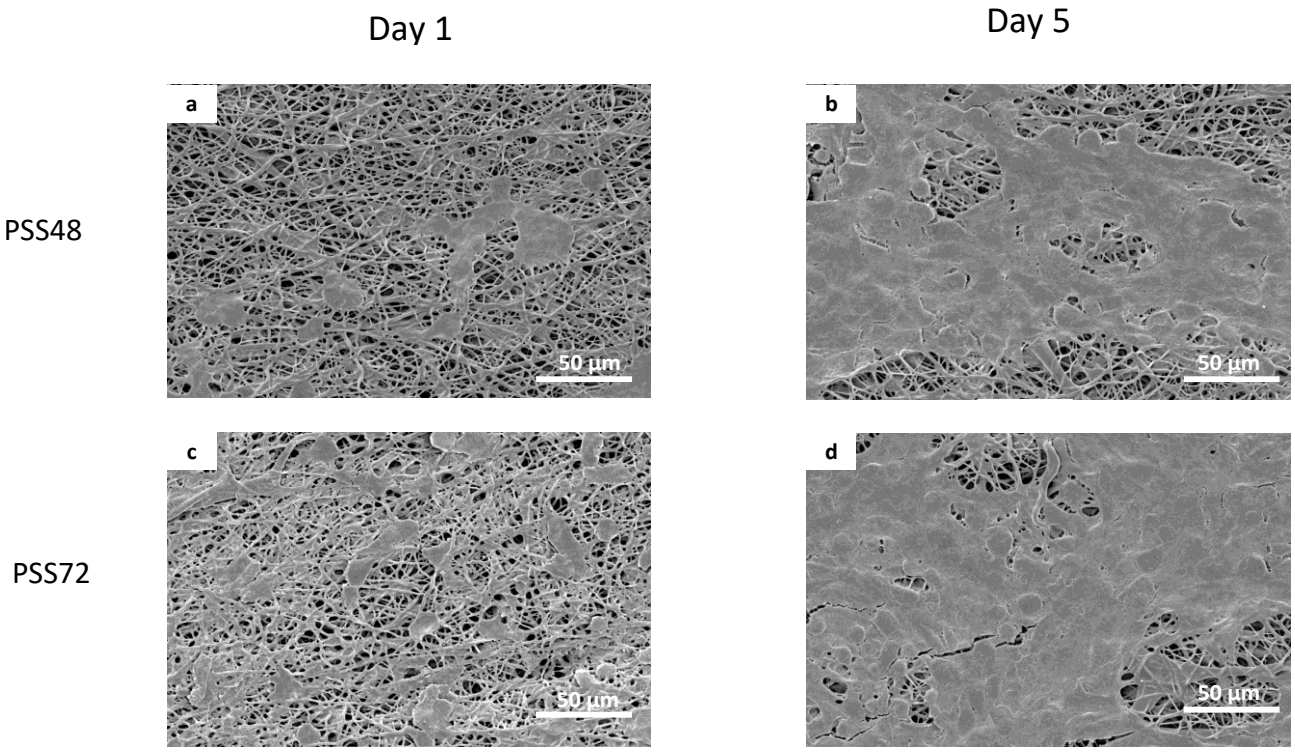


Figure 3.12: SEM images of 3T3 fibroblast cells cultivated on PSS48 and PSS72 fibrous scaffolds.

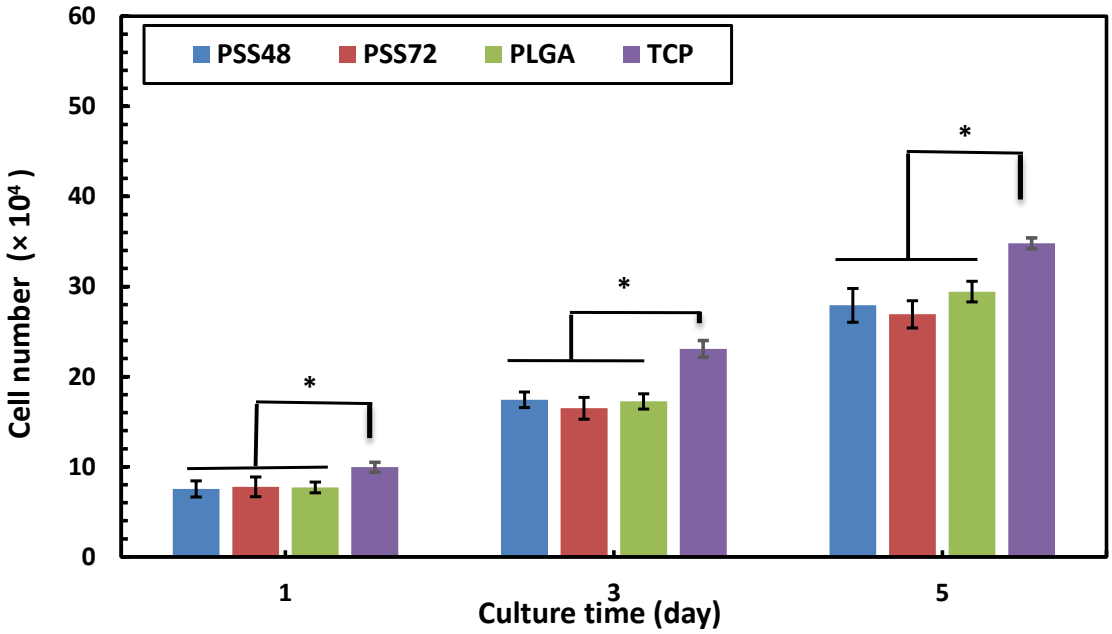


Figure 3.13: Proliferation of 3T3 cells cultured on PSS48, PSS72 and PLGA for 5 days. Four replicates of each sample were tested using PrestoBlue® assay and the averages are presented ±SD ($p < 0.05$).

3.4. Conclusions

In this study, elastomeric fibrous scaffolds of PSS have been electrospun with the assistance of PVA as a sacrificial carrier. Uniform fibrous scaffolds have been produced by optimising electrospinning conditions. PVA polymer could be partially removed by washing with hot dH_2O at 90^oC for 4h after crosslinking. Under hydrated conditions, PSS fibrous scaffolds show non-linear and elastic mechanical properties. Moreover, PSS scaffolds supported adhesion, spreading and proliferation of 3T3 cells *in vitro*. Therefore, PSS fibrous scaffolds could be a candidate for different types of soft tissue engineering applications.

4. Chapter four

Biodegradable poly(serinol sebacate) as a coating material for aligned polycaprolactone fibres

4.1. Introduction

Electrospinning of nanofibres is a technique of growing interest for different applications, such as tissue engineering[256], drug delivery[257,258], wound dressing[259], water filtration[260], biosensors[261] and enzyme immobilisation[262]. The technique was developed by Formhals and has been widely studied and developed over the recent decades[263,264]. Among the techniques of producing nanoscale fibres, electrospinning is unique in terms of its simplicity, controllability and cost-effectiveness. The electrospinning process occurs when a polymer solution possesses sufficient entanglement concentration[246]. A flow jet of a low molecular weight polymer solution breaks up into droplets instead of being a continuous jet, a technique termed electrospraying. In contrast, a polymer solution with sufficient entanglement concentration provides a stable jet, and when the solvent is evaporated the jet becomes unstable and enters the bending instability region, which accounts for fibre drawing on the collector[245].

Number of reports have studied the correlation between polymer entanglement concentration and the ability to electrospin the polymer solution. The first investigation was reported by McKee et al.[265], they observed that the suitable polymer concentration to produce bead-free fibres was 2-2.5 times Ce. Kong et al.[266] investigated the entanglement concentration of amylose starch for effective electrospinning. De Gennes [20] developed a scaling theory by plotting the specific viscosity of linear polymer solutions in a good solvent versus different concentrations in order to estimate the entanglement concentration (Ce)[267]. The plot was divided into four different regimes: a dilute regime with specific viscosity (ηsp) correlated to the power law of $C^{1.0}$; a semi-dilute unentangled regime with $\eta sp \sim C^{1.25}$; a semi-dilute entangled regime with $\eta sp \sim C^{3.7\text{-}4.8}$ and a concentrated regime with $\eta sp \sim C^{3.6.}$. The specific viscosity of the PCL80 semi-dilute unentangled regime was found to be proportional to $C^{1.34}$. This result is close to the predicted value theoretically ($C^{1.25}$) for the semi-dilute unentangled regime of linear polymers in a good solvent[267]. On the other hand, the semi-dilute entangled regime shows that $\eta_{sp} \alpha C^{3.99}$ is in a good agreement with the theoretical values for sodium hyaluronate ($\eta_{sp} \alpha C^{4.1}$)[268]. The entanglement concentration (C_e) of PCL80 was then determined to perform the electrospinning process by plotting the specific viscosity data against solution concentrations.

PCL is an interesting linear polyester due to its many advantages, such as its biocompatibility, biodegradability and low cost synthesis. Moreover, PCL has been approved by the Food and Drug Administration as a biodegradable suture (Monocryl® suture) and drug delivery device (Capronor®) since the 1980s.

These advantages make PCL an attractive polymer for electrospun scaffolds. To enhance the hydrophilicity of PCL scaffolds, bioactive molecules such as fibronectin or collagen have been used in forms of surface coating or blending with PCL[269–271]. However, PCL electrospun scaffold have been developed and amply investigated in literature. To the best of the author knowledge, Correlation between the PCL rheology and fibre structure and alignment have not been previously studied. For example, the relationships of entanglement concentration (C_e) and

molecular weight of a PCL solution on the processes of electrospinning and fibre orientation are deficient.

PSS, a biocompatible and biodegradable elastomer based on the polymerization of serinol and sebacic acid, has been designed and synthesised in our laboratory recently. In general, PSS is synthesised in two steps: polycondensation of equimolar molar of serinol and sebacic acid followed by heat treatment at 110^{o}C to produce cured PSS elastomer. However, high treatment temperature may limit its potential applications with sensitive biomaterials such as proteins or low melting temperature polymers such as PCL.

In this chapter, PCL/PSS composite scaffolds were fabricated by a safe, cost-effective and simple method to enhance the biological responses of PCL in different biomedical applications. PCL scaffolds were prepared using different concentrations of PCL solution and two different molecular weights, to determine the effect of entangled concentration on the ability of electrospinning and to eliminate the instability jet region and control the fibre alignment. The produced PCL scaffolds were then treated with uncured PSS polymer to improve its hydrophilicity and biocompatibility.

4.2. Experimental Procedure

4.2.1. Materials

PCL with two different Mn of 45 and 80 kDa, sebacic acid (99.5%), serinol (98%), hexafluoroisopropanol (HFIP, 99.5%), Sudan Black and trypsin EDTA solution were purchased from Sigma Aldrich. Methanol (99.8%) and dichloromethane (DCM) were purchased from Fisher Chemical. Cell culture supplies including Dulbecco's Modified Eagle's Medium (DMEM) media (Gibco Life Technologies, UK), (1% v/v) L-glutamine, 1% antibiotic (penicillin/streptomycin), (10% v/v) fetal bovine serum (FBS) and 4′,6-diamidino-2-phenylindole (DAPI) were purchased from Thermo Fisher Scientific, UK. All reagents and solvents were used without further purification.

4.2.2. Synthesis of PSS pre-polymer and PSS/PCL composite scaffold preparation

PSS elastomer with serinol to sebacic acid ratio of 1:1 was synthesized according to the procedure mentioned in chapter two. Serinol and sebacic acid were charged into a 100 ml three-neck round bottom flask at 1:1 molar ratio. The flask was heated at 110^{o}C for 16 hours under inert atmosphere (nitrogen gas) under constant stirring. The resultant PSS prepolymer was cooled to the room temperature. The gel point was determined as that when the polymer no longer dissolve in methanol. At the end of the reaction, a viscous yellow coloured PSS pre-polymer was obtained. The products were then subjected to water sedimentation and methanol dissolution repeatedly to remove unreacted monomers. Thereafter, the PSS was dissolved in methanol at a concentration of 0.3 and 0.6 g/ml with continuous stirring at room temperature for 24 hours. The PSS solutions were dropped onto the surface of aligned PCL scaffolds at 20 µl/cm^2 using an adjustable volume micropipette, then the scaffolds were dried using freeze dryer to obtain PSS/PCL scaffolds. The produced composite scaffolds were coded as P3 and P6 based on the concentration of the PSS solution.

4.2.3. Solution preparation and electrospinning setup

PCL solutions of different concentrations were prepared by dissolving the polymer in DCM under continuous stirring at room temperature for 24 hours. The process of electrospinning was performed by using an Electrospinning kit (IME Technology), which has a special syringe pump (Harvard) equipped with humidity and temperature sensors. The PCL solution was placed in a 10 ml glass syringe (Becton Dickinson®) and then mounted in the syringe pump. The power supply was connected to the 22 gauge blunt needle (Sterican®) and 20 cm working distance was used. The solutions were injected at a constant flow rate of 1 ml/h and under voltage of 20 kV, while the temperature was kept constant at 20±1^{o}C. Fibres were collected on aluminium foil which was placed around the mandrel collector.

4.2.4. Rheology

PCL/DCM solution of concentrations ranged from 1 to 10% (w/v) were prepared using the two different molecular weights for rheological characterisation and to determine concentration regimes. Zero shear rate viscosity was measured using concentric cylinders geometry in a strain controlled rheometer (Anton Paar) at 25 ± 0.1 C^{o}. The shear rate swept from 1 to 1000 s^{-1}.

4.2.5. SEM of the electrospun scaffold

The morphology of the PCL electrospun scaffolds and PSS/PCL composite scaffolds were examined using a scanning electron microscope (JSM-6060LV). The scaffolds were placed on the carbon tape on a metallic holder and then coated with a thin layer of gold using a gold coater (Leica EM SCD005) at 10 mA for 280 seconds. Diameter of the produced nanofiber were measured from the SEM micrographs of randomly selected 200 fibres using ImageJ software(National Institutes of Health, USA) according to the method published erilerly[242]Fast Fourier Transform (FFT) was used to evaluate fibre alignment; FFT converts the real space in the data image into a corresponding mathematically frequency space[272]. The SEM image was converted to a TIF file and 8-bit greyscale captured at 1024×1024 pixels using ImageJ software. A circular projection was drawn on the FFT image and a radial sum was then conducted to generate a graphical depiction of the frequency distribution. The degree of fibre alignment in the SEM images was reflected by the shape and height of the peak in the FFT plot[273].

4.2.6. Fourier Transform Infrared (FTIR)

The chemical bonds of the P3, P6 and PCL composite scaffolds were investigated by Fourier Transform Infrared (FTIR) spectroscopy, The FTIR spectra was in range of 700–4000 cm^{-1} and recorded on Thermo Scientific Nicolet IR 200 FT-IR. The data were analysed using Omnic 8.0 software (Thermo Scientific).

4.2.7. Water contact angle

The water contact angles of PCL and PSS/PCL composite scaffolds were measured using a Cam 200 machine (KSV, instrument Ltd) (n = 3). To place a droplet of distilled water (dH_2O) on the surface of the samples, a 21-gauge needle was used. The image of the water droplet was captured using a digital camera and the contact angle was measured using Cam 200 software (KSV, instrument Ltd).

4.2.8. Cytocompatibility

4.2.8.1. Sterilization of Nanofiber Mats.

All the produced fibrous scaffolds were cut into discs of 15 mm diameter: 15 mm and placed in 24 well-plate and supported with sterile rings (Cell Crown, Sigma-Aldrich) to prevent the fibrous scaffold from floating in the culture medium. Afterwards, the composite scaffolds (P3, P6) and control PCL aligned fibrous scaffolds were sterilised under UV light for 30 minutes, followed by washing three times with PBS prior to cell seeding.

4.2.8.2. Cell culture

The fibroblast cells (3T3) cells were cultured in Dulbecco's Modified Eagle Medium (DMEM), supplemented with 1% Penicillin/Streptomycin and 10% Fatal Bovine Serum (FBS). The cell culture medium was used as a negative control, and the PCL aligned fibrous scaffold were used as a positive control. The scaffold discs were placed in 48-well plates (Falcon, BD Bioscience, UK) containing 1 ml of DMEM, and then seeded with fibroblast cells at the density of 10×10^4 cells/sample. The fibrous scaffolds were then cultured under standard incubation conditions of 5% CO_2 humid air and at 37 ^oC. The media was change every 2 days.

4.2.8.3. Cell viability and attachment

Fibroblast cells were seeded on the composites scaffolds and harvested after 12 h. The fibrous scaffolds were washed with PBS to remove unattached cells and fixed with 3% glutaraldehyde for 2 hours, and then washed with PBS. Subsequently, the scaffolds were dehydrated with a series concentration of alcohols (50%, 70%, 90%, 100% v/v). Spreading and attachment of the cells were assessed using SEM.

4.2.8.4. Cell proliferation

The cell proliferation was examined over a period of 5 days using PrestoBlue (PB) Assay (thermos fisher scientific, UK) according to the manufacturer's protocol. The Prestoblue assay can be used to analyse the time-dependant cell proliferations, based on the ability of viable cells to reduce resazurin dye (blue) to resorufin (pink). Briefly, seeded scaffolds (n=4) were transferred to a new 48-well plate containing fresh culture medium. PB solution (10% v/v) was added into each well and incubated at 37°C for 2 h. Reduced PB (100 µL) was then placed in 96-well plate to measure the fluorescence intensity using microplate reader at excitation/emission wavelengths of 530/590 nm. Cells seeded on TCPs was used as control.

4.2.8.5. Fluorescent nuclear staining

The composite scaffolds and PCL fibrous scaffolds were seeded with 3T3 fibroblast cells were fixed in 4% paraformaldehyde solution after 5 days in medium culture to examine cell attachment and spreading, and then washed twice with PBS. Cells membrane permeabilisation with 300 µl of blocking buffer (PBS, 10% FBS, 1% triton) for 30 minutes. Cell nuclei were stained with DAPI for 5 mins. DAPI solution was prepared according to manufacture protocol and diluted 1:1,000 in PBS. Thereafter, the scaffolds were washed trice in PBS and fluorescence images were examine using a Zeiss LSM 510 Meta laser scanning confocal microscope, equipped with a 543 nm HeNe laser.

4.3. Statistics

Statistical analysis was expressed as mean ± standard deviation (SD), and carried out by one-way analysis of variance (ANOVA) with Tukey's post-hoc analysis. The data were considered to be significantly different if p-value becomes less than 0.05.

4.4. Results and discussion

4.4.1. Rheological properties of PCL solutions

The solution concentration regimes of PCL were determined using rheology measurements. Flow curves of viscosity as a function of shear rate for PCL80 (Mn = 80 kDa) in DCM with varying solution concentrations are given in Figure 4.1. All PCL solutions followed a Newtonian behaviour over this range of shear rates up to 7% (w/v) of PCL80 and 13% (w/v) of PCL45. However, as PCL concentrations were increased, shear thinning would become apparent.

The specific viscosity of the PCL80 semi-dilute unentangled regime was found to be proportional to $C^{1.34}$. This result is close to the predicted value theoretically ($C^{1.25}$) for the semi-dilute unentangled regime of linear polymers in a good solvent[267], and also for the reported value of Gelose starch in 100% Dimethyl sulfoxide solution ($\eta_{sp} \alpha C^{1.4}$)[266]. On the other hand, the semi-dilute entangled regime shows that $\eta_{sp} \alpha C^{3.99}$ is in a good agreement with the theoretical values and some reported experimental values for nylon-6,6 ($\eta_{sp} \alpha C^{3.28}$) [268] and sodium hyaluronate ($\eta_{sp} \alpha C^{4.1}$)[268].

The zero shear viscosities (η_0) of different PCL molecular weights were approximated determined from the viscosity flow curves. The solution contribution to η_0 was evaluated by measuring specific viscosity (η_{sp}) of the PCL solutions, where $\eta_{sp} = (\eta_0 - \eta_s)/\eta_s$ and η_s is the viscosity of the solvent (DCM). The entanglement concentration (C_e) of PCL80 was determined by plotting the specific viscosity data against PCL solution concentration. Figure 4.1 shows the η_{sp} dependence of the concentration for PCL 80. The C_e was determined to be 5.5% (w/v) from the intercept of the slopes of semi-dilute unentangled and semi-dilute entangled regimes (Figure 4.2).

The flow curve of PCL45 was also performed (Figure 4.3) and the C_e value was determined from the change in the power of the semi-dilute unentangled from 1.347 to 4.999 at 7 wt%. Decrease of the PCL molecular weight from 80 to 45 kDa led to increase in the entanglement concentration from 6 to 8 wt%. The reason for this is that the PCL solution with high molecular weight has higher hydrodynamic volume and requires a lower solution concentration before the chains start entangling and constraining one another.

Moreover, we hypothesised that the fibre orientation can be adjusted by reducing the bending instability region of the jet, providing patterned deposition of the fibre on the surface of the mandrel collector.

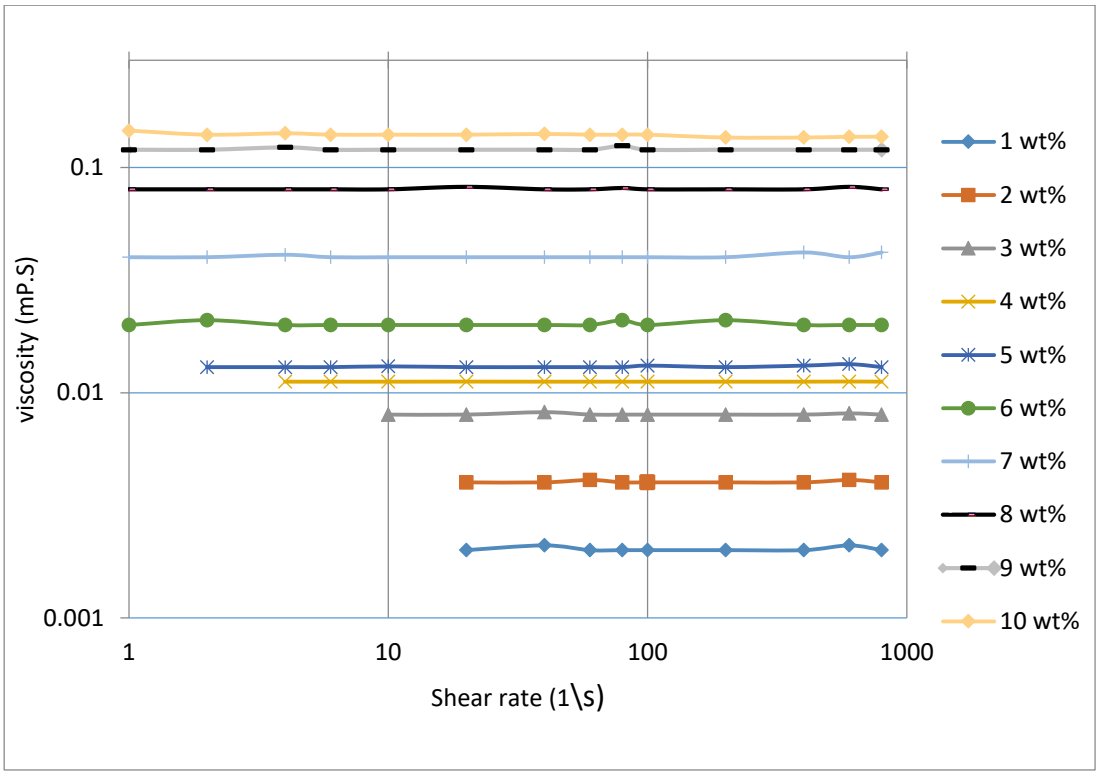


Figure 4.1: Viscosity curves of PCL 80 as a function of PCL concentration (w/v %).

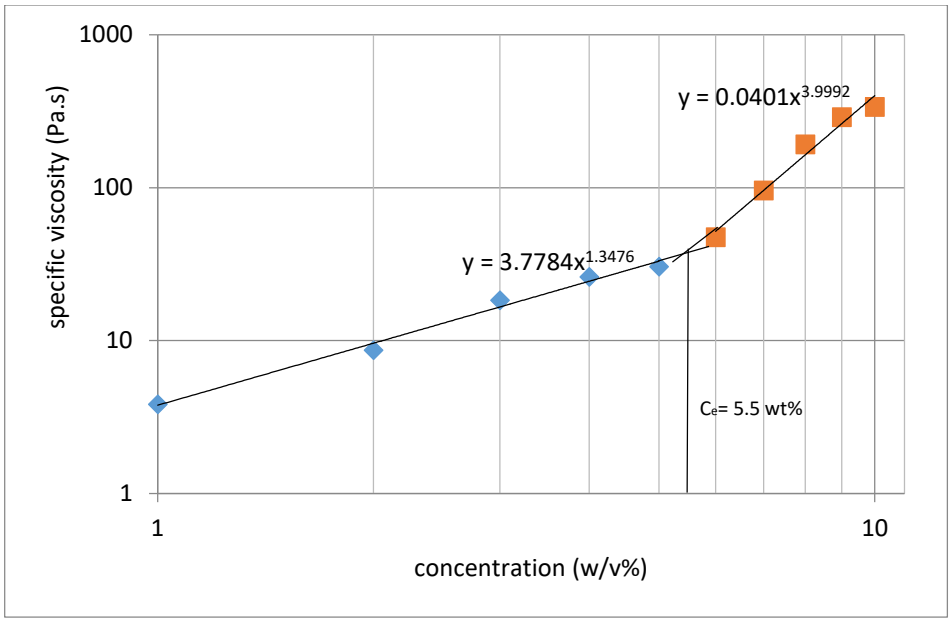


Figure 4.2. Plot of specific viscosity dependence on PCL80 concentration to determine the entanglement concentration.

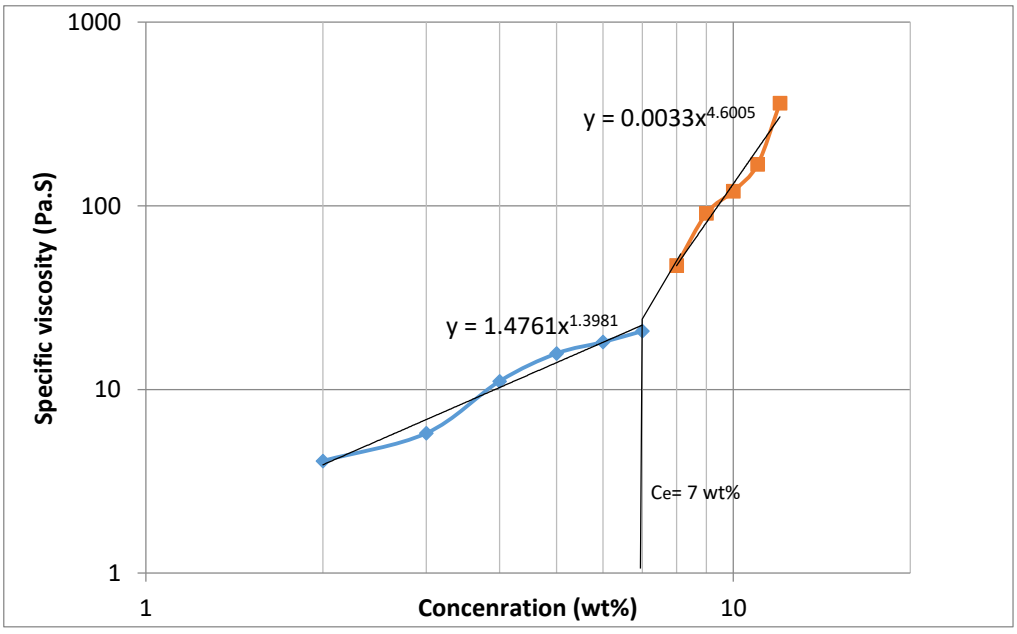


Figure 4.3: Plot of specific viscosity dependence on PCL45 concentration

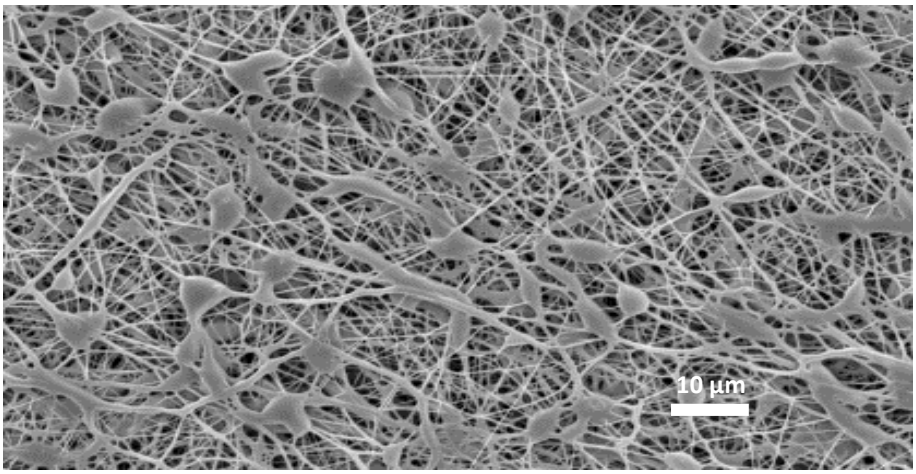
4.4.2. Electrospinning

Different concentrations of PCL/DCM solution from each molecular weight were electrospun. The experiments were performed using a stationary collector and SEM was utilised to evaluate the fibre morphology. In addition, good spinning condition is to produce uniform, continuous and beads free nanofibres (Figure 4.4c) while poor condition would lead is too short and weak fibres to be removed from the collector, and lack of uniformity and presence of beads are also expected (Figure 4.4a, 4.4b). It should be noted that all the parameters during the electrospinning process were held identical; ~20^{o}C temperature, 50% humidity, 4 ml/h flow rate from the nozzle of the syringe, and a 20 cm the distance between the tip of the syringe and the collector.

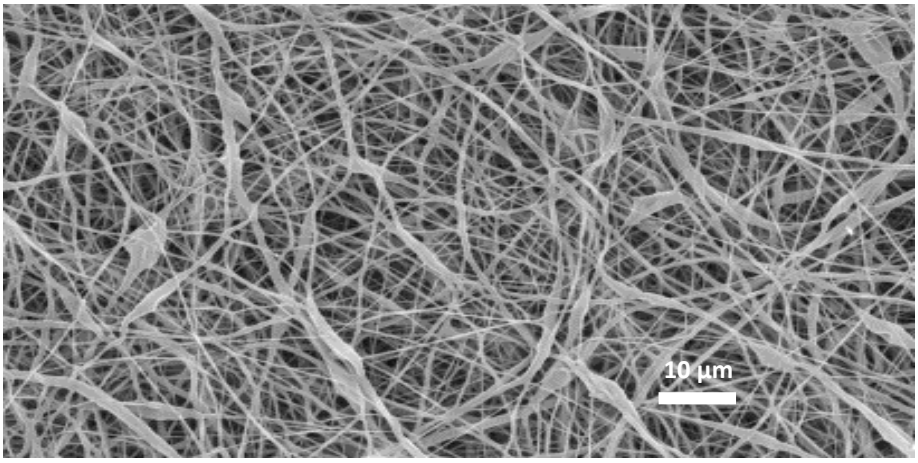
Figure 4.5 shows SEM images of PCL 80 electrospun fibres obtained from three different concentrations (6, 7 and 10%). For the solution with concentration below C_e (5.5%), the entanglements between polymer chains were not sufficient to yield a stable jet and overcome the solution surface tension, only irregular droplets were produced. When the concentration of PCL 80 solution increased to 5.5% (C_e concentration), irregular fibres and few droplets were observed. At this concentration, the polymer chains started to get close and constrain each other.

Between 6 and 9 wt %, above the C_e value, the average fibre diameter increased (Figure 4.5) and the entanglement between polymer chains became high enough to stabilise the electrospinning jet. However, some beads were still present. For the 10 wt% concentration, a solution of almost double the C_e, the entanglement level of the polymer chains became adequate to prevent any bead formation (Figure 4.5c), to obtain a highly stable jet and consequently generate uniform continuous fibres. These findings revealed a good agreement with the previously reported results [265,266,268].

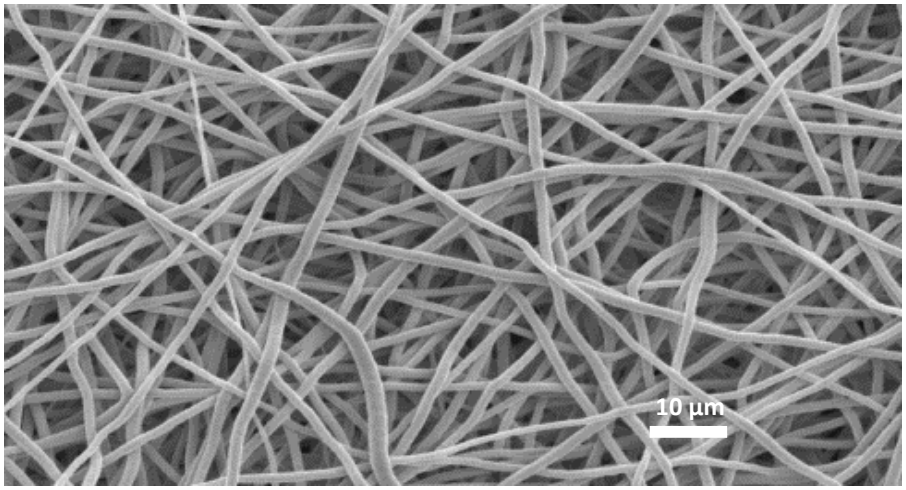
The same electrospinning optimisation experiment was conducted on a lower molecular weight PCL (PCL 45). Figure 4.4a shows SEM micrographs of electrospinning of 8 wt% of PCL45 solution which resulted in irregular fibres and beads. Stable jet and uniform fibres were obtained when the concentration was increased above C_e of PCL 45/DCM solution (12%). Electrospinning of 15 wt% solution produced bead-free fibres with an average diameter of 1.5 µm. Therefore, to produce bead-free fibres, the solution concentration should be higher than C_e Finally, as PCL 45 possesses a higher C_e than PCL 80, the equivalent fibre diameter with from different molecular weights can be obtained by increasing the concentration of PCL45.



a: 8 wt%

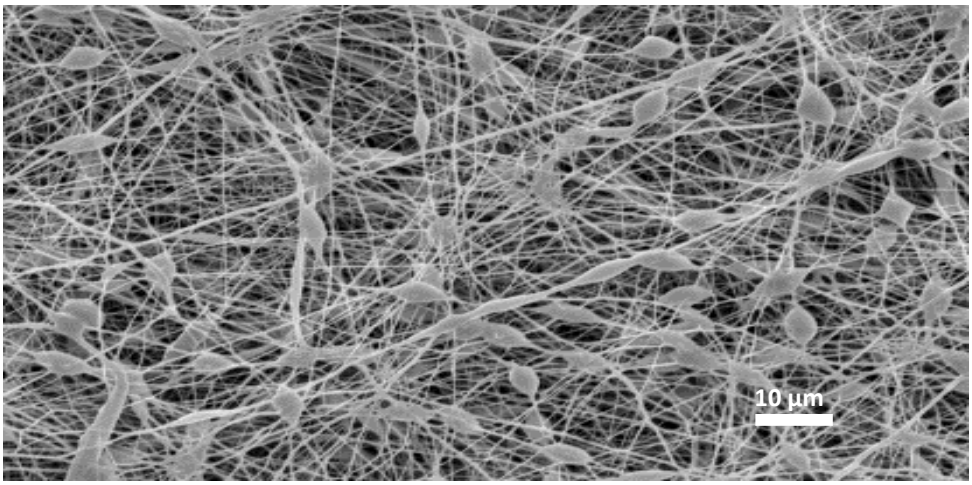


b: 10 wt%

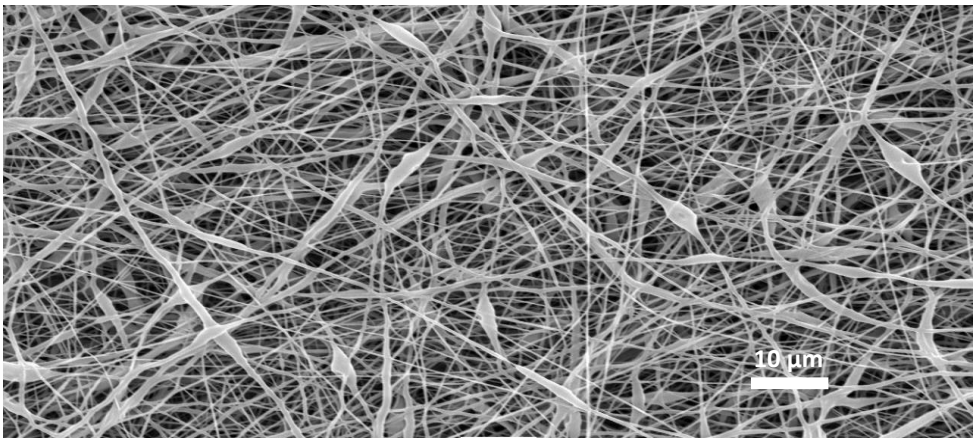


c: 15 wt%

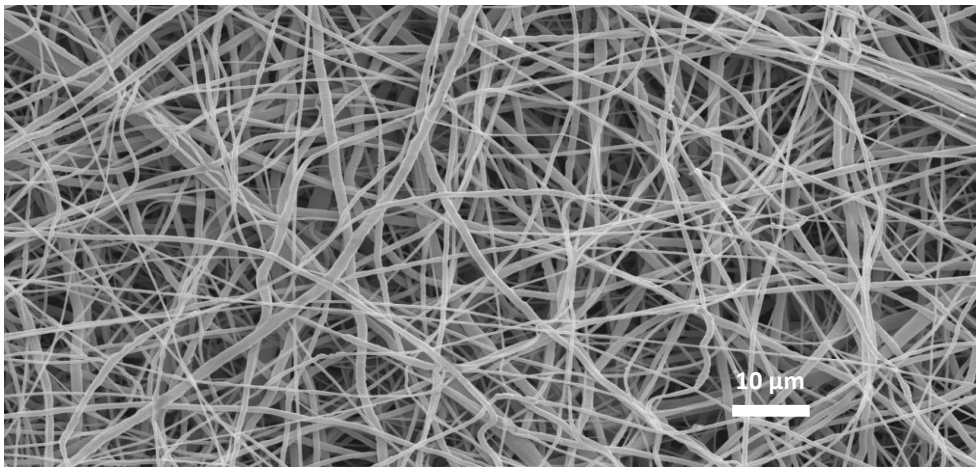
Figure 4.4: SEM micrographs of electrospun PCL 45 fibres (C_e = 12 wt%) at different concentrations.



a: 6 wt%



b: 7 wt%



c: 10 wt%

Figure 4.5: SEM images of electrospun PCL 80 fibres (C_e = 5.5 wt%) at different concentrations

4.4.3. Fibre alignment

Controlling the electrospun fibre alignment has been achieved by different techniques. For example, the alignment degree can be adjusted by varying the speed of the rotating mandrel[273,274]. Li et al. used two parallel electrodes to control the fibre orientation[275]. External electric field method has been used to decrease the bending instability by using auxiliary electrodes to manipulate the deposition area and jet path[157]. However, it is difficult to have a universal design for special equipment. Even at high rotational speeds with the mandrel collector, the degree of fibre alignment remains challengeable. Some studies reported poor alignment despite using very high rotational speeds[276,277]; however, a combination of using a mandrel collector and supplementary electrodes has found to offer better control on the fibre alignment[278,279]. The effects of the solute on solution viscosity, concentration of solvent, conductivity and process parameters such as flow rate of the polymer solution, the distance between the needle tip and the collector, the applied voltage and humidity have been extensively investigated for a range of natural and synthetic polymers[118,280,281]. In addition, researchers have also explored the effects of varying solution concentration on the fibre morphology[116].

The experimental observations of the electrospun jet and bending instability regions using 5 wt%, 10 wt%, 12 wt%, 14 wt%, 16 wt%, 18 wt% and 20 wt% of PCL 80 are shown in Figure 4.6. The stable jet and bending instability regions with C_e of 5.5 wt% were unclear due to the interruption of the droplets during the electrospinning process. When the polymer solution increased to 10 wt%, a stable jet was clear due to the increase in polymer chain entanglement and overcame the surface tension (Figure 4.6). However, the bending instability started midway of the distance between the nozzle and the surface of the stationary collector. By using a low rotational speed of 100 rpm, the fibre was deposited randomly due to buckling on the surface of the collector (Figure 4.7(a)). Furthermore, even at high speed (2000 rpm), no fibre alignment was observed.

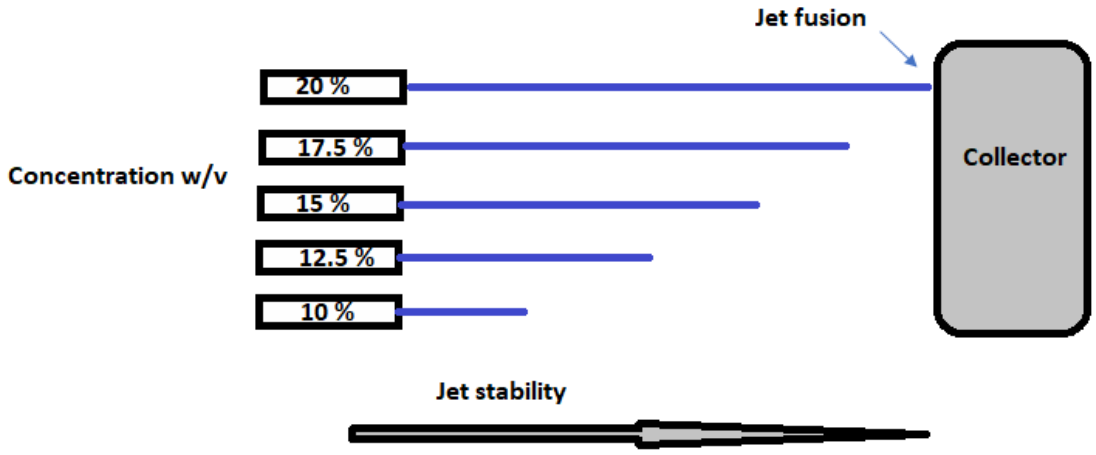
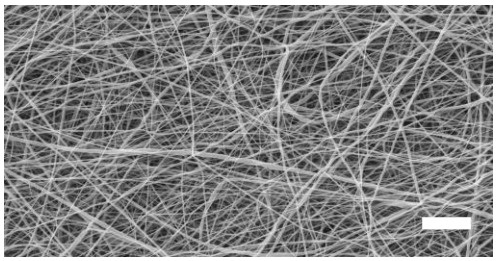


Figure 4.6: Schematic of the electrospinning stable jet using different PCL80 solution concentrations.

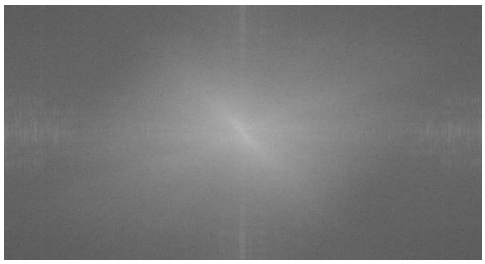
For the polymer solutions between 10 wt% and 20 wt%, the polymer chain entanglements increased, the length of the stable jet region increased gradually (Figure 4.6). Nevertheless, at high rotational speeds (2000 rpm), the fibre alignment increased due to the inhibition of the bending instability region.

At 20 wt% polymer concentration, the bending instability region was completely suppressed between the needle and the mandrel collector; the jet travelled in a straight line and the deposition area grew from a small spot to a circle of a few millimetres in width. On the other hand, no bending instability region was observed either with the mandrel collector, with slight deviation near the surface of the collector and fibre angle, which may be due to air flow induced by the rotation of the collector or by tugging of the jet by the mandrel collector. At higher rotational speed (2000 rpm), the fibre was highly aligned (Figure 4.7(c)).

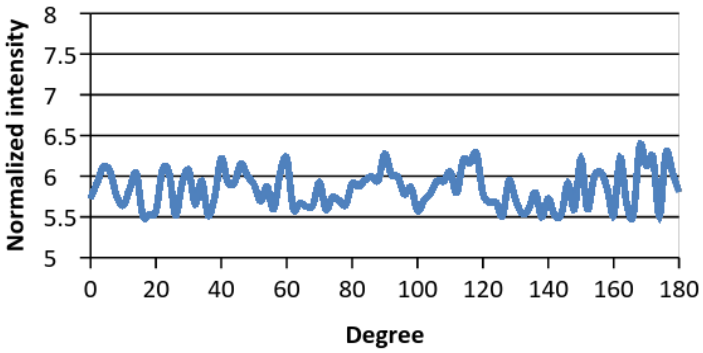
FFT analysis was used to characterise the electrospun fibre alignment. The degree of alignment was evaluated by the shape and height of the peak generated by the plot of the pixel intensity versus the angle of acquisition. PCL 80 electrospun from a concentration of 10 wt% showed no evidence of fibre alignment at a rotational speed of 2000 rpm; the highest value of the intensity was 6.25 arbitrary units (Figure 4.7(a)). FFT values for PCL 80 electrospun from a concentration of 15 wt% increased as a function of concentration (Figure 4.7(b)). At a concentration of 20 wt%, alignment values exhibited evidence of fibre alignment with intensity values exceeding 7 (Figure 4.7(c)).



a: PCL80 (10 wt%)

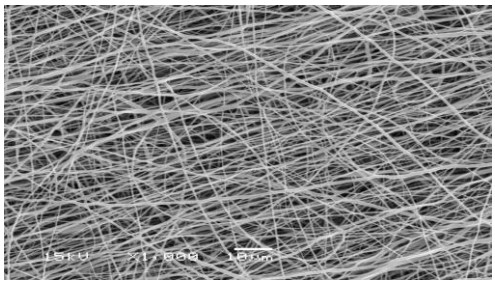


b: PCL80 (10 wt%)

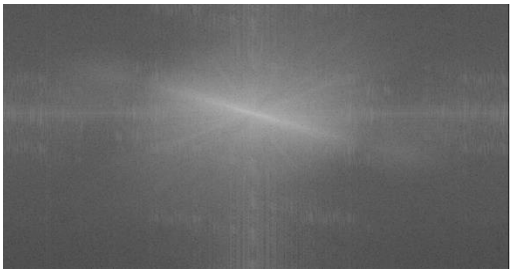


c: PCL80 (10 wt%)

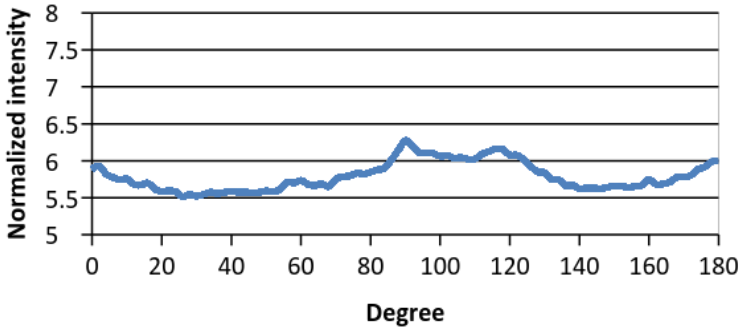
Figure 4.7(a): SEM images of random electrospun PCL80 fibres (a), FFT output images (b) and plots of Pixel intensity versus the angle acquisition(c)**.**



d: PCL80 (15 wt%)

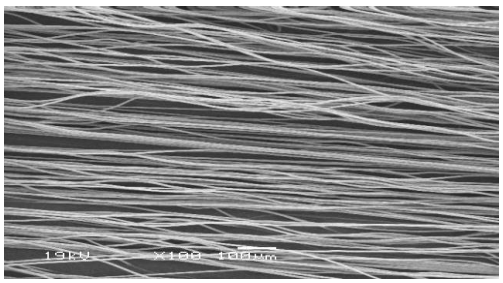


e: PCL80 (15 wt%)

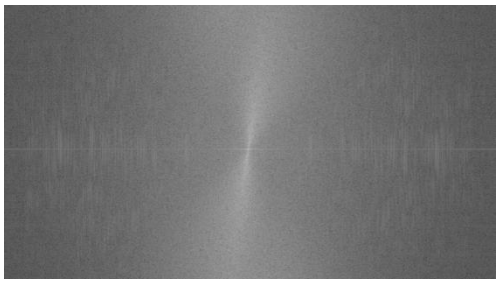


f: PCL80 (15 wt%)

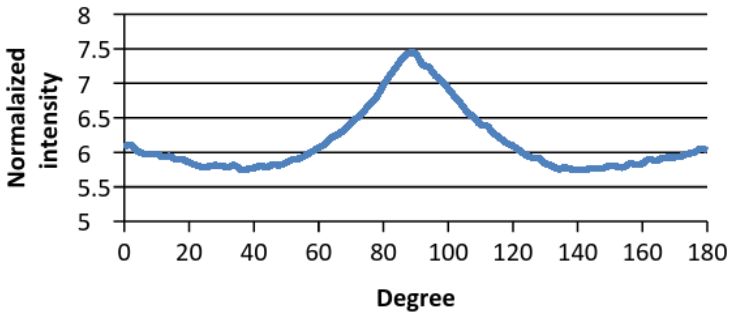
Figure 4.7(b): SEM images of a partially aligned electrospun PCL80 fibres (a), FFT output images (b) and plots of pixel intensity versus the angle acquisition (c).



h: PCL 80 (20 wt%)



i: PCL 80 (20 wt%)



j: PCL 80 (20 wt%)

Figure 4.7(c): SEM images of an aligned electrospun PCL80 fibres (a), FFT output images (b), and plots of pixel intensity versus the angle acquisition (c).

4.4.4. Chemical characterization

The FT-IR spectra of the P3 and P6 composite scaffolds were compared with PCL aligned scaffold and PSS pre-polymer to study their composition (see Figure 4.8). The FT-IR spectrum of PCL aligned scaffold displaying characteristic carbonyl stretching vibration at 1721 cm^{-1} and also showed peak at 1161 cm^{-1} corresponding to C-O-C[282,283]. PSS pre-polymer displayed carbonyl stretching vibration at 1722 cm^{-1}, amide carbonyl absorption at 1655 cm^{-1} and vibration of N-H at 1562 cm^{-1} as reported earlier in chapter two.

In case of P3 and P6, the carbonyl stretching peaks were observed at PCL and PSS pre-polymer spectra were also observed in P3 and P6 scaffolds, while amide carbonyl absorption, stretching of hydroxyl groups and vibration of N-H were presented in PSS pre-polymer, P3 and P6 scaffolds spectra and absent in the spectra of aligned electrospun PCL scaffold as expected. Altogether, these results confirm presence of both PCL and PSS in the composite PSS/PCL scaffolds.

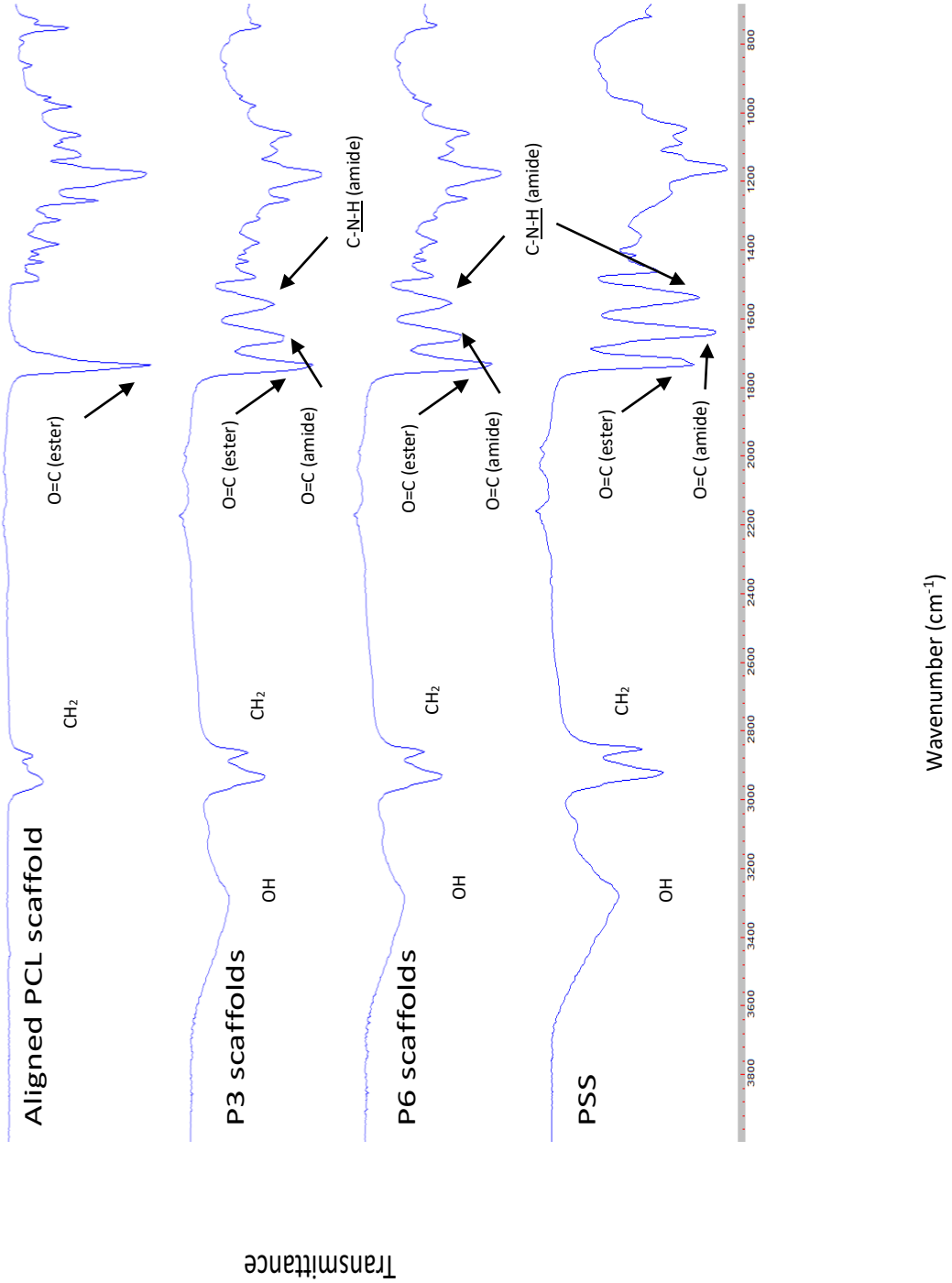


Figure 4.8: FTIR spectra of aligned PCL80 scaffold, P3, P6 and PSS pre-polymer synthesised at 110ºC for 22 hours showed strong signals of amide and ester bonds at 1650 cm^{-1} and 1760 cm^{-1}, respectively.

4.4.5. Characterization of PCL Nanofibers and PSS/PCL composites

The diameter of PCL aligned fibre was found to be in range of 2.14-7.4 μm, with a mean diameter of 4.34±0.34 μm. The SEM images of the PCL aligned nanofibers produced by spinning 20% of PCL80, P3 and P4 scaffolds are shown in Figure 4.9. The images of all electrospun scaffolds showed smooth and uniform fibre. However, P3 and P4 scaffolds show some blocked pores as a result of post-treatment with PSS pre-polymer.

4.4.6. Water contact angles

Contact angle measurements were performed to explore the hydrophilicity of the PCL80, P3 and P6 scaffolds. The water contact angle for PCL aligned scaffolds was found to be 104.3±8.2°. After treatment with PSS pre-polymer, the water contact angles decreased to 76.4±6.3° and 74.2±3.9° for P3 and P6 respectively. This reflects the enhancement in the hydrophobicity of PCL scaffolds by modification with PSS. This reduction in the water contact angles could be attributed to the presence of free amine functional groups[284]. Consequently, P3 and P6 are expected to own better cytocompatibility which would beneficial for tissue engineering applications. However, the topography of the aligned PCL scaffold differed significantly from that of the P3 and P6 scaffolds. Specifically, the aligned PCL scaffold was composed of micro-scale fibres, resulting in the generation of a rough and porous structure, but the P3 and P6 scaffolds showed a different topography, with changes in the porous structure. These topographical differences could result in changes in the water drop contact angle values. Therefore, further investigations are required to investigate the effect of the topographical differences. The Wilhelmy balance method has been proven to be a reliable technique for studying WCA on individual fibres of known diameter.

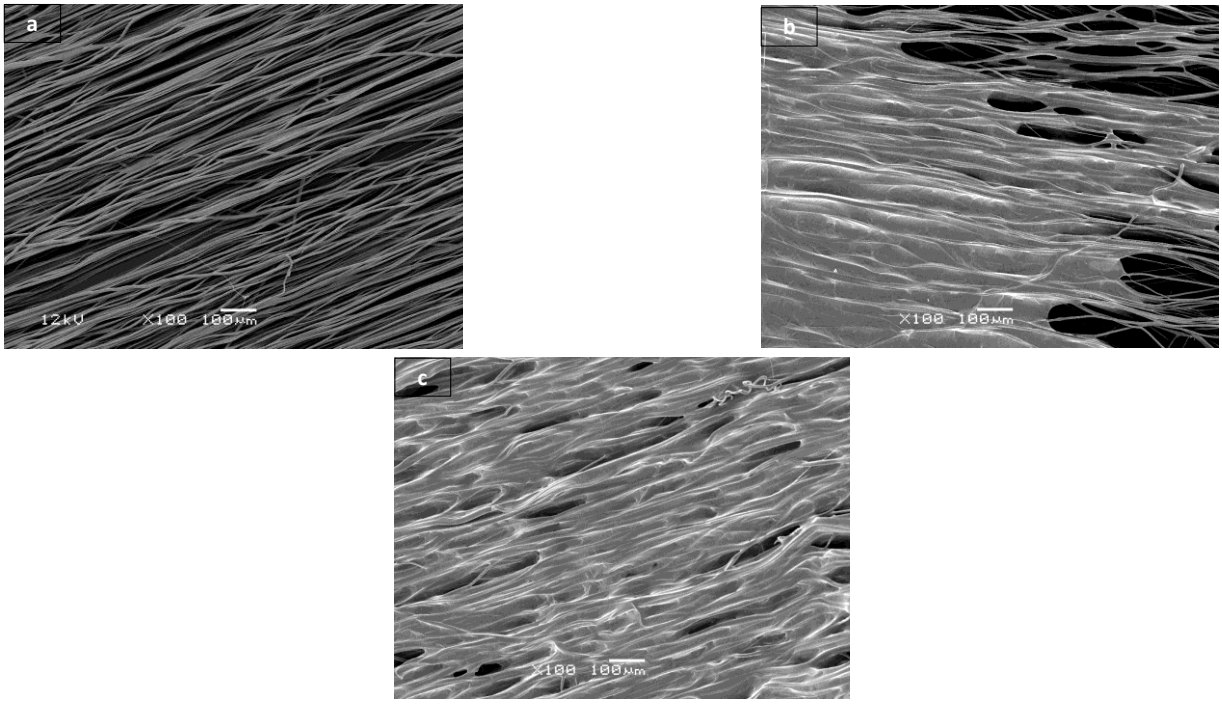


Figure 4.9: SEM images of (a) PCL aligned fibre scaffolds and composite with different amount of PSS coating ((b) P3 scaffolds, (c) P6 scaffolds). Scale bar = 100 µm.

4.4.7. Cell attachment and proliferation

3T3 fibroblast cells were seeded on PCL aligned scaffolds as well as P3 and P6. Figure 4.10 shows the SEM images of PCL, P3 and P6 scaffolds 1 day post-seeding. It was found that cells were rounded on PCL aligned scaffolds, whereas no cells were found on the surface of P3 and P6 which can be attributed to removal of the PSS pre-polymer coating during dehydration process by using methanol.

DAPI nuclear staining was used to observe the response of 3T3 fibroblast cells on the three scaffolds to substrate topology. The fibrous scaffolds provided appropriate surface for guided cell attachment, oriented along the longitudinal axis of the fibre direction and allowed cells to proliferate until largely coat the surface at day 5 (Figure 4.11). In addition, 3T3 fibroblasts cells maintain their typical morphology after proliferation.

Quantitative analysis of cell proliferation by Prestoblue assay demonstrated significant reduction in the number of cells on PCL aligned scaffolds as compared to P3, P6 and TCP on day 5 (Figure. 4.12). Amount of PSS on the surface of the scaffolds did not show any significant difference in cell proliferation on the composite scaffolds. Moreover, addition of PGS to PCL resulted in enhanced cell proliferation comparable to TCP, which was considered as a positive control. However, on day 3 cells proliferated faster on TCP than P3 and P6 scaffolds.

Cell studies on P3 and P6 scaffolds clearly showed that PSS promoted cell attachment and proliferation on these scaffolds. Although PCL aligned scaffolds mimics many aspects of natural ECM structure of skeletal muscle, the hydrophobicity of PCL leads to lower cell attachment and proliferation.

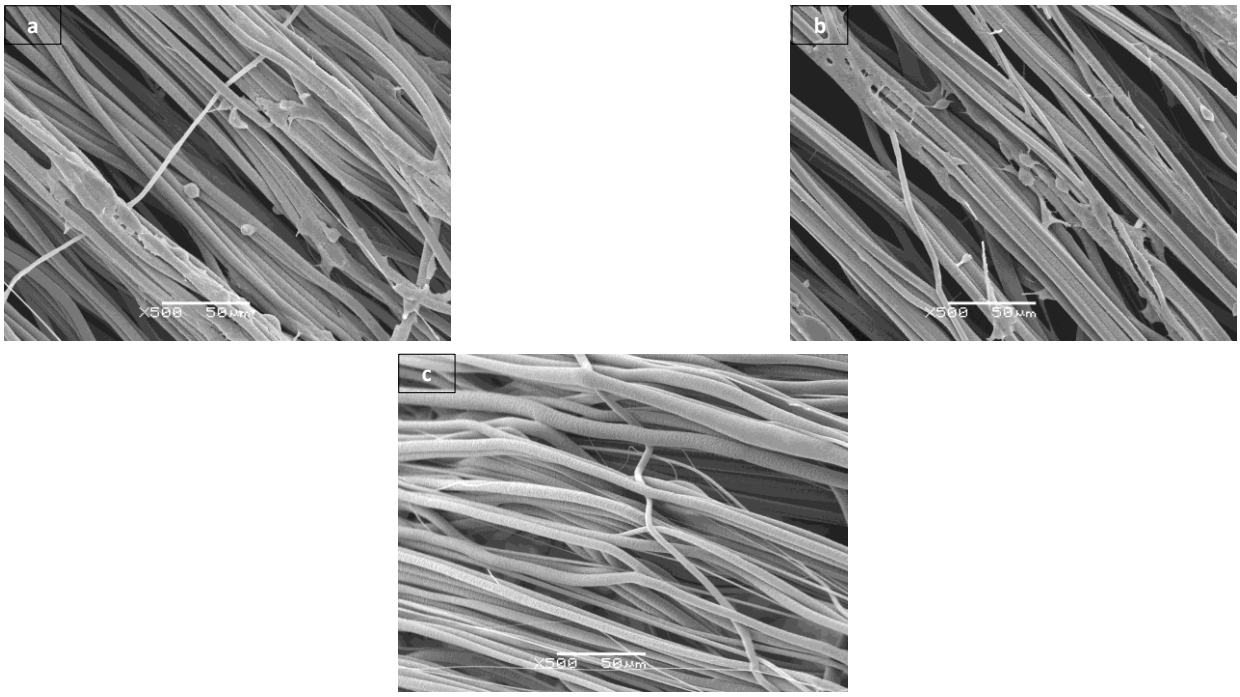


Figure 4.10: SEM images showing 3T3 fibroblast cells growing at day one on (a, b) aligned electrospun PCL scaffolds (c) P3 scaffolds. Scale bar = 50 µm.

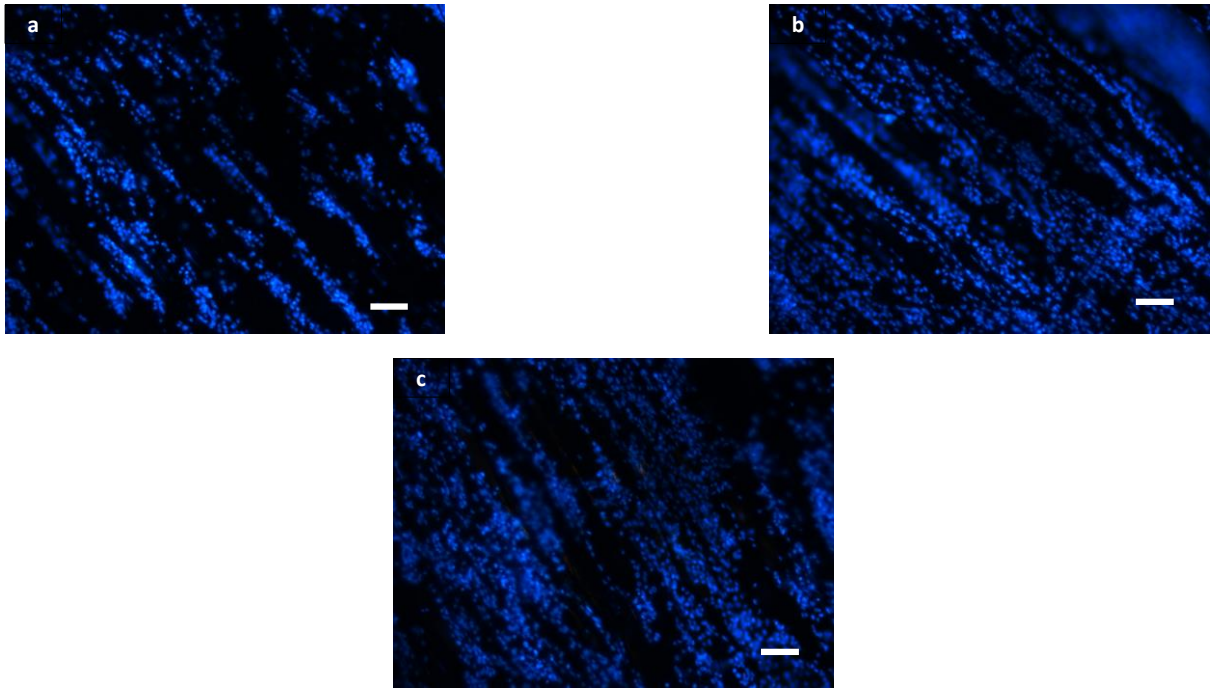


Figure 4.11: Fluorescence microscopy images of the (a) PCL aligned scaffolds, (b)P3 and (c)P6 surface cultured with fibroblasts for 5 days. Scale bar = 100 µm.

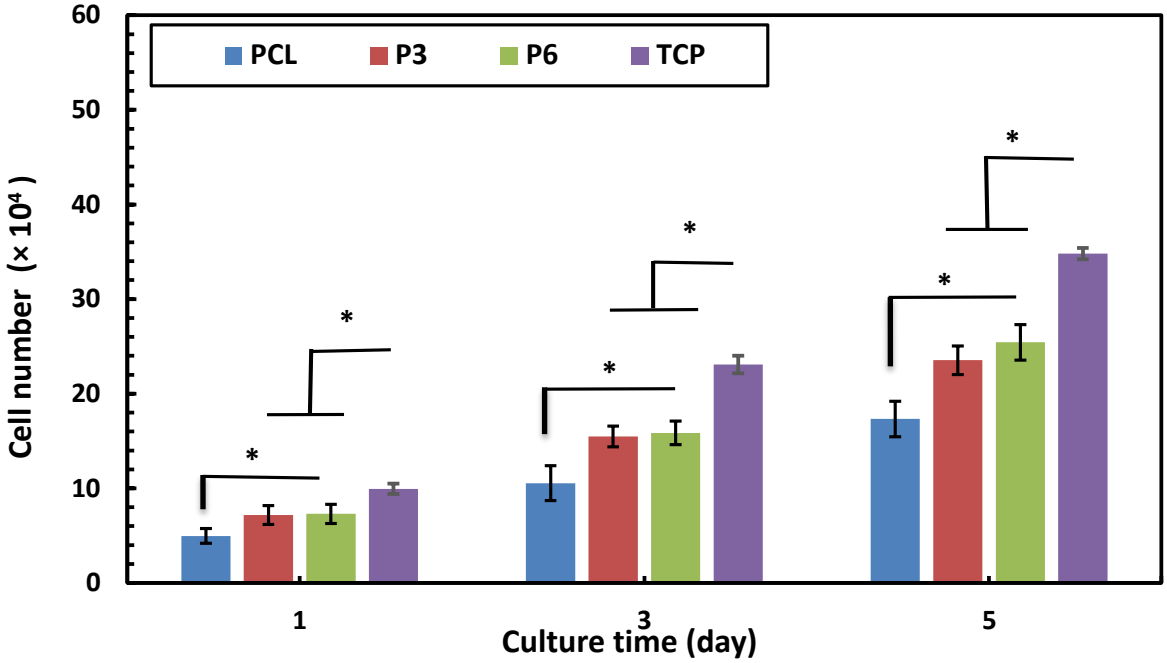


Figure 4.12: Proliferation of 3T3 cells cultured on PCL aligned scaffolds, P3 and P6 for 5 days. Four replicates of each sample were tested using PrestoBlue® assay and the averages are presented ±SD ($p < 0.05$).

4.5. Conclusions

Correlation between solution rheology and electro-spinnability, fibre morphology and fibre alignment of PCL with different molecular weights was studied. Depending on the solution viscosity, fibre morphology can be divided into three different levels: droplets region, and irregular fibre with beads region and bead-free fibres. For PCL 80 and 45, with concentrations of less than 5.5 wt% and 8 wt% respectively, a stable jet could not be generated. To obtain bead-free fibres, the concentration of PCL solution should be 1.5-1.8 times the entanglement concentration. For PCL 80, the solution concentration should be increased 3.6 times to eliminate the bending instability region and enhance fibre deposition and alignment on the rotating collector.

Contact angle measurements revealed improved wettability of P3 and P6 scaffolds compared to aligned PCL only scaffolds. Thus, improved cell adhesion and proliferation on P3 and P6 scaffolds may be attributed to the higher hydrophilicity of these scaffolds compared to pure PCL scaffolds alone. Moreover, insignificant differences in cell attachment and proliferation between P3 and P6 scaffolds may be due to their similar hydrophilicity.

5. Chapter five

General discussion, future work and conclusion

5.1. General discussion

The aim of this PhD project was to introduce a synthetic, biodegradable and elastic material for soft tissue engineering. The newly synthesised polymer, PSS, offers the advantages of both natural and synthetic polyester biomaterials as a suitable material for soft tissue engineering applications. The pre-polymer of PSS retained a much wider range of solubility in common organic solvents compared to APS. This finding proves valuable for better monitoring aspects, such as chemical synthesis using different techniques like NMR spectroscopy and GPC, and processability in many different fabrication processes. Moreover, the thermal analysis indicate that PSS samples would have rubber-like elastomeric behavior at a physiological temperature.

The swelling properties of biomaterials play an important role in tissue engineering applications due to the influences of the degree of swelling on degradation behavior, mechanical properties and diffusion properties of the scaffold[285,286]. The water uptake capacity of PSS decreased slightly with an increase in curing duration which can be attributed to the decrease in accessible spaces for PBS diffusion[217] between the PSS molecular chains. The low percentage of swelling in PBS could potentially help to maintain the mechanical properties of PSS post implantation.

Degradation profiles of polymers are commonly affected by their chemical structure. PSS, as a polyester amide, can be degraded under physiological conditions because of the hydrolysable nature of the amide and ester chemical bonds[287,288]. The gradual degradation curves suggest that PSS degrades via surface eroding, similar to APS and PGS[86,197]. The degradation behaviour of a thermoplastic polymer such as poly(lactic-co-glycolic acid) PLGA, one of the most widely biodegradable polymers in tissue engineering research, exhibited heterogeneous degradation characterized by holes developed in the surface and the formation of large cracks[88]. Heterogeneous degradation is usually not preferred as it can cause sudden mechanical failure of the scaffold due to unpredictable change in mechanical behaviour during degradation[37]. It was proposed that this behaviour could be one of the main reasons for mechanical failure of these conventional thermoplastic polymers *in vivo*[289]. On the other hand, thermoset elastomers usually show homogeneous surface degradation characterized by surface erosion and consequently exhibit a gradual change in their mechanical performance[86,197], as observed in the current study for PSS. In addition, the presence of amide groups decreases the degradation rate, due to the suppression of the hydrolysis and esterase enzymes' activity, which is part of the immune system defence that is excreted by macrophages[290].

Previous studies have demonstrated that curing temperatures and curing durations had a significant influence on mechanical properties of elastomeric polymers[291,292]. PSS elastomers showed slight gradual change (not statistically significant) in mechanical behaviors after degradation in accordance with previous studies[293,294], which is demonstrate an advantage over traditional thermoplastic polymer such as PLGA, PCL and PLA and their co-polymers as these thermoplastic polymer show inconsistency in the mechanical behaviors during degradation process.

Similar to natural elastomers, PSS polymers exhibit a low elastic modulus, high tensile strength, large elongation percentage and slow degradation rate. PSS polymers are simple to synthesise and inexpensive to produce. The PSS biomaterials described in this thesis were synthesised from an amino alcohol with a diacid; other types of amino alcohols could also be used, including tris (hydroxymethyl) aminomethane, 1,4-diamino-2, 3-butanediol and 1,3-diamino-2-propano, in order to achieve a broad range of material properties. Other types of diacids could also be used, including azelaic acid, suberic acid and adipic acid.

It is essential to examine the cytotoxicity of cells towards a new polymer in order for it to qualify as a biocompatible material[295]. The *in vitro* response of 3T3 fibroblast cells on PSS films demonstrates the fibroblast cells' ability to interact with this new biomaterial, as confirmed by the maintenance of the cells' attachment, spreading, morphology and metabolic activity, in comparison to TCP.

The synthesised PSS elastomers offered adjustable and predictable degradation and mechanical properties via changing the curing durations. They also followed almost a linear degradation profile against degradation time in PBS and no significant change was seen in their mechanical performance after immersion in degradation media. Moreover, a good cyctocompatibility response was obtained for PSS materials, approximately similar to TCP. The aforementioned advantages would potentially make this material a good candidate for tissue engineering applications, drug delivery and diagnostic system

Electrospun fibre scaffolds with porous structure similar to those of native ECM have been demonstrated enhancement in cell adhesion, proliferation, differentiation and maturation thereby by improving the nutrient exchange and waste products excretion[296,297]. A PSS elastomeric fibrous scaffold for soft tissue engineering was fabricated through the use of an electrospinning technique. A water-soluble PVA polymer was utilised as a carrier material in order to facilitate the electrospinning process, and the optimal electrospinning parameters were established. Following heat treatment that was performed to crosslink the PSS polymer, the PVA carrier was washed off with hot water, resulting in a porous elastomeric scaffold of PSS fibres. Water was used in order to avoid damage to the morphology of the fibres, which can be caused by the use of organic solvent. The FTIR results confirmed successful electrospun of PSS fibrous scaffold and partial elimination of the carrier polymer from the scaffold.

The elastic modulus of wet PSS48 and PSS72 fibrous scaffolds were slightly lower than the PSS48 film, while the elongation percentage was significantly higher. This could be ascribed to the remaining PVA polymer within the scaffolds. In addition, the water could also decrease the friction between the fibres by acting as a lubricant[250], thus the wet fibrous scaffold could stretch easily compared with dry conditions. Therefore, the PSS fibrous scaffolds demonstrated tuneable mechanical properties via altering the curing time which could offer promising constructs for different tissue engineering applications.

The gradual degradation of PSS scaffolds suggested that the scaffold followed surface degradation mechanism[252]. Unlike heterogeneous degradation, homogenous degradation is typically preferred as it maintains the geometry of the fibrous scaffold with gradual and predictable decrease in the mechanical properties to obviate catastrophic sudden mechanical failure modes.

Swelling property plays an important role in the selection of scaffold materials for biomedical applications as the pore sizes would increase when fibrous scaffolds swell. The wider pores would facilitate the cell attachment and cells penetration into the inter-network of the scaffolds and grow *in vitro* with a three dimensional geometry[298], and also could lead to more effective diffusion and distribution of the cell culture nutrients. The water uptake of the PSS fibrous scaffolds increased initially after one week and reached ~100% at week two. The initial increase in swelling ratio could be due to the absorption of water in the first stage of degradation[253].

PVA was chosen as a carrier polymer due to the fact that it is water-soluble, and can thus be safely removed by dissolution in water, PVA has a high melting temperature meaning that it does not melt during the crosslinking process. On the other hand, PCL scaffolds were used in the last chapter to improve its hydrophilicity and biocompatibility, without the need for the crosslinking process.

The PSS elastomeric fibrous scaffolds demonstrated good biocompatibility and mechanical properties. Under tissue culture conditions, the PSS scaffolds demonstrated effective cytocompatibility in direct contact with 3T3 fibroblast monolayers. The PSS scaffolds revealed a low elastic modulus and a high elongation percentage under aqueous conditions, which may indicate future effectiveness in soft tissue engineering applications. Therefore, the combination of the PSS elastomeric scaffolds' cytocompatibility and mechanical properties make this material a promising candidate for a variety of applications in soft tissue engineering, such as in the cardiac muscles and lungs.

The use of PCL for drug delivery and scaffold fabrication has increased within the tissue engineering field during the past decade[299]. However, PCL scaffolds have limited biological applications due to poor cell attachment as a result of the relatively low hydrophilicity of PCL[300]. To enhance the hydrophilicity of PCL scaffolds, PCL scaffolds were produced using two different molecular weights and different concentrations of PCL, to determine the effect of entangled concentration on the ability of electrospinning. The produced PCL scaffolds were then treated with uncured PSS polymer to improve its hydrophilicity and biocompatibility.

Electrospun fibres are desirable for biomedical applications with anisotropic properties such as tissue engineering scaffolds. Generally, the random fibre is appropriate in the tissue engineering field, as it mimics the topography of the extracellular matrix. In addition, aligned fibres can also offer some advantages such as guiding the contact between cells in the case of the engineering of skeletal muscle tissue, which is normally aligned in the human body[274]. For PCL 80, the studies showed the solution concentration should be increased 3.6 times to eliminate the bending instability region and enhance fibre deposition and alignment on the rotating collector.

The adsorption of biological molecules to the surface of the scaffolds is linked to its hydrophilicity[300]. Typically, the threshold for defining hydrophilic materials is a contact angle smaller than 90°[301]. Contact angle measurements showed improved wettability of P3 and P6 scaffolds compared to aligned PCL only scaffolds. Thus, improved cell adhesion and proliferation on P3 and P6 scaffolds may be due to the higher hydrophilicity of these scaffolds compared to pure PCL scaffolds alone.

5.2.Future work

5.2.1. In vivo studies

One of the important objectives of the scaffolds is to support cell attachment, spreading, proliferation and differentiation on the scaffold, which leads to the regeneration of the injured tissues and organs. As a result, it is necessary to perform *in vitro* and *in vivo* studies with a variety of cell types, such as neural stem cells for neutral tissue engineering and endothelial progenitor cells for cardiac tissue engineering, and to study these cells' adhesion and migration abilities; this is an important step in the study of biomedical applications. In addition, scaffolds are expected to expose the tissue fluids, enzymes and mechanical stresses of the native tissue; thus, it is necessary to study the kinetic properties of scaffolds' degradation *in vivo*, as well as the effects of mechanical stresses and degradation on the mechanical properties and structure of the fibrous scaffolds.

5.2.2. Surface modification of PSS

Cells' ability to attach and spread on the scaffolds can be significantly affected by the chemistry of the biomaterial's surface. There are some that can be conducted on the surface of the PSS biomaterial in order to meet the special requirements of the cells' interaction with the biomaterial. These techniques include grafting bioactive groups through chemical modification, structural modification (such as porosity) and the immobilisation of bioactive groups (such as growth factors and peptides) on the surface of the PSS biomaterial, in order to promote cell attachment, proliferation and signalling.

5.3.Conclusions

PSS polymers are a new biomaterial that offer a variety of potential applications, such as tissue engineering and drug delivery. This PhD thesis demonstrates the synthesis and optimisation of the properties of a PSS biomaterial, newly electrospun elastomeric PSS scaffolds and the use of this polymer as a coating material for aligned polycaprolactone fibres. The results demonstrate that this newly developed biomaterial has tuneable mechanical properties, good cytocompatibility and a slow degradation rate, as well as the possibility that this biomaterial could be fabricated as an elastic scaffold, specifically through the use of an electrospinning technique. This technique may be a promising candidate in the application of soft tissue engineering, particularly with respect to drug delivery systems. In addition, this thesis proves that PSS biomaterials can be utilised as coating agents in order to enhance the hydrophilicity of polycaprolactone aligned fibres. Future work will focus on the completion of *in vivo* studies, using different types of cells for soft tissue engineering, simultaneously studying cells' behaviour on the modified PSS surface; this can be achieved through the use of different surface modification techniques.

References

1. Atala A. Engineering tissues, organs and cells. *J Tissue Eng Regen Med*. 2007;1(2):83-96.
2. Prokop A. Bioartificial Organs in the Twenty-first Century. *Ann N Y Acad Sci*. 2001;944(1):472-490.
3. Polak JM, Bishop AE. Stem cells and tissue engineering: past, present, and future. *Ann N Y Acad Sci*. 2006;1068(1):352-366.
4. Cohen S, Baño MC, Cima LG, et al. Design of synthetic polymeric structures for cell transplantation and tissue engineering. *Clin Mater*. 1993;13(1):3-10.
5. Drury JL, Mooney DJ. Hydrogels for tissue engineering: scaffold design variables and applications. *Biomaterials*. 2003;24(24):4337-4351.
6. Katari R, Peloso A, Orlando G. Tissue engineering and regenerative medicine: semantic considerations for an evolving paradigm. *Front Bioeng Biotechnol*. 2015;2:57.
7. Badylak SF, Nerem RM. Progress in tissue engineering and regenerative medicine. *Proc Natl Acad Sci*. 2010;107(8):3285-3286.
8. Fisher MB, Mauck RL. Tissue engineering and regenerative medicine: recent innovations and the transition to translation. *Tissue Eng Part B Rev*. 2013;19(1):1-13.
9. Dvir T, Timko BP, Kohane DS, Langer R. Nanotechnological strategies for engineering complex tissues. *Nat Nanotechnol*. 2011;6(1):13-22.
10. Driessen-Mol A, Rutten MCM, Driessen NJB, et al. Autologous human tissue-engineered heart valves: prospects for systemic applications. 2006.
11. Schenke-Layland K, Opitz F, Gross M, et al. Complete dynamic repopulation of decellularized heart valves by application of defined physical signals—an in vitro study. *Cardiovasc Res*. 2003;60(3):497-509.
12. Ko IK, Lee SJ, Atala A, Yoo JJ. In situ tissue regeneration through host stem cell recruitment. *Exp Mol Med*. 2013;45(11):e57.
13. Patience C, Takeuchi Y, Weiss RA. Zoonosis in xenotransplantation. *Curr Opin Immunol*. 1998;10(5):539-542.
14. Fishman JM, Lowdell MW, Urbani L, et al. Immunomodulatory effect of a decellularized skeletal muscle scaffold in a discordant xenotransplantation model. *Proc Natl Acad Sci*. 2013;110(35):14360-14365.
15. Fishman JM, Ansari T, Sibbons P, De Coppi P, Birchall MA. Decellularized rabbit cricoarytenoid dorsalis muscle for laryngeal regeneration. *Ann Otol Rhinol Laryngol*. 2012;121(2):129-138.
16. Daly KA, Liu S, Agrawal V, et al. Damage associated molecular patterns within xenogeneic biologic scaffolds and their effects on host remodeling. *Biomaterials*. 2012;33(1):91-101.

17. Wiles K, Fishman JM, De Coppi P, Birchall MA. The host immune response to tissue-engineered organs: current problems and future directions. *Tissue Eng Part B Rev*. 2016;22(3):208-219.
18. Evans ND, Gentleman E, Polak JM. Scaffolds for stem cells. *Mater Today*. 2006;9(12):26-33.
19. Niklason LE, Gao J, Abbott WM, et al. Functional arteries grown in vitro. *Science (80-)*. 1999;284(5413):489-493.
20. Lovett M, Lee K, Edwards A, Kaplan DL. Vascularization strategies for tissue engineering. *Tissue Eng Part B Rev*. 2009;15(3):353-370.
21. Kim B-S, Park I-K, Hoshiba T, et al. Design of artificial extracellular matrices for tissue engineering. *Prog Polym Sci*. 2011;36(2):238-268.
22. Hollister SJ. Porous scaffold design for tissue engineering. *Nat Mater*. 2005;4(7):518.
23. Goldberg M, Langer R, Jia X. Nanostructured materials for applications in drug delivery and tissue engineering. *J Biomater Sci Polym Ed*. 2007;18(3):241-268.
24. Bose S, Vahabzadeh S, Bandyopadhyay A. Bone tissue engineering using 3D printing. *Mater Today*. 2013;16(12):496-504.
25. Senel-Ayaz HG, Perets A, Govindaraj M, Brookstein D, Lelkes PI. Textile-templated electrospun anisotropic scaffolds for tissue engineering and regenerative medicine. In: *Engineering in Medicine and Biology Society (EMBC), 2010 Annual International Conference of the IEEE*. IEEE; 2010:255-258.
26. Hutmacher DW. Scaffolds in tissue engineering bone and cartilage. In: *The Biomaterials: Silver Jubilee Compendium*. Elsevier; 2006:175-189.
27. Babensee JE, Anderson JM, McIntire L V, Mikos AG. Host response to tissue engineered devices. *Adv Drug Deliv Rev*. 1998;33(1-2):111-139.
28. Brown BN, Valentin JE, Stewart-Akers AM, McCabe GP, Badylak SF. Macrophage phenotype and remodeling outcomes in response to biologic scaffolds with and without a cellular component. *Biomaterials*. 2009;30(8):1482-1491.
29. Phelps EA, Garcia AJ. Update on therapeutic vascularization strategies. 2009.
30. O'Brien FJ, Harley BA, Yannas I V, Gibson LJ. The effect of pore size on cell adhesion in collagen-GAG scaffolds. *Biomaterials*. 2005;26(4):433-441.
31. Murphy CM, Haugh MG, O'Brien FJ. The effect of mean pore size on cell attachment, proliferation and migration in collagen–glycosaminoglycan scaffolds for bone tissue engineering. *Biomaterials*. 2010;31(3):461-466.
32. Whelan A, Lee KS. *Developments in Rubber Technology—2: Synthetic Rubbers*. Vol 37. Springer Science & Business Media; 2013.

33. McDevitt TC, Woodhouse KA, Hauschka SD, Murry CE, Stayton PS. Spatially organized layers of cardiomyocytes on biodegradable polyurethane films for myocardial repair. *J Biomed Mater Res Part A*. 2003;66(3):586-595.
34. Chen Q, Liang S, Thouas GA. Elastomeric biomaterials for tissue engineering. *Prog Polym Sci*. 2013;38(3):584-671.
35. Webb AR, Yang J, Ameer GA. Biodegradable polyester elastomers in tissue engineering. *Expert Opin Biol Ther*. 2004;4(6):801-812.
36. Bettinger CJ. Biodegradable elastomers for tissue engineering and cell–biomaterial interactions. *Macromol Biosci*. 2011;11(4):467-482.
37. Amsden B. Curable, biodegradable elastomers: emerging biomaterials for drug delivery and tissue engineering. *Soft Matter*. 2007;3(11):1335-1348.
38. Zhang LQ, Shi R. Novel elastomers for biomedical applications. *Curr Top Elastomers Res ed AK Bhowmick*. 2008;1104.
39. Yoda R. Elastomers for biomedical applications. *J Biomater Sci Polym Ed*. 1998;9(6):561-626.
40. Ma PX. Scaffolds for tissue fabrication. *Mater today*. 2004;7(5):30-40.
41. Zhu J. Bioactive modification of poly (ethylene glycol) hydrogels for tissue engineering. *Biomaterials*. 2010;31(17):4639-4656.
42. Burdick JA, Anseth KS. Photoencapsulation of osteoblasts in injectable RGD-modified PEG hydrogels for bone tissue engineering. *Biomaterials*. 2002;23(22):4315-4323.
43. Jia L, Prabhakaran MP, Qin X, Kai D, Ramakrishna S. Biocompatibility evaluation of protein-incorporated electrospun polyurethane-based scaffolds with smooth muscle cells for vascular tissue engineering. *J Mater Sci*. 2013;48(15):5113-5124.
44. McBane JE, Sharifpoor S, Cai K, Labow RS, Santerre JP. Biodegradation and in vivo biocompatibility of a degradable, polar/hydrophobic/ionic polyurethane for tissue engineering applications. *Biomaterials*. 2011;32(26):6034-6044.
45. Parenteau-Bareil R, Gauvin R, Berthod F. Collagen-based biomaterials for tissue engineering applications. *Materials (Basel)*. 2010;3(3):1863-1887.
46. Rnjak-Kovacina J, Wise SG, Li Z, et al. Tailoring the porosity and pore size of electrospun synthetic human elastin scaffolds for dermal tissue engineering. *Biomaterials*. 2011;32(28):6729-6736.
47. Ahmed TAE, Dare E V, Hincke M. Fibrin: a versatile scaffold for tissue engineering applications. *Tissue Eng Part B Rev*. 2008;14(2):199-215.
48. Li Q, Williams CG, Sun DDN, Wang J, Leong K, Elisseeff JH. Photocrosslinkable polysaccharides based on chondroitin sulfate. *J Biomed Mater Res Part A*. 2004;68(1):28-33.
49. Zia KM, Zia F, Zuber M, Rehman S, Ahmad MN. Alginate based

polyurethanes: A review of recent advances and perspective. *Int J Biol Macromol*. 2015;79:377-387.
50. Novakovic GV, Eschenhagen T, Mummery C. Myocardial tissue engineering: in vitro models. *Cold Spring Harb Perspect Med*. 2014;4(3):a014076.
51. Zieber L, Or S, Ruvinov E, Cohen S. Microfabrication of channel arrays promotes vessel-like network formation in cardiac cell construct and vascularization in vivo. *Biofabrication*. 2014;6(2):24102.
52. Chen Q-Z, Harding SE, Ali NN, Lyon AR, Boccaccini AR. Biomaterials in cardiac tissue engineering: ten years of research survey. *Mater Sci Eng R Reports*. 2008;59(1):1-37.
53. Sharma SK, Mudhoo A. *A Handbook of Applied Biopolymer Technology: Synthesis, Degradation and Applications*. Royal Society of Chemistry; 2011.
54. Seal BL, Otero TC, Panitch A. Polymeric biomaterials for tissue and organ regeneration. *Mater Sci Eng R Reports*. 2001;34(4):147-230.
55. Legge NR. Thermoplastic elastomers. *Rubber Chem Technol*. 1987;60(3):83-117.
56. Shackelford JF, Han Y-H, Kim S, Kwon S-H. *CRC Materials Science and Engineering Handbook*. CRC press; 2016.
57. Bajaj P, Schweller RM, Khademhosseini A, West JL, Bashir R. 3D biofabrication strategies for tissue engineering and regenerative medicine. *Annu Rev Biomed Eng*. 2014;16:247-276.
58. Storey RF, Hickey TP. Degradable polyurethane networks based on D, L-lactide, glycolide, ε-caprolactone, and trimethylene carbonate homopolyester and copolyester triols. *Polymer (Guildf)*. 1994;35(4):830-838.
59. Kucińska-Lipka J, Gubańska I, Janik H. Gelatin-modified polyurethanes for soft tissue scaffold. *Sci World J*. 2013;2013.
60. KUCIŃSKA-LIPKA J, GUBAŃSKA IGA, Janik H. Polyurethanes modified with natural polymers for medical application Part I. POLYURETHANE/CHITOSAN AND POLYURETHANE/COLLAGEN. *Polimery*. 2013;58(9).
61. Gibas I, Janik H. Medical polyurethanes with different hard segments content obtained from polycaprolactone diol, aliphatic diisocyanates and butanediol. *Polish J Appl Chem*. 2009;53(1):9-14.
62. Gogolewski S, Galletti G, Ussia G. Polyurethane vascular prostheses in pigs. *Colloid Polym Sci*. 1987;265(9):774-778.
63. Chiono V, Mozetic P, Boffito M, et al. Polyurethane-based scaffolds for myocardial tissue engineering. *Interface Focus*. 2014;4(1):20130045.
64. Da L, Gong M, Chen A, et al. Composite elastomeric polyurethane

scaffolds incorporating small intestinal submucosa for soft tissue engineering. *Acta Biomater*. 2017.

65. Kakisis JD, Liapis CD, Breuer C, Sumpio BE. Artificial blood vessel: the Holy Grail of peripheral vascular surgery. *J Vasc Surg*. 2005;41(2):349-354.
66. Guelcher SA, Patel V, Gallagher K, et al. Synthesis of polyurethane foam scaffolds for bone tissue engineering. In: *Proc. AIChE Anual Meeting Austin*. ; 2004.
67. Grad S, Kupcsik L, Gorna K, Gogolewski S, Alini M. The use of biodegradable polyurethane scaffolds for cartilage tissue engineering: potential and limitations. *Biomaterials*. 2003;24(28):5163-5171.
68. Sharifi-Aghdam M, Faridi-Majidi R, Derakhshan MA, Chegeni A, Azami M. Preparation of collagen/polyurethane/knitted silk as a composite scaffold for tendon tissue engineering. *Proc Inst Mech Eng Part H J Eng Med*. 2017:0954411917697751.
69. Vermette P, Laroche G, Guidoin R. Biomedical applications of polyurethanes. 2001.
70. Sinclair RG. Copolymers of D, L-lactide and epsilon caprolactone. August 1977.
71. Huang Y, Chang R, Han L, Shan G, Bao Y, Pan P. ABA-Type Thermoplastic Elastomers Composed of Poly (ε-caprolactone-co-δ-valerolactone) Soft Midblock and Polymorphic Poly (lactic acid) Hard End blocks. *ACS Sustain Chem Eng*. 2015;4(1):121-128.
72. Chu B, Zhang L, Qu Y, et al. Synthesis, characterization and drug loading property of Monomethoxy-Poly (ethylene glycol)-Poly (ε-caprolactone)-Poly (D, L-lactide)(MPEG-PCLA) copolymers. *Sci Rep*. 2016;6.
73. Boland E, Wnek G. Tailoring tissue engineering scaffolds using electrostatic processing techniques: a study of poly (glycolic acid) electrospinning. *... Sci Part A*. 2001. http://www.tandfonline.com/doi/abs/10.1081/MA-100108380. Accessed March 2, 2014.
74. Pitt GG, Gratzl MM, Kimmel GL, Surles J, Sohindler A. Aliphatic polyesters II. The degradation of poly (DL-lactide), poly (ε-caprolactone), and their copolymers in vivo. *Biomaterials*. 1981;2(4):215-220.
75. Pitt CG, Hendren RW, Schindler A, Woodward SC. The enzymatic surface erosion of aliphatic polyesters. *J Control Release*. 1984;1(1):3-14.
76. Serrano MC, Vavra AK, Jen M, et al. Poly (diol-co-citrate) s as Novel Elastomeric Perivascular Wraps for the Reduction of Neointimal Hyperplasia. *Macromol Biosci*. 2011;11(5):700-709.
77. Serrano MC, Gutiérrez MC, Jiménez R, Ferrer ML, del Monte F. Synthesis of novel lidocaine-releasing poly (diol-co-citrate) elastomers by using deep

eutectic solvents. *Chem Commun*. 2012;48(4):579-581.
78. Sant S, Iyer D, Gaharwar AK, Patel A, Khademhosseini A. Effect of biodegradation and de novo matrix synthesis on the mechanical properties of valvular interstitial cell-seeded polyglycerol sebacate–polycaprolactone scaffolds. *Acta Biomater*. 2013;9(4):5963-5973.
79. Kelch S, Steuer S, Schmidt AM, Lendlein A. Shape-memory polymer networks from oligo [(ε-hydroxycaproate)-co-glycolate] dimethacrylates and butyl acrylate with adjustable hydrolytic degradation rate. *Biomacromolecules*. 2007;8(3):1018-1027.
80. Bos RRM, Rozema FB, Boering G, et al. Degradation of and tissue reaction to biodegradable poly (L-lactide) for use as internal fixation of fractures: a study in rats. *Biomaterials*. 1991;12(1):32-36.
81. Wang Y, Ameer GA, Sheppard BJ, Langer R. A tough biodegradable elastomer. *Nat Biotechnol*. 2002;20(6):602-606.
82. Chiba M, Komatsu K. Mechanical responses of the periodontal ligament in the transverse section of the rat mandibular incisor at various velocities of loading in vitro. *J Biomech*. 1993;26(4-5):561-570.
83. Komatsu K, Chiba M. The effect of velocity of loading on the biomechanical responses of the periodontal ligament in transverse sections of the rat molar in vitro. *Arch Oral Biol*. 1993;38(5):369-375.
84. Meyers MA, Chen P-Y, Lin AY-M, Seki Y. Biological materials: structure and mechanical properties. *Prog Mater Sci*. 2008;53(1):1-206.
85. Nijst CLE, Bruggeman JP, Karp JM, et al. Synthesis and characterization of photocurable elastomers from poly (glycerol-co-sebacate). *Biomacromolecules*. 2007;8(10):3067-3073.
86. Pomerantseva I, Krebs N, Hart A, Neville CM, Huang AY, Sundback CA. Degradation behavior of poly (glycerol sebacate). *J Biomed Mater Res Part A*. 2009;91(4):1038-1047.
87. Liang S-L, Yang X-Y, Fang X-Y, Cook WD, Thouas GA, Chen Q-Z. In vitro enzymatic degradation of poly (glycerol sebacate)-based materials. *Biomaterials*. 2011;32(33):8486-8496.
88. Wang Y, Kim YM, Langer R. In vivo degradation characteristics of poly (glycerol sebacate). *J Biomed Mater Res Part A*. 2003;66(1):192-197.
89. Sundback CA, Shyu JY, Wang Y, et al. Biocompatibility analysis of poly (glycerol sebacate) as a nerve guide material. *Biomaterials*. 2005;26(27):5454-5464.
90. Sales VL, Engelmayr GC, Johnson JA, et al. Protein precoating of elastomeric tissue-engineering scaffolds increased cellularity, enhanced extracellular matrix protein production, and differentially regulated the phenotypes of circulating endothelial progenitor cells. *Circulation*. 2007;116(11 suppl):I-55.

91. Engelmayr Jr GC, Cheng M, Bettinger CJ, Borenstein JT, Langer R, Freed LE. Accordion-like honeycombs for tissue engineering of cardiac anisotropy. *Nat Mater*. 2008;7(12):1003.
92. Yang J, Webb AR, Ameer GA. Novel citric acid-based biodegradable elastomers for tissue engineering. *Adv Mater*. 2004;16(6):511-516.
93. Yang J, Webb AR, Pickerill SJ, Hageman G, Ameer GA. Synthesis and evaluation of poly (diol citrate) biodegradable elastomers. *Biomaterials*. 2006;27(9):1889-1898.
94. Zhao H, Ameer GA. Modulating the mechanical properties of poly (diol citrates) via the incorporation of a second type of crosslink network. *J Appl Polym Sci*. 2009;114(3):1464-1470.
95. Motlagh D, Allen J, Hoshi R, Yang J, Lui K, Ameer G. Hemocompatibility evaluation of poly (diol citrate) in vitro for vascular tissue engineering. *J Biomed Mater Res Part A*. 2007;82(4):907-916.
96. Yang J, Motlagh D, Webb AR, Ameer GA. Novel biphasic elastomeric scaffold for small-diameter blood vessel tissue engineering. *Tissue Eng*. 2005;11(11-12):1876-1886.
97. Bettinger CJ, Bruggeman JP, Borenstein JT, Langer RS. Amino alcohol-based degradable poly (ester amide) elastomers. *Biomaterials*. 2008;29(15):2315-2325.
98. Tsang VL, Bhatia SN. Three-dimensional tissue fabrication. *Adv Drug Deliv Rev*. 2004;56(11):1635-1647.
99. Liu CZ, Czernuszka JT. Development of biodegradable scaffolds for tissue engineering: a perspective on emerging technology. *Mater Sci Technol*. 2007;23(4):379-391.
100. Liu C, Xia Z, Czernuszka JT. Design and development of three-dimensional scaffolds for tissue engineering. *Chem Eng Res Des*. 2007;85(7):1051-1064.
101. Ramakrishna S, Fujihara K, Teo W-E, Yong T, Ma Z, Ramaseshan R. Electrospun nanofibers: solving global issues. *Mater today*. 2006;9(3):40-50.
102. Fong H, Liu W, Wang C-S, Vaia RA. Generation of electrospun fibers of nylon 6 and nylon 6-montmorillonite nanocomposite. *Polymer (Guildf)*. 2002;43(3):775-780.
103. Hendricks CD, Carson RS, Hogan JJ, Schneider JM. Photomicrography of electrically sprayed heavy particles. *AIAA J*. 1964;2(4):733-737.
104. Koombhongse S, Liu W, Reneker DH. Flat polymer ribbons and other shapes by electrospinning. *J Polym Sci Part B Polym Phys*. 2001;39(21):2598-2606.
105. Shin YM, Hohman MM, Brenner MP, Rutledge GC. Experimental characterization of electrospinning: the electrically forced jet and

instabilities. *Polymer (Guildf)*. 2001;42(25):9955-9967.
106. Bosworth L, Downes S. *Electrospinning for Tissue Regeneration*. Elsevier; 2011.
107. Li J, Connell S, Shi R. Biomimetic architectures for tissue engineering. In: *Biomimetics Learning from Nature*. Intech; 2010.
108. Bini TB, Gao S, Wang S, Lim A, Hai L Ben, Ramakrishna S. Electrospun poly (L-lactide-co-glycolide) biodegradable polymer nanofibre tubes for peripheral nerve regeneration. *Nanotechnology*. 2004;15(11):1459.
109. Liu H, Hsieh Y. Ultrafine fibrous cellulose membranes from electrospinning of cellulose acetate. *J Polym Sci Part B Polym Phys*. 2002;40(18):2119-2129.
110. Sill TJ, von Recum HA. Electrospinning: applications in drug delivery and tissue engineering. *Biomaterials*. 2008;29(13):1989-2006.
111. Bertea A, Manea LR, Popa A. The Influence of Process Parameters on the Characteristics of Electrospun 3D Nanostructures. In: *IOP Conference Series: Materials Science and Engineering*. Vol 209. IOP Publishing; 2017:12074.
112. Deitzel JM, Kleinmeyer J, Harris DEA, Tan NCB. The effect of processing variables on the morphology of electrospun nanofibers and textiles. *Polymer (Guildf)*. 2001;42(1):261-272.
113. Matabola KP, Moutloali RM. The influence of electrospinning parameters on the morphology and diameter of poly (vinyledene fluoride) nanofibers-effect of sodium chloride. *J Mater Sci*. 2013;48(16):5475-5482.
114. Bhardwaj N, Kundu SC. Electrospinning: a fascinating fiber fabrication technique. *Biotechnol Adv*. 2010;28(3):325-347.
115. Zhang C, Yuan X, Wu L, Han Y, Sheng J. Study on morphology of electrospun poly (vinyl alcohol) mats. *Eur Polym J*. 2005;41(3):423-432.
116. Zong X, Kim K, Fang D, Ran S, Hsiao BS, Chu B. Structure and process relationship of electrospun bioabsorbable nanofiber membranes. *Polymer (Guildf)*. 2002;43(16):4403-4412.
117. Li Z, Wang C. Effects of working parameters on electrospinning. In: *One-Dimensional Nanostructures*. Springer; 2013:15-28.
118. Megelski S, Stephens JS, Chase DB, Rabolt JF. Micro-and nanostructured surface morphology on electrospun polymer fibers. *Macromolecules*. 2002;35(22):8456-8466.
119. Macossay J, Marruffo A, Rincon R, Eubanks T, Kuang A. Effect of needle diameter on nanofiber diameter and thermal properties of electrospun poly (methyl methacrylate). *Polym Adv Technol*. 2007;18(3):180-183.
120. Yarin AL, Koombhongse S, Reneker DH. Bending instability in electrospinning of nanofibers. *J Appl Phys*. 2001;89(5):3018-3026.
121. Teo WE, Ramakrishna S. A review on electrospinning design and

nanofibre assemblies. *Nanotechnology*. 2006;17(14):R89.
122. Pillay V, Dott C, Choonara YE, et al. A review of the effect of processing variables on the fabrication of electrospun nanofibers for drug delivery applications. *J Nanomater*. 2013;2013.
123. Haider S, Al-Zeghayer Y, Ali FAA, et al. Highly aligned narrow diameter chitosan electrospun nanofibers. *J Polym Res*. 2013;20(4):105.
124. Zargham S, Bazgir S, Tavakoli A, Rashidi AS, Damerchely R. The Effect of Flow Rate on Morphology and Deposition Area of Electrospun Nylon 6 Nanofiber. *J Eng Fabr Fibers*. 2012;7(4).
125. Sun B, Long YZ, Zhang HD, et al. Advances in three-dimensional nanofibrous macrostructures via electrospinning. *Prog Polym Sci*. 2014;39(5):862-890.
126. Haider A, Haider S, Kang I-K. A comprehensive review summarizing the effect of electrospinning parameters and potential applications of nanofibers in biomedical and biotechnology. *Arab J Chem*. 2015.
127. Du J, Zhang X. Role of polymer–salt–solvent interactions in the electrospinning of polyacrylonitrile/iron acetylacetonate. *J Appl Polym Sci*. 2008;109(5):2935-2941.
128. Fong H, Chun I, Reneker DH. Beaded nanofibers formed during electrospinning. *Polymer (Guildf)*. 1999;40(16):4585-4592.
129. Czech T, Ramakrishna S, Sundarrajan S. Electrospinning and electrospraying techniques for nanocomposite non-woven fabric production. *Fibres Text East Eur*. 2009;17:77-81.
130. Huang C, Chen S, Lai C, et al. Electrospun polymer nanofibres with small diameters. *Nanotechnology*. 2006;17(6):1558.
131. Lannutti J, Reneker D, Ma T, Tomasko D, Farson D. Electrospinning for tissue engineering scaffolds. *Mater Sci Eng C*. 2007;27(3):504-509.
132. Koski A, Yim K, Shivkumar S. Effect of molecular weight on fibrous PVA produced by electrospinning. *Mater Lett*. 2004;58(3):493-497.
133. Zhao YY, Yang QB, Lu X-F, Wang C, Wei Y. Study on correlation of morphology of electrospun products of polyacrylamide with ultrahigh molecular weight. *J Polym Sci Part B Polym Phys*. 2005;43(16):2190-2195.
134. Huan S, Liu G, Han G, et al. Effect of experimental parameters on morphological, mechanical and hydrophobic properties of electrospun polystyrene fibers. *Materials (Basel)*. 2015;8(5):2718-2734.
135. Pelipenko J, Kristl J, Janković B, Baumgartner S, Kocbek P. The impact of relative humidity during electrospinning on the morphology and mechanical properties of nanofibers. *Int J Pharm*. 2013;456(1):125-134.
136. Zhang Y, Lim CT, Ramakrishna S, Huang Z-M. Recent development of polymer nanofibers for biomedical and biotechnological applications. *J*

Mater Sci Mater Med. 2005;16(10):933-946.
137. Zahedi P, Rezaeian I, Ranaei-Siadat S, Jafari S, Supaphol P. A review on wound dressings with an emphasis on electrospun nanofibrous polymeric bandages. *Polym Adv Technol*. 2010;21(2):77-95.
138. Katti DS, Robinson KW, Ko FK, Laurencin CT. Bioresorbable nanofiber-based systems for wound healing and drug delivery: Optimization of fabrication parameters. *J Biomed Mater Res Part B Appl Biomater*. 2004;70(2):286-296.
139. Thakur R, Florek C, Kohn J, Michniak B. Electrospun nanofibrous polymeric scaffold with targeted drug release profiles for potential application as wound dressing. *Int J …*. 2008. http://www.sciencedirect.com/science/article/pii/S0378517308005310. Accessed March 2, 2014.
140. Bölgen N, Vargel I, Korkusuz P, Menceloğlu YZ, Pişkin E. In vivo performance of antibiotic embedded electrospun PCL membranes for prevention of abdominal adhesions. *J Biomed Mater Res Part B Appl Biomater*. 2007;81(2):530-543.
141. Hong Y, Fujimoto K, Hashizume R, et al. Generating elastic, biodegradable polyurethane/poly (lactide-co-glycolide) fibrous sheets with controlled antibiotic release via two-stream electrospinning. *Biomacromolecules*. 2008;9(4):1200-1207.
142. Xie J, Wang C-H. Electrospun micro-and nanofibers for sustained delivery of paclitaxel to treat C6 glioma in vitro. *Pharm Res*. 2006;23(8):1817.
143. Yih TC, Al-Fandi M. Engineered nanoparticles as precise drug delivery systems. *J Cell Biochem*. 2006;97(6):1184-1190.
144. Kenawy E-R, Bowlin GL, Mansfield K, et al. Release of tetracycline hydrochloride from electrospun poly (ethylene-co-vinylacetate), poly (lactic acid), and a blend. *J Control release*. 2002;81(1-2):57-64.
145. Luong-Van E, Grøndahl L, Chua KN, Leong KW, Nurcombe V, Cool SM. Controlled release of heparin from poly (ε-caprolactone) electrospun fibers. *Biomaterials*. 2006;27(9):2042-2050.
146. Zeng J, Xu X, Chen X, et al. Biodegradable electrospun fibers for drug delivery. *J Control release*. 2003;92(3):227-231.
147. Luu Y, Kim K, Hsiao B. Development of a nanostructured DNA delivery scaffold via electrospinning of PLGA and PLA–PEG block copolymers. *J Control …*. 2003. http://www.sciencedirect.com/science/article/pii/S016836590300097X. Accessed March 2, 2014.
148. Taepaiboon P, Rungsardthong U, Supaphol P. Drug-loaded electrospun mats of poly (vinyl alcohol) fibres and their release characteristics of four model drugs. *Nanotechnology*. 2006;17(9):2317.

149. Jiang H, Fang D, Hsiao B, Chu B, Chen W. Preparation and characterization of ibuprofen-loaded poly (lactide-co-glycolide)/poly (ethylene glycol)-g-chitosan electrospun membranes. *J Biomater Sci Polym Ed*. 2004;15(3):279-296.
150. Kim TG, Lee DS, Park TG. Controlled protein release from electrospun biodegradable fiber mesh composed of poly (ε-caprolactone) and poly (ethylene oxide). *Int J Pharm*. 2007;338(1-2):276-283.
151. Xu X, Yang L, Xu X, et al. Ultrafine medicated fibers electrospun from W/O emulsions. *J Control Release*. 2005;108(1):33-42.
152. Wang M, Wang L, Huang Y. Electrospun hydroxypropyl methyl cellulose phthalate (HPMCP)/erythromycin fibers for targeted release in intestine. *J Appl Polym Sci*. 2007;106(4):2177-2184.
153. Pornsopone V, Supaphol P, Rangkupan R, Tantayanon S. Electrospun methacrylate-based copolymer/indomethacin fibers and their release characteristics of indomethacin. *J Polym Res*. 2007;14(1):53-59.
154. Chew SY, Wen J, Yim EKF, Leong KW. Sustained release of proteins from electrospun biodegradable fibers. *Biomacromolecules*. 2005;6(4):2017-2024.
155. Matthews JA, Wnek GE, Simpson DG, Bowlin GL. Electrospinning of collagen nanofibers. *Biomacromolecules*. 2002;3(2):232-238.
156. Kenawy E-R, Layman JM, Watkins JR, et al. Electrospinning of poly (ethylene-co-vinyl alcohol) fibers. *Biomaterials*. 2003;24(6):907-913.
157. Stankus JJ, Guan J, Wagner WR. Fabrication of biodegradable elastomeric scaffolds with sub-micron morphologies. *J Biomed Mater Res Part A*. 2004;70(4):603-614.
158. Mo XM, Xu CY, Kotaki MEA, Ramakrishna S. Electrospun P (LLA-CL) nanofiber: a biomimetic extracellular matrix for smooth muscle cell and endothelial cell proliferation. *Biomaterials*. 2004;25(10):1883-1890.
159. Venugopal J, Zhang YZ, Ramakrishna S. Fabrication of modified and functionalized polycaprolactone nanofibre scaffolds for vascular tissue engineering. *Nanotechnology*. 2005;16(10):2138.
160. Baker SC, Atkin N, Gunning PA, et al. Characterisation of electrospun polystyrene scaffolds for three-dimensional in vitro biological studies. *Biomaterials*. 2006;27(16):3136-3146.
161. Yoshimoto H, Shin YM, Terai H, Vacanti JP. A biodegradable nanofiber scaffold by electrospinning and its potential for bone tissue engineering. *Biomaterials*. 2003;24(12):2077-2082.
162. Shin M, Yoshimoto H, Vacanti JP. In vivo bone tissue engineering using mesenchymal stem cells on a novel electrospun nanofibrous scaffold. *Tissue Eng*. 2004;10(1-2):33-41.
163. Kim K, Yu M, Zong X, Chiu J, Fang D. Control of degradation rate and

hydrophilicity in electrospun non-woven poly (D, L-lactide) nanofiber scaffolds for biomedical applications. *Biomaterials*. 2003. http://www.sciencedirect.com/science/article/pii/S0142961203004071. Accessed March 2, 2014.

164. Nair LS, Bhattacharyya S, Bender JD, et al. Fabrication and optimization of methylphenoxy substituted polyphosphazene nanofibers for biomedical applications. *Biomacromolecules*. 2004;5(6):2212-2220.
165. Badami AS, Kreke MR, Thompson MS, Riffle JS, Goldstein AS. Effect of fiber diameter on spreading, proliferation, and differentiation of osteoblastic cells on electrospun poly (lactic acid) substrates. *Biomaterials*. 2006;27(4):596-606.
166. Sakai S, Yamada Y, Yamaguchi T, Kawakami K. Prospective use of electrospun ultra-fine silicate fibers for bone tissue engineering. *Biotechnol J Healthc Nutr Technol*. 2006;1(9):958-962.
167. Zhang J, Qi H, Wang H, et al. Engineering of vascular grafts with genetically modified bone marrow mesenchymal stem cells on poly (propylene carbonate) graft. *Artif Organs*. 2006;30(12):898-905.
168. Fang J, Niu H, Lin T, Wang X. Applications of electrospun nanofibers. *Chinese Sci Bull*. 2008;53(15):2265.
169. Xu C, Yang F, Wang S, Ramakrishna S. In vitro study of human vascular endothelial cell function on materials with various surface roughness. *J Biomed Mater Res Part A An Off J Soc Biomater Japanese Soc Biomater Aust Soc Biomater Korean Soc Biomater*. 2004;71(1):154-161.
170. Yang F, Xu CY, Kotaki M, Wang S, Ramakrishna S. Characterization of neural stem cells on electrospun poly (L-lactic acid) nanofibrous scaffold. *J Biomater Sci Polym Ed*. 2004;15(12):1483-1497.
171. Yang F, Murugan R, Wang S, Ramakrishna S. Electrospinning of nano/micro scale poly (L-lactic acid) aligned fibers and their potential in neural tissue engineering. *Biomaterials*. 2005. http://www.sciencedirect.com/science/article/pii/S0142961204008567. Accessed March 2, 2014.
172. Sangsanoh P, Waleetorncheepsawat S, Suwantong O, et al. In vitro biocompatibility of schwann cells on surfaces of biocompatible polymeric electrospun fibrous and solution-cast film scaffolds. *Biomacromolecules*. 2007;8(5):1587-1594.
173. Vacanti JP, Langer R. Tissue engineering: the design and fabrication of living replacement devices for surgical reconstruction and transplantation. *Lancet*. 1999;354:S32-S34.
174. Sahoo S, Chung C, Khetan S, Burdick JA. Hydrolytically degradable hyaluronic acid hydrogels with controlled temporal structures. *Biomacromolecules*. 2008;9(4):1088-1092.

175. Burdick JA, Chung C, Jia X, Randolph MA, Langer R. Controlled degradation and mechanical behavior of photopolymerized hyaluronic acid networks. *Biomacromolecules*. 2005;6(1):386-391.
176. Sawhney AS, Pathak CP, Hubbell JA. Bioerodible hydrogels based on photopolymerized poly (ethylene glycol)-co-poly (α-hydroxy acid) diacrylate macromers. *Macromolecules*. 1993;26(4):581-587.
177. Liu J. *Synthesis, Characterization and Applications of New Photocurable and Biodegradable Elastomers*. ProQuest; 2008.
178. Anderson DG, Tweedie CA, Hossain N, et al. A combinatorial library of photocrosslinkable and degradable materials. *Adv Mater*. 2006;18(19):2614-2618.
179. Duan N, Geng X, Ye L, et al. A vascular tissue engineering scaffold with core–shell structured nano-fibers formed by coaxial electrospinning and its biocompatibility evaluation. *Biomed Mater*. 2016;11(3):35007.
180. Siriwardane ML, Pfister BJ. Engineering three-dimensional nervous tissue constructs based on fiber-gel substrates. In: *Proceedings of the 2010 IEEE 36th Annual Northeast Bioengineering Conference (NEBEC)*. IEEE; 2010:1-2.
181. Zimmermann W-H, Melnychenko I, Eschenhagen T. Engineered heart tissue for regeneration of diseased hearts. *Biomaterials*. 2004;25(9):1639-1647.
182. Hunt NC, Grover LM. Cell encapsulation using biopolymer gels for regenerative medicine. *Biotechnol Lett*. 2010;32(6):733-742.
183. Raghunath J, Rollo J, Sales KM, Butler PE, Seifalian AM. Biomaterials and scaffold design: key to tissue-engineering cartilage. *Biotechnol Appl Biochem*. 2007;46(2):73-84.
184. Patel A, Fine B, Sandig M, Mequanint K. Elastin biosynthesis: the missing link in tissue-engineered blood vessels. *Cardiovasc Res*. 2006;71(1):40-49.
185. Lanza R, Langer R, Vacanti JP. *Principles of Tissue Engineering*. Academic press; 2011.
186. Kai D, Prabhakaran MP, Jin G, Ramakrishna S. Guided orientation of cardiomyocytes on electrospun aligned nanofibers for cardiac tissue engineering. *J Biomed Mater Res Part B Appl Biomater*. 2011;98(2):379-386.
187. Boland ED, Wnek GE, Simpson DG, Pawlowski KJ, Bowlin GL. Tailoring tissue engineering scaffolds using electrostatic processing techniques: a study of poly (glycolic acid) electrospinning. *J Macromol Sci Part A*. 2001;38(12):1231-1243.
188. Lendlein A, Langer R. Biodegradable, elastic shape-memory polymers for potential biomedical applications. *Science (80-)*. 2002;296(5573):1673-1676.

189. Liu X, Holzwarth JM, Ma PX. Functionalized synthetic biodegradable polymer scaffolds for tissue engineering. *Macromol Biosci*. 2012;12(7):911-919.
190. Stuckey DJ, Ishii H, Chen Q-Z, et al. Magnetic resonance imaging evaluation of remodeling by cardiac elastomeric tissue scaffold biomaterials in a rat model of myocardial infarction. *Tissue Eng Part A*. 2010;16(11):3395-3402.
191. Garlotta D. A literature review of poly (lactic acid). *J Polym Environ*. 2001;9(2):63-84.
192. Liang S-L, Cook WD, Thouas GA, Chen Q-Z. The mechanical characteristics and in vitro biocompatibility of poly (glycerol sebacate)-Bioglass® elastomeric composites. *Biomaterials*. 2010;31(33):8516-8529.
193. Gaharwar AK, Nikkhah M, Sant S, Khademhosseini A. Anisotropic poly (glycerol sebacate)-poly (ϵ-caprolactone) electrospun fibers promote endothelial cell guidance. *Biofabrication*. 2014;7(1):15001.
194. Sant S, Hwang CM, Lee S, Khademhosseini A. Hybrid PGS–PCL microfibrous scaffolds with improved mechanical and biological properties. *J Tissue Eng Regen Med*. 2011;5(4):283-291.
195. Eslami M, Vrana NE, Zorlutuna P, et al. Fiber-reinforced hydrogel scaffolds for heart valve tissue engineering. *J Biomater Appl*. 2014:0885328214530589.
196. Eglin D, Mortisen D, Alini M. Degradation of synthetic polymeric scaffolds for bone and cartilage tissue repairs. *Soft Matter*. 2009;5(5):938-947.
197. Bettinger CJ, Bruggeman JP, Borenstein JT, Langer R. In vitro and in vivo degradation of poly (1, 3-diamino-2-hydroxypropane-co-polyol sebacate) elastomers. *J Biomed Mater Res Part A*. 2009;91(4):1077-1088.
198. Wang J, Boutin KG, Abdulhadi O, et al. Fully Biodegradable Airway Stents Using Amino Alcohol-Based Poly (ester amide) Elastomers. *Adv Healthc Mater*. 2013;2(10):1329-1336.
199. Mukundan S, Sant V, Goenka S, Franks J, Rohan LC, Sant S. Nanofibrous composite scaffolds of poly (ester amides) with tunable physicochemical and degradation properties. *Eur Polym J*. 2015;68:21-35.
200. Rickerby J, Prabhakar R, Patel A, Knowles J, Brocchini S. A biomedical library of serinol-derived polyesters. *J Control release*. 2005;101(1):21-34.
201. Tomlinson R, Klee M, Garrett S, Heller J, Duncan R, Brocchini S. Pendent chain functionalized polyacetals that display pH-dependent degradation: A platform for the development of novel polymer therapeutics. *Macromolecules*. 2002;35(2):473-480.
202. Bieberich E, Kawaguchi T, Robert KY. N-acylated serinol is a novel ceramide mimic inducing apoptosis in neuroblastoma cells. *J Biol Chem*.

2000;275(1):177-181.
203. Nicholas GM, Li R, MacMillan JB, Molinski TF. Antifungal activity of bifunctional sphingolipids. intramolecular synergism within long-chain α, ω-bis-aminoalcohols. *Bioorg Med Chem Lett*. 2002;12(16):2159-2162.
204. Boffito M, Gioffredi E, Chiono V, et al. Novel polyurethane-based thermosensitive hydrogels as drug release and tissue engineering platforms: design and in vitro characterization. *Polym Int*. 2016;65(7):756-769.
205. Yun D, Famili A, Lee YM, Jenkins PM, Freed CR, Park D. Biomimetic poly (serinol hexamethylene urea) for promotion of neurite outgrowth and guidance. *J Biomater Sci Polym Ed*. 2014;25(4):354-369.
206. Park D, Wu W, Wang Y. A functionalizable reverse thermal gel based on a polyurethane/PEG block copolymer. *Biomaterials*. 2011;32(3):777-786.
207. Mortensen PB, Gregersen N. The biological origin of ketotic dicarboxylic aciduria: In vivo and in vitro investigations of the ω-oxidation of C6–C16-monocarboxylic acids in unstarved, starved and diabetic rats. *Biochim Biophys Acta (BBA)-Lipids Lipid Metab*. 1981;666(3):394-404.
208. Grego A V, Mingrone G. Dicarboxylic acids, an alternate fuel substrate in parenteral nutrition: an update. *Clin Nutr*. 1995;14(3):143-148.
209. Kerativitayanan P, Tatullo M, Khariton M, Joshi P, Perniconi B, Gaharwar AK. Nanoengineered Osteoinductive and Elastomeric Scaffolds for Bone Tissue Engineering. 2017.
210. Flory PJ. *Principles of Polymer Chemistry*. Cornell University Press; 1953.
211. Claridge TDW. *High-Resolution NMR Techniques in Organic Chemistry*. Vol 27. Elsevier; 2016.
212. Li X, Lu X, Lin Y, et al. Synthesis and characterization of hyperbranched poly (ester-amide) s from commercially available dicarboxylic acids and multihydroxyl primary amines. *Macromolecules*. 2006;39(23):7889-7899.
213. Xue Y, Patel A, Sant V, Sant S. PEGylated poly (ester amide) elastomers with tunable physico-chemical, mechanical and degradation properties. *Eur Polym J*. 2015;72:163-179.
214. Young RJ, Lovell PA. *Introduction to Polymers*. CRC press; 2011.
215. Berg JM, Tymoczko JL, Stryer L. Biochemistry, ; W. H. 2002.
216. Fan Q, Xiao C. Effects of crosslinking density on structure and properties of interpenetrating polymer networks from polyurethane and nitroguar gum. *Polym Compos*. 2008;29(7):758-767.
217. De SK, Aluru NR, Johnson B, Crone WC, Beebe DJ, Moore J. Equilibrium swelling and kinetics of pH-responsive hydrogels: Models, experiments, and simulations. *J Microelectromechanical Syst*. 2002;11(5):544-555.

218. Agrawal CM, Huang D, Schmitz JP, Athanasiou KA. Elevated temperature degradation of a 50: 50 copolymer of PLA-PGA. *Tissue Eng*. 1997;3(4):345-352.
219. Li X, Hong AT-L, Naskar N, Chung H-J. Criteria for quick and consistent synthesis of poly (glycerol sebacate) for tailored mechanical properties. *Biomacromolecules*. 2015;16(5):1525-1533.
220. Ceonzo K, Gaynor A, Shaffer L, Kojima K, Vacanti CA, Stahl GL. Polyglycolic acid-induced inflammation: role of hydrolysis and resulting complement activation. *Tissue Eng*. 2006;12(2):301-308.
221. Reis RL, San Román J. *Biodegradable Systems in Tissue Engineering and Regenerative Medicine*. Crc Press; 2004.
222. Jia Y, Wang W, Zhou X, Nie W, Chen L, He C. Synthesis and characterization of poly (glycerol sebacate)-based elastomeric copolyesters for tissue engineering applications. *Polym Chem*. 2016;7(14):2553-2564.
223. Morrow DA, Donahue TLH, Odegard GM, Kaufman KR. Transversely isotropic tensile material properties of skeletal muscle tissue. *J Mech Behav Biomed Mater*. 2010;3(1):124-129.
224. Chen EJ, Novakofski J, Jenkins WK, O'Brien WD. Young's modulus measurements of soft tissues with application to elasticity imaging. *IEEE Trans Ultrason Ferroelectr Freq Control*. 1996;43(1):191-194.
225. Toursel T, Stevens L, Granzier H, Mounier Y. Passive tension of rat skeletal soleus muscle fibers: effects of unloading conditions. *J Appl Physiol*. 2002;92(4):1465-1472.
226. Sant S, Hancock MJ, Donnelly JP, Iyer D, Khademhosseini A. Biomimetic gradient hydrogels for tissue engineering. *Can J Chem Eng*. 2010;88(6):899-911.
227. Bat E, Zhang Z, Feijen J, Grijpma DW, Poot AA. Biodegradable elastomers for biomedical applications and regenerative medicine. *Regen Med*. 2014;9(3):385-398.
228. Godier AFG, Marolt D, Gerecht S, Tajnsek U, Martens TP, Vunjak-Novakovic G. Engineered microenvironments for human stem cells. *Birth Defects Res Part C Embryo Today Rev*. 2008;84(4):335-347.
229. Park H, Cannizzaro C, Vunjak-Novakovic G, Langer R, Vacanti CA, Farokhzad OC. Nanofabrication and microfabrication of functional materials for tissue engineering. *Tissue Eng*. 2007;13(8):1867-1877.
230. Li W, Laurencin CT, Caterson EJ, Tuan RS, Ko FK. Electrospun nanofibrous structure: a novel scaffold for tissue engineering. *J Biomed Mater Res*. 2002;60(4):613-621.
231. Jain KK. Role of nanotechnology in developing new therapies for diseases of the nervous system. 2006.
232. Li Y, Thouas GA, Chen Q-Z. Biodegradable soft elastomers:

synthesis/properties of materials and fabrication of scaffolds. *RSC Adv*. 2012;2(22):8229-8242.
233. Freed LE, Engelmayr GC, Borenstein JT, Moutos FT, Guilak F. Advanced material strategies for tissue engineering scaffolds. *Adv Mater*. 2009;21(32-33):3410-3418.
234. Sarti B, Scandola M. Viscoelastic and thermal properties of collagen/poly (vinyl alcohol) blends. *Biomaterials*. 1995;16(10):785-792.
235. Aoi K, Takasu A, Okada M. New chitin-based polymer hybrids, 1. Miscibility of poly (vinyl alcohol) with chitin derivatives. *Macromol Rapid Commun*. 1995;16(10):757-761.
236. Kuchaiyaphum P, Punyodom W, Watanesk S, Watanesk R. Composition optimization of polyvinyl alcohol/rice starch/silk fibroin-blended films for improving its eco-friendly packaging properties. *J Appl Polym Sci*. 2013;129(5):2614-2620.
237. Kumar HMPN, Prabhakar MN, Prasad CV, et al. Compatibility studies of chitosan/PVA blend in 2% aqueous acetic acid solution at 30 C. *Carbohydr Polym*. 2010;82(2):251-255.
238. Chaouat M, Le Visage C, Baille WE, et al. A novel cross-linked poly (vinyl alcohol)(PVA) for vascular grafts. *Adv Funct Mater*. 2008;18(19):2855-2861.
239. Kobayashi M, Toguchida J, Oka M. Development of polyvinyl alcohol-hydrogel (PVA-H) shields with a high water content for tendon injury repair. *J Hand Surg Am*. 2001;26(5):436-440.
240. Hassan CM, Peppas NA. Structure and applications of poly (vinyl alcohol) hydrogels produced by conventional crosslinking or by freezing/thawing methods. In: *Biopolymers· PVA Hydrogels, Anionic Polymerisation Nanocomposites*. Springer; 2000:37-65.
241. Park H, Park K, Shalaby WSW. *Biodegradable Hydrogels for Drug Delivery*. CRC Press; 2011.
242. Ghasemi-Mobarakeh L, Semnani D, Morshed M. A novel method for porosity measurement of various surface layers of nanofibers mat using image analysis for tissue engineering applications. *J Appl Polym Sci*. 2007;106(4):2536-2542.
243. Pham QP, Sharma U, Mikos AG. Electrospinning of polymeric nanofibers for tissue engineering applications: a review. *Tissue Eng*. 2006;12(5):1197-1211.
244. Graessley W. The entanglement concept in polymer rheology. *Entanglement Concept Polym Rheol*. 1974:1-179.
245. Shin YM, Hohman MM, Brenner MP, Rutledge GC. Electrospinning: A whipping fluid jet generates submicron polymer fibers. *Appl Phys Lett*. 2001;78(8):1149-1151.

246. Hohman MM, Shin M, Rutledge G, Brenner MP. Electrospinning and electrically forced jets. I. Stability theory. *Phys fluids*. 2001;13(8):2201-2220.
247. Jeffries EM, Allen RA, Gao J, Pesce M, Wang Y. Highly elastic and suturable electrospun poly (glycerol sebacate) fibrous scaffolds. *Acta Biomater*. 2015;18:30-39.
248. Socrates G. *Infrared and Raman Characteristic Group Frequencies: Tables and Charts*. John Wiley & Sons; 2004.
249. Ye M, Mohanty P, Ghosh G. Morphology and properties of poly vinyl alcohol (PVA) scaffolds: impact of process variables. *Mater Sci Eng C*. 2014;42:289-294.
250. Xu B, Li Y, Zhu C, Cook WD, Forsythe J, Chen Q. Fabrication, mechanical properties and cytocompatibility of elastomeric nanofibrous mats of poly (glycerol sebacate). *Eur Polym J*. 2015;64:79-92.
251. Hodge RM, Bastow TJ, Edward GH, Simon GP, Hill AJ. Free volume and the mechanism of plasticization in water-swollen poly (vinyl alcohol). *Macromolecules*. 1996;29(25):8137-8143.
252. Lyu S, Untereker D. Degradability of polymers for implantable biomedical devices. *Int J Mol Sci*. 2009;10(9):4033-4065.
253. Zulkifli FH, Hussain FSJ, Rasad MSBA, Yusoff MM. In vitro degradation study of novel HEC/PVA/collagen nanofibrous scaffold for skin tissue engineering applications. *Polym Degrad Stab*. 2014;110:473-481.
254. Puri M. Food Bioactives: Extraction and Biotechnology Applications. 2017.
255. Li Y, Cook WD, Moorhoff C, Huang W, Chen Q. Synthesis, characterization and properties of biocompatible poly (glycerol sebacate) pre-polymer and gel. *Polym Int*. 2013;62(4):534-547.
256. Di Martino A, Sittinger M, Risbud M V. Chitosan: a versatile biopolymer for orthopaedic tissue-engineering. *Biomaterials*. 2005;26(30):5983-5990.
257. Xie Z, Buschle-Diller G. Electrospun poly (D, L-lactide) fibers for drug delivery: The influence of cosolvent and the mechanism of drug release. *J Appl Polym Sci*. 2010;115(1):1-8.
258. Prabaharan M, Grailer JJ, Pilla S, Steeber DA, Gong S. Folate-conjugated amphiphilic hyperbranched block copolymers based on Boltorn® H40, poly (l-lactide) and poly (ethylene glycol) for tumor-targeted drug delivery. *Biomaterials*. 2009;30(16):3009-3019.
259. Vargas EAT, do Vale Baracho NC, De Brito J, De Queiroz AAA. Hyperbranched polyglycerol electrospun nanofibers for wound dressing applications. *Acta Biomater*. 2010;6(3):1069-1078.
260. Tian Y, Wu M, Liu R, et al. Electrospun membrane of cellulose acetate for heavy metal ion adsorption in water treatment. *Carbohydr Polym*.

2011;83(2):743-748.
261. Shin YJ, Wang M, Kameoka J. Electrospun nanofiber biosensor for measuring glucose concentration. *J Photopolym Sci Technol*. 2009;22(2):235-237.
262. Chen J-P, Ho K-H, Chiang Y-P, Wu K-W. Fabrication of electrospun poly (methyl methacrylate) nanofibrous membranes by statistical approach for application in enzyme immobilization. *J Memb Sci*. 2009;340(1):9-15.
263. Li D, Xia Y. Direct fabrication of composite and ceramic hollow nanofibers by electrospinning. *Nano Lett*. 2004;4(5):933-938.
264. Anton F. Process and apparatus for preparing artificial threads. October 1934.
265. McKee MG, Wilkes GL, Colby RH, Long TE. Correlations of solution rheology with electrospun fiber formation of linear and branched polyesters. *Macromolecules*. 2004;37(5):1760-1767.
266. Kong L, Ziegler GR. Role of molecular entanglements in starch fiber formation by electrospinning. *Biomacromolecules*. 2012;13(8):2247-2253.
267. De Gennes P-G. *Scaling Concepts in Polymer Physics*. Cornell university press; 1979.
268. Abbasi A, Nasef MM, Takeshi M, Faridi-Majidi R. Electrospinning of nylon-6, 6 solutions into nanofibers: rheology and morphology relationships. 高分子科学. 2014;32(6):793-804.
269. Powell HM, Boyce ST. Engineered human skin fabricated using electrospun collagen–PCL blends: morphogenesis and mechanical properties. *Tissue Eng Part A*. 2009;15(8):2177-2187.
270. Phipps MC, Clem WC, Catledge SA, et al. Mesenchymal stem cell responses to bone-mimetic electrospun matrices composed of polycaprolactone, collagen I and nanoparticulate hydroxyapatite. *PLoS One*. 2011;6(2):e16813.
271. Nerurkar NL, Elliott DM, Mauck RL. Mechanics of oriented electrospun nanofibrous scaffolds for annulus fibrosus tissue engineering. *J Orthop Res*. 2007;25(8):1018-1028.
272. ALEXANDER JK, FUSS B, COLELLO RJ. Electric field-induced astrocyte alignment directs neurite outgrowth. *Neuron Glia Biol*. 2006;2(2):93-103.
273. Ayres C, Bowlin GL, Henderson SC, et al. Modulation of anisotropy in electrospun tissue-engineering scaffolds: Analysis of fiber alignment by the fast Fourier transform. *Biomaterials*. 2006;27(32):5524-5534.
274. Aviss KJ, Gough JE, Downes S. Aligned electrospun polymer fibres for skeletal muscle regeneration. *Eur Cell Mater*. 2010;19:193-204.
275. Li D, Wang Y, Xia Y. Electrospinning of polymeric and ceramic nanofibers as uniaxially aligned arrays. *Nano Lett*. 2003;3(8):1167-1171.

276. Na H, Li Q, Sun H, Zhao C, Yuan X. Anisotropic mechanical properties of hot-pressed PVDF membranes with higher fiber alignments via electrospinning. *Polym Eng Sci*. 2009;49(7):1291-1298.
277. Gaumer J, Prasad A, Lee D, Lannutti J. Structure–function relationships and source-to-ground distance in electrospun polycaprolactone. *Acta Biomater*. 2009;5(5):1552-1561.
278. Tong H-W, Wang M. Electrospinning of aligned biodegradable polymer fibers and composite fibers for tissue engineering applications. *J Nanosci Nanotechnol*. 2007;7(11):3834-3840.
279. Sundaray B, Subramanian V, Natarajan TS, Xiang R-Z, Chang C-C, Fann W-S. Electrospinning of continuous aligned polymer fibers. *Appl Phys Lett*. 2004;84(7):1222-1224.
280. Lee KH, Kim HY, La YM, Lee DR, Sung NH. Influence of a mixing solvent with tetrahydrofuran and N, N-dimethylformamide on electrospun poly (vinyl chloride) nonwoven mats. *J Polym Sci part B Polym Phys*. 2002;40(19):2259-2268.
281. Reneker DH, Chun I. Nanometre diameter fibres of polymer, produced by electrospinning. *Nanotechnology*. 1996;7(3):216.
282. Elzubair A, Elias CN, Suarez JCM, Lopes HP, Vieira MVB. The physical characterization of a thermoplastic polymer for endodontic obturation. *J Dent*. 2006;34(10):784-789.
283. Elzein T, Nasser-Eddine M, Delaite C, Bistac S, Dumas P. FTIR study of polycaprolactone chain organization at interfaces. *J Colloid Interface Sci*. 2004;273(2):381-387.
284. Shabani I, Haddadi-Asl V, Seyedjafari E, Babaeijandaghi F, Soleimani M. Improved infiltration of stem cells on electrospun nanofibers. *Biochem Biophys Res Commun*. 2009;382(1):129-133.
285. Place ES, Evans ND, Stevens MM. Complexity in biomaterials for tissue engineering. *Nat Mater*. 2009;8(6):457-470.
286. Huebsch N, Mooney DJ. Inspiration and application in the evolution of biomaterials. *Nature*. 2009;462(7272):426-432.
287. Qian Z, Li S, He Y, Zhang H, Liu X. Hydrolytic degradation study of biodegradable polyesteramide copolymers based on ε-caprolactone and 11-aminoundecanoic acid. *Biomaterials*. 2004;25(11):1975-1981.
288. Karimi P, Rizkalla AS, Mequanint K. Versatile biodegradable poly (ester amide) s derived from α-amino acids for vascular tissue engineering. *Materials (Basel)*. 2010;3(4):2346-2368.
289. Makadia HK, Siegel SJ. Poly lactic-co-glycolic acid (PLGA) as biodegradable controlled drug delivery carrier. *Polymers (Basel)*. 2011;3(3):1377-1397.
290. Hu W-J, Eaton JW, Ugarova TP, Tang L. Molecular basis of biomaterial-

mediated foreign body reactions. *Blood*. 2001;98(4):1231-1238.
291. Bruggeman JP, de Bruin B-J, Bettinger CJ, Langer R. Biodegradable poly (polyol sebacate) polymers. *Biomaterials*. 2008;29(36):4726-4735.
292. Rai R, Tallawi M, Grigore A, Boccaccini AR. Synthesis, properties and biomedical applications of poly (glycerol sebacate)(PGS): a review. *Prog Polym Sci*. 2012;37(8):1051-1078.
293. Patel A, Gaharwar AK, Iviglia G, et al. Highly elastomeric poly (glycerol sebacate)-co-poly (ethylene glycol) amphiphilic block copolymers. *Biomaterials*. 2013;34(16):3970-3983.
294. Sun Z-J, Wu L, Huang W, et al. The influence of lactic on the properties of poly (glycerol–sebacate–lactic acid). *Mater Sci Eng C*. 2009;29(1):178-182.
295. Nair LS, Laurencin CT. Biodegradable polymers as biomaterials. *Prog Polym Sci*. 2007;32(8):762-798.
296. Kim E-S, Ahn EH, Dvir T, Kim D-H. Emerging nanotechnology approaches in tissue engineering and regenerative medicine. *Int J Nanomedicine*. 2014;9(Suppl 1):1.
297. Yang HS, Ieronimakis N, Tsui JH, et al. Nanopatterned muscle cell patches for enhanced myogenesis and dystrophin expression in a mouse model of muscular dystrophy. *Biomaterials*. 2014;35(5):1478-1486.
298. Shanmugasundaram N, Ravichandran P, Reddy PN, Ramamurty N, Pal S, Rao KP. Collagen–chitosan polymeric scaffolds for the in vitro culture of human epidermoid carcinoma cells. *Biomaterials*. 2001;22(14):1943-1951.
299. Cipitria A, Skelton A, Dargaville TR, Dalton PD, Hutmacher DW. Design, fabrication and characterization of PCL electrospun scaffolds—a review. *J Mater Chem*. 2011;21(26):9419-9453.
300. Ghasemi-Mobarakeh L, Prabhakaran MP, Morshed M, Nasr-Esfahani M-H, Ramakrishna S. Electrospun poly (ε-caprolactone)/gelatin nanofibrous scaffolds for nerve tissue engineering. *Biomaterials*. 2008;29(34):4532-4539.
301. Law K-Y. Definitions for hydrophilicity, hydrophobicity, and superhydrophobicity: getting the basics right. 2014.